2017-09-01

Large-Scale Testing of Low-Strength Cellular Concrete for Skewed Bridge Abutments

Tyler Kirk Remund

Large-Scale Testing of Low-Strength Cellular Concrete for Skewed Bridge Abutments

Tyler Kirk Remund

A thesis submitted to the faculty of
Brigham Young University
in partial fulfillment of the requirements for the degree of

Master of Science

Kyle M. Rollins, Chair
W. Spencer Guthrie
Fernando S. Fonseca

Department of Civil and Environmental Engineering

Brigham Young University

ABSTRACT

Large-Scale Testing of Low-Strength Cellular Concrete for Skewed Bridge Abutments

Tyler Kirk Remund
Department of Civil and Environmental Engineering, BYU
Master of Science

Low-strength cellular concrete consists of a cement slurry that is aerated prior to placement. It remains a largely untested material with properties somewhere between those of soil, geofoam, and typical controlled low-strength material (CLSM). The benefits of using this material include its low density, ease of placement, and ability to self-compact. Although the basic laboratory properties of this material have been investigated, little information exists about the performance of this material in the field, much less the passive resistance behavior of this material in the field.

In order to evaluate the use of cellular concrete as a backfill material behind bridge abutments, two large-scale tests were conducted. These tests sought to better understand the passive resistance, the movement required to reach this resistance, the failure mechanism, and skew effects for a cellular concrete backfill. The tests used a pile cap with a backwall face 5.5 ft (1.68 m) tall and 11 ft (3.35 m) wide. The backfill area had walls on either side running parallel to the sides of the pile cap to allow the material to fail in a 2D fashion. The cellular concrete backfill for the 30° skew test had an average wet density of 29.6 pcf (474 kg/m^3) and a compressive strength of 57.6 psi (397 kPa). The backfill for the 0° skew test had an average wet density of 28.6 pcf (458 kg/m^3) and a compressive strength of 50.9 psi (351 kPa). The pile cap was displaced into the backfill area until failure occurred. A total of two tests were conducted, one with a 30° skew wedge attached to the pile cap and one with no skew wedge attached.

It was observed that the cellular concrete backfill mainly compressed under loading with no visible failure at the surface. The passive-force curves showed the material reaching an initial peak resistance after movement equal to 1.7-2.6% of the backwall height and then remaining near this strength or increasing in strength with any further deflection. No skew effects were observed; any difference between the two tests is most likely due to the difference in concrete placement and testing.

Key words: abutments, abutment lateral resistance, backfill, cellular concrete, controlled low-strength material, foam concrete, passive force, passive pressure on abutments

ACKNOWLEDGEMENTS

I thank Dr. Kyle M. Rollins for allowing me to work on this project, which was both interesting and fun. I appreciate Dr. Rollin's efforts to teach and guide me as well as his example of hard work and dedication. I thank the other members of my committee, Dr. Guthrie and Dr. Fonseca, for their time and advice as I worked to finish this project. Dr. Guthrie, in particular, helped me understand various aspects of concrete behavior even though I had not taken corresponding courses. I am grateful to Dr. Franke, who introduced me to geotechnical engineering, an area of civil engineering I did not even know about at the time but have since grown to love.

I appreciate the sacrifices of my wife Claire and son Boyd who dealt with long periods without me. Claire supported me through this long endeavor. I thank Dave Anderson and Rodney Mayo for their expertise, problem-solving ability, and patience as we dealt with several setbacks. I thank Clay Hansen and Kirk Kauer for enduring many long, hot days at the Salt Lake Airport in order to prepare the site and complete all of the tests; they remained enthusiastic throughout the entire process.

Funding for this study was provided by Federal Highway Administration (FHWA) pooled fund TPF-5(264) supported by the departments of transportation from the states of California, Minnesota, Montana, New York, Oregon, Utah, and Wisconsin. Utah served as the lead agency with David Stevens as the project manager. This support is gratefully acknowledged. I also express appreciation to the Salt Lake City Airport Department for providing access to the test site used in this study, to Cell-Crete Corporation for donating the cellular concrete material, and to Ryan Maw at Gerhart-Cole for his advice and help with laboratory testing.

TABLE OF CONTENTS

LIST OF TABLES

LIST OF FIGURES

1 INTRODUCTION

Bridge abutments are often designed to rely on the passive resistance of the adjacent soil during thermal expansion or earthquake events. Tests have shown that skewed bridge abutments have a significantly lower amount of available passive resistance compared to non-skewed abutments (Jessee 2012, Rollins 2002), but when placed in translational motion these abutments are designed as if the skew did not exist (FHWA 2014). Various backfill materials have been tested to remedy this problem by imparting extra passive resistance to the abutment. Cellular concrete has not been tested as a backfill material for skewed abutments.

Cellular concrete has multiple properties that make it desirable as a backfill material. Cellular concrete has a low density and is able to self-compact. Due to these properties, the material can be placed quickly and with less manpower compared to traditional backfills. The low density also reduces or eliminates settlement.

1.1 Research Objectives

The objectives of this research were as follows:

1. Determine the effect of skew angle on the passive resistance of a cellular concrete backfill
2. Determine the displacement required to mobilize peak passive resistance of cellular concrete

3. Determine the passive force-displacement relationship for cellular concrete backfill
4. Develop a method for characterizing cellular concrete backfill strength

1.2 Scope of Work

A passive force-deflection test was conducted using an existing pile cap to simulate a non-skewed abutment and a 30° skew wedge to simulate a skewed abutment. Cellular concrete backfill was placed in front of the pile cap or skew wedge and allowed to cure. Concrete cylinders were prepared during concrete placement to characterize the backfill strength. Two actuators were used to displace the pile cap into the cellular concrete backfill, and the load required to do so was measured. A grid pattern was painted onto the backfill surface so that individual points could be surveyed and the movement of each point observed. String potentiometers measured the longitudinal movement in the backfill more precisely at 2-ft (0.62-m) intervals. Potentiometers were also placed behind the pile cap to measure the longitudinal movement of the pile cap.

Data were collected and analyzed to determine the movement of the backfill and characterize the passive resistance of the backfill. The unconfined compressive strength (UCS) of the cellular concrete was determined and used in calculating the passive resistance of the backfill. The computed result was then compared to the measured result in the field for accuracy.

1.3 Outline of Report

This thesis includes seven chapters. Chapter 2 explains what is currently known about cellular concrete and provides a summary of other tests on skewed bridge abutments with typical backfill materials. Chapter 3 explains how this study was conducted with an overview of the test site and the testing procedures. Chapter 4 describes the properties of the cellular concrete used.

Chapter 5 presents the full-scale test results. Chapter 6 analyzes these results by comparing them with PYCAP-computed results and the design procedure for a granular backfill. Lastly, Chapter 7 provides the conclusions of this study and recommendations for future research.

2 LITERATURE REVIEW

2.1 Low-Strength Cellular Concrete

In actual fact, cellular concrete is not a true concrete consisting of cement, aggregates, and water. It is more of a cement slurry that has been aerated prior to placement. Cellular concrete is also known as foam concrete or aerated concrete. Unlike conventional concrete, it generally does not contain coarse aggregate. It also contains 50-80% more air voids than a typical concrete (Grutzeck 2005). The large amount of air voids does compromise compressive strength and durability compared to other concrete mixtures (Panesar 2013), but it also produces a lightweight material that is self-consolidating.

2.1.1 Physical Properties

2.1.1.1 Shrinkage

Cellular concrete experiences a high amount of shrinkage due to the absence of aggregates, up to 10 times more than a conventional concrete. This can be reduced by using lightweight aggregate, adding fly ash or sand, or using the autoclave curing method (Ramamurthy 2009). Nambiar (2009) found that shrinkage can be reduced by increasing the foam content. This reduction in shrinkage is due to a reduction in the amount of paste and amount of pores due to increasing foam content. An increase in foam content increases the size of and combines micropores. The removal of water from larger-sized pores does not contribute

to shrinkage (Nambiar 2009). As the foam volume increases the number of small micropores (which contribute to shrinkage) decreases thus reducing the overall shrinkage.

2.1.1.2 Unit Weight

Cellular concrete has a significantly lower unit weight compared to typical concrete or even typical soils. Caltrans categorizes cellular concrete into six classes with densities ranging from 24 to 90 pcf (384 to 1442 kg/m^3) as summarized in Table 2-1. Classes II through IV are most commonly used in practice.

Table 2-1: Caltrans Cellular Concrete Classes

Cellular Concrete Class	Cast Density (pcf)	Minimum 28-day Compressive Strength (psi)
I	24-29	10
II	30-35	40
III	36-41	80
IV	42-49	120
V	50-79	160
VI	80-90	300

2.1.1.3 Unconfined Compressive Strength

The compressive strength of cellular concrete is affected by multiple factors including age, density, water content, method of curing, and the particle-size distribution of sand in the mixture (Ramamurthy, 2009). The dry density of cellular concrete has been found to be the largest factor affecting strength (Kearsley and Wainwright 2001). This is particularly true for low-density cellular concretes (Nambiar and Ramamurthy 2006). Since the dry density of cellular concretes is primarily affected by the volume of voids, this concept is illustrated well by

comparing porosity to strength. Figure 2-1 shows that, as porosity increases, the compressive strength of the concrete decreases (Nambiar 2008).

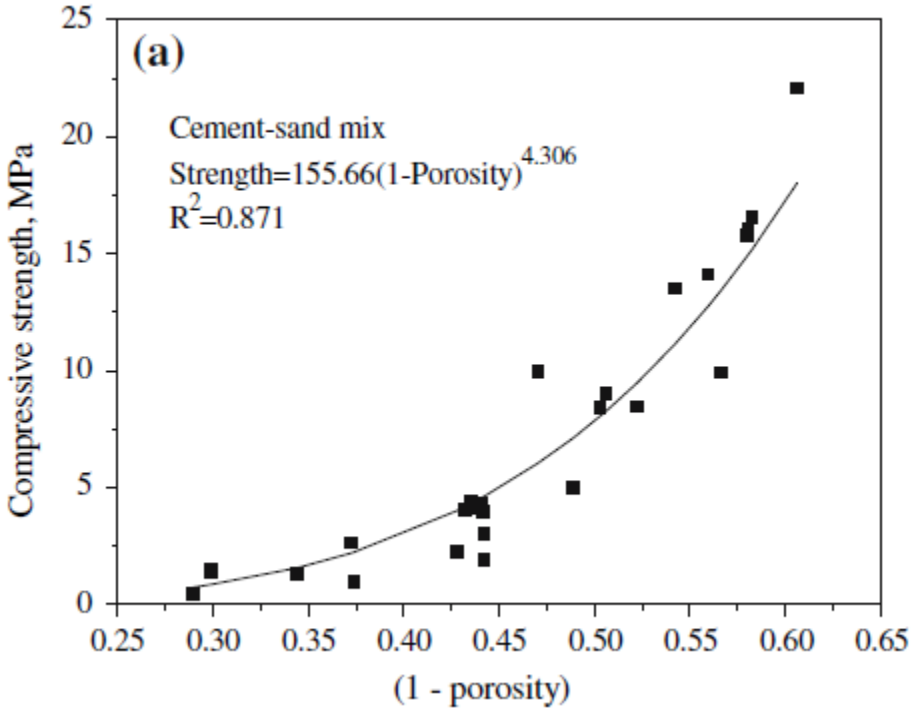

Figure 2-1: Compressive strength vs. porosity for cement-sand mixture (Nambiar 2008).

The compressive strength of low-density cellular concrete is primarily controlled by the foam volume rather than changes in material properties (Nambiar and Ramamurthy 2006). It has been observed that small changes in water-cement ratio do not markedly affect the strength of cellular concrete in the way that would be expected for a normal-weight concrete (Jones and McCarthy 2006). Tam et al. 1987 concluded that the combined effects of the water-cement ratio and air-cement ratio should be considered when the volume of air voids approaches the volume of water voids for moist-cured cellular concrete. Kearsley and Wainwright (2001) found that large amounts of cement (up to 75%) could be replaced with fly ash without any noticeable negative effect on long-term compressive strength. Kearsley and Wainwright (2001) used a

graded fly ash complying with South African Bureau of Standards 1491 and an ungraded fly ash. Although concretes with high fly ash contents needed more time to cure, they could reach higher strengths than their cement-only counterparts. Kearsley and Wainwright (2001) noted that their results apply only to well-cured specimens.

The curing method can also have an effect on compressive strength. Humid air curing at 104° F (40^{O} C) is reported to produce higher compressive strengths than water curing (Kearsley and Booysens 1998). The autoclaving curing method can also increase strength, although this method is generally used for pre-cast structural concrete and is not applicable to backfill materials (Ramamurthy 2009).

Normal concrete gains approximately 70% of its 28-day strength within the first 7 days (Zemajtis). Since low-density cellular concrete typically has cement contents below that of a normal concrete, it follows that curing times would be faster. Nambiar and Ramamurthy (2006) tested a cellular concrete comprised of a cement-sand mixture that had a dry density of 49.1 pcf (787 kg/m^3). The cellular concrete was immersed in water and then tested for compressive strength. Nambiar and Ramamurthy (2006) found only a 2.5% strength gain between 7 and 28 days and a 28.3 % strength gain between 7 and 90 days.

In order to allow future excavation of the backfill, UCS values must not exceed approximately 200 psi (1379 kPa) for mechanical excavation and 50 psi (345 kPa) for manual excavation (NRMCA 2000). Typically, state DOTs limit the strength of controlled low-strength materials (CLSM) to between 50 psi and 150 psi (345 kPa and 1034 kPa) so that future excavation remains possible. Figure 2-2 shows the range of acceptable UCS values for several

state DOTs. The UCS of cellular concrete is generally tested in accordance with ASTM C495 (Standard Test Method for Compressive Strength of Lightweight Insulating Concrete).

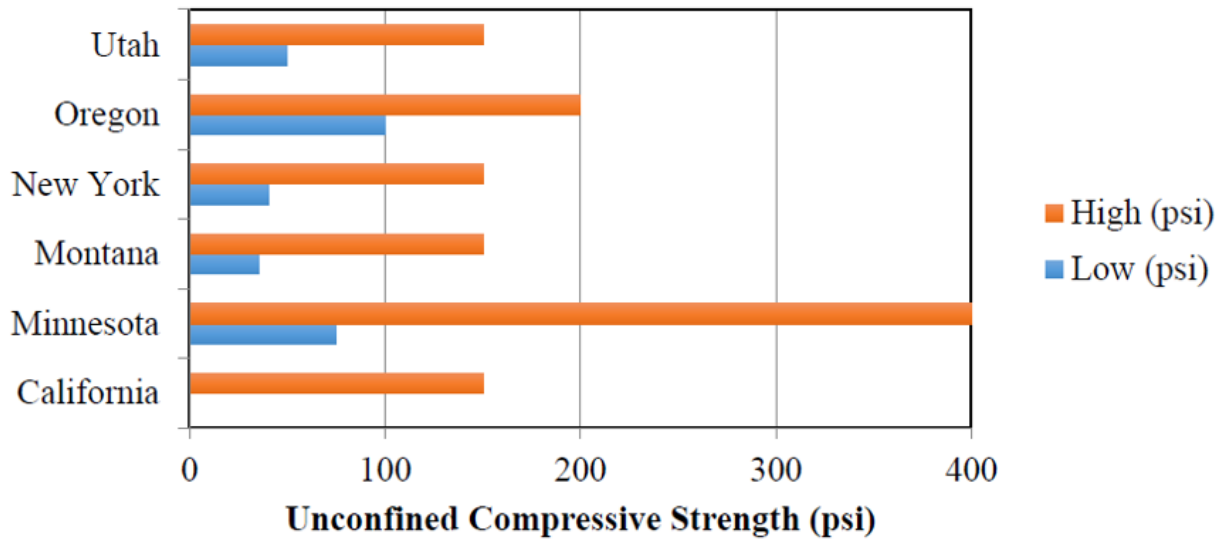

Figure 2-2: UCS range for CLSM mixtures by state (Wagstaff 2016).

An independent laboratory, Gerhart-Cole, tested the UCS of Class II and Class IV (low-density) cellular concrete (Maw and Cole 2015). The cellular concrete samples were provided by Cell-Crete Corporation and were classified according to the Caltrans criteria. UCS results show that the Class II material generally exceeded the manufacturer's suggested values. However, the Class IV material did not meet the minimum recommended values. Gerhart-Cole noted that the mixture design for the Class IV concrete was unique to the project and may not be best classified as a Class IV concrete. Table 2-2 presents Gerhart Cole's UCS results.

Table 2-2: UCS Results (Maw and Cole 2015)

Cellular Concrete Class	Minimum UCS (psi) [a]	Cast Date (MM/YR)	UCS (psi)	Unit Weight (pcf)	Strain at Peak Strength (%)
II	40	11/14	65.5	24.3	8.3
		11/14	62.4	23.9	7.3
		02/15	*23.4*	28.0	5.8
		02/15	*25.9*	27.5	5.8
		02/15	*30.5*	29.1	3.5
IV (low-density)	120	02/15	*81.8*	32.1	0.9
		02/15	*105.6*	33.5	1.9
		02/15	*111.7*	33.2	2.9
		02/15	*96.0*	34.0	2.1
		02/15	*118.6*	32.7	1.4
		02/15	*108.5*	31.3	1.9

[a] Value suggested by Elastizell (2000).
[b] UCS values not meeting minimum in italics.

2.1.1.4 Triaxial Test Results

Gerhart-Cole also performed isotropically consolidated, drained and undrained triaxial tests (Maw and Cole 2015). The results presented here are from the drained tests. These tests were conducted with confining pressures of 2.5 psi, 5 psi, 12.5 psi, and 30 psi (17.2 kPa, 34.5 kPa, 86.2 kPa, and 206.8 kPa). Figure 2-3 shows the Mohr's circle results for a Class II cellular concrete. Shear strength ranges between 20 psi and 30 psi (137.9 kPa and 206.8 kPa) and does not appear to increase with higher confining pressures. Figure 2-4 shows the Mohr's circle results for a Class IV cellular concrete. The shear strength is about 20 psi (137.8 kPa) higher than that of the Class II concrete at 40-50 psi (275.8-344.7 kPa). There is also, once again, no noticeable increase in shear strength with higher confining pressures. These results support a 0˚ friction angle assumption. Figure 2-5 shows the stress vs. strain curves for cylinders at the four

confining pressures previously mentioned. Even at high levels of strain, the samples are able to retain most of their peak strength.

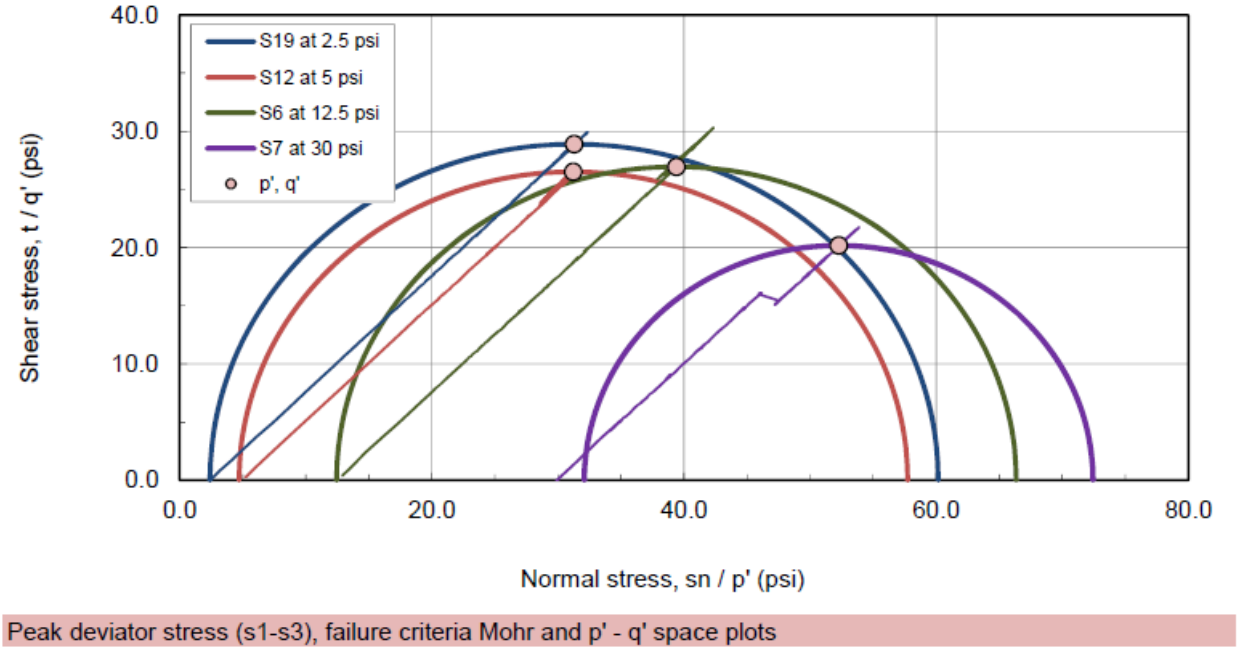

Figure 2-3: Class II cellular concrete effective stress results.

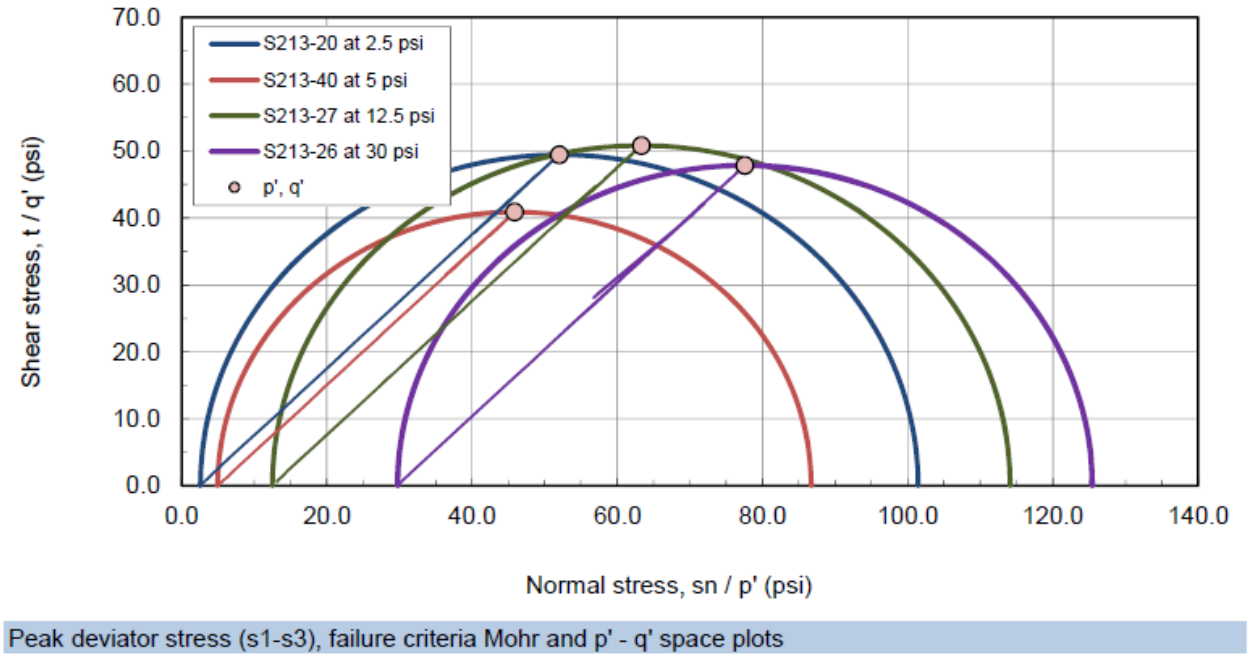

Figure 2-4: Class IV cellular concrete effective stress results.

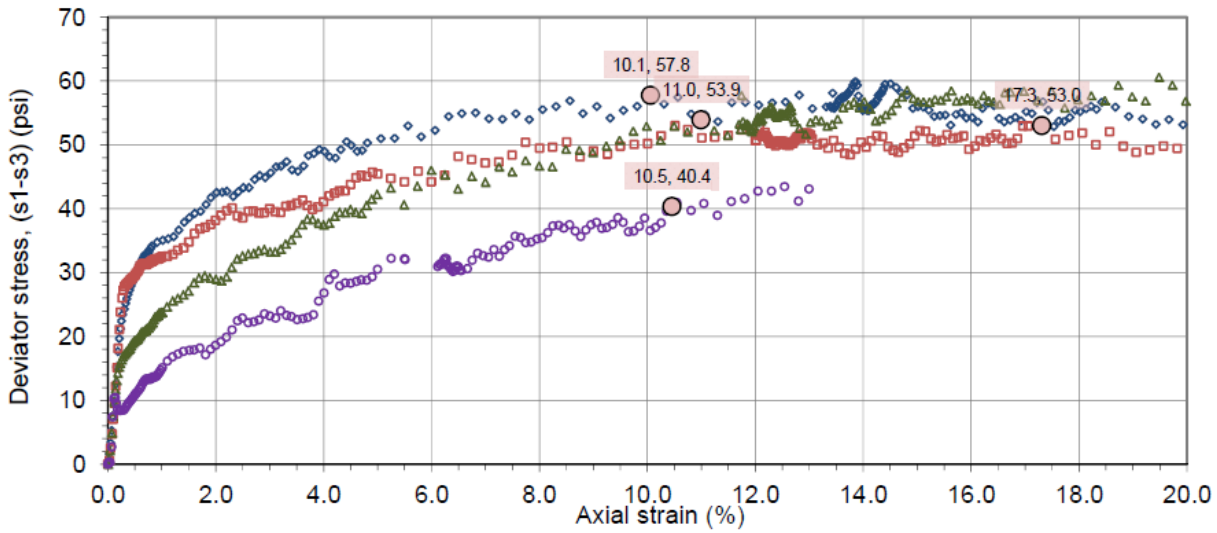

Figure 2-5: Stress vs. strain curve for Class II cellular concrete samples.

2.1.1.5 Water Absorption

Moisture transport in cellular concrete is better represented through sorptivity than through permeability (Ramamurthy 2009). Sorptivity is the ability to transfer water through capillary action. As the foam volume increases, the sorptivity, like absorption, decreases. This is due to the reduction in cement paste and the increase in porosity and pore sizes. The amount of cement paste influences the number of capillary pores that are able to form (Ramamurthy 2009). Since capillary action is the primary form of moisture transport, less cement paste means less water absorption. Greater porosity, which occurs as a result of increasing pore sizes, does not increase water absorption since a large portion of the air voids are not connected; these air voids actually increase the tortuosity of the water transport path (Nambiar and Ramamurthy 2007). Consequently, lower density cellular concretes have lower water absorption.

Freeze-thaw resistance for cellular concrete depends on several factors. Tikalsky et al. (2004) tested several cellular concrete mixtures at 150 freeze-thaw cycles and determined that cellular concretes with 28-day compressive strengths above 145 psi (1 MPa) and with low absorptivity performed well in freeze-thaw testing. The density and permeability of the sample did not appear to be significant. One high-density, high-strength mixture was able to perform well despite having a high water absorption. The one low-density, low-strength mixture tested used a large amount of fly ash in place of cement. It was concluded that this mixture had marginal performance due to low early-strength gain and a high level of water absorption.

2.1.1.6 Hydraulic Conductivity

Gerhart-Cole measured the hydraulic conductivity of Class II and IV cellular concrete using a triaxial cell with a flexible membrane (Maw and Cole 2015). The moist unit weight of the samples ranged between 27.1 pcf and 33.5 pcf. Specimens were tested at different confining stresses to determine if seepage around the sides of the sample affected the results. Gerhart-Cole found that higher density samples had a slightly higher hydraulic conductivity. This observation supports the idea of water transport through capillary action presented in Section 2.1.1.5. Table 2-3 shows the hydraulic conductivity values for both Class II and Class IV (denser) cellular concrete. Hydraulic conductivity for all samples ranged between 1.7E-04 cm/sec and 1.2E-03 cm/sec.

Table 2-3: Cellular Concrete Hydraulic Conductivity (Back Pressure, Flexible Wall).

Cellular Concrete Class	Cast Date (MM/YR)	Sample ID	Hydraulic Conductivity $K_{average}$[a] (cm/sec)	Moist Unit Weight (pcf)	Confining Stress (psi)
II	07/14	13	1.9E-04	29.2	5.0
	07/14	13	1.7E-04	29.2	12.5
	07/14	19	7.7E-04	27.1	5.0
	07/14	19	7.2E-04	27.1	12.5
IV (low density)	02/15	213-31	1.2E-03	31.2	5.0
	02/15	213-21	9.5E-04	33.5	12.5

[a] Corrected to 20° C.

2.1.1.7 Shear Strength

Little information exists about the shear strength of cellular concrete. Legatski and Mansour (1961) tested Elastizell cellular concrete mixtures with sand that had densities between 40 pcf and 120 pcf (641 kg/m^3 and 1922 kg/m^3). Shear strength in diagonal tension was determined by centrally loading a 50-in.- (127-cm-) long beam, reinforced with two #4 bars, over a 36-in. (91-cm) span. They found that shear strength could be expressed as a percentage of the compressive strength in accordance with ACI 318-56 Table 305(a) with reduced maximum values. This method provides a very conservative estimate of strength compared to their test values as shown in Figure 2-6.

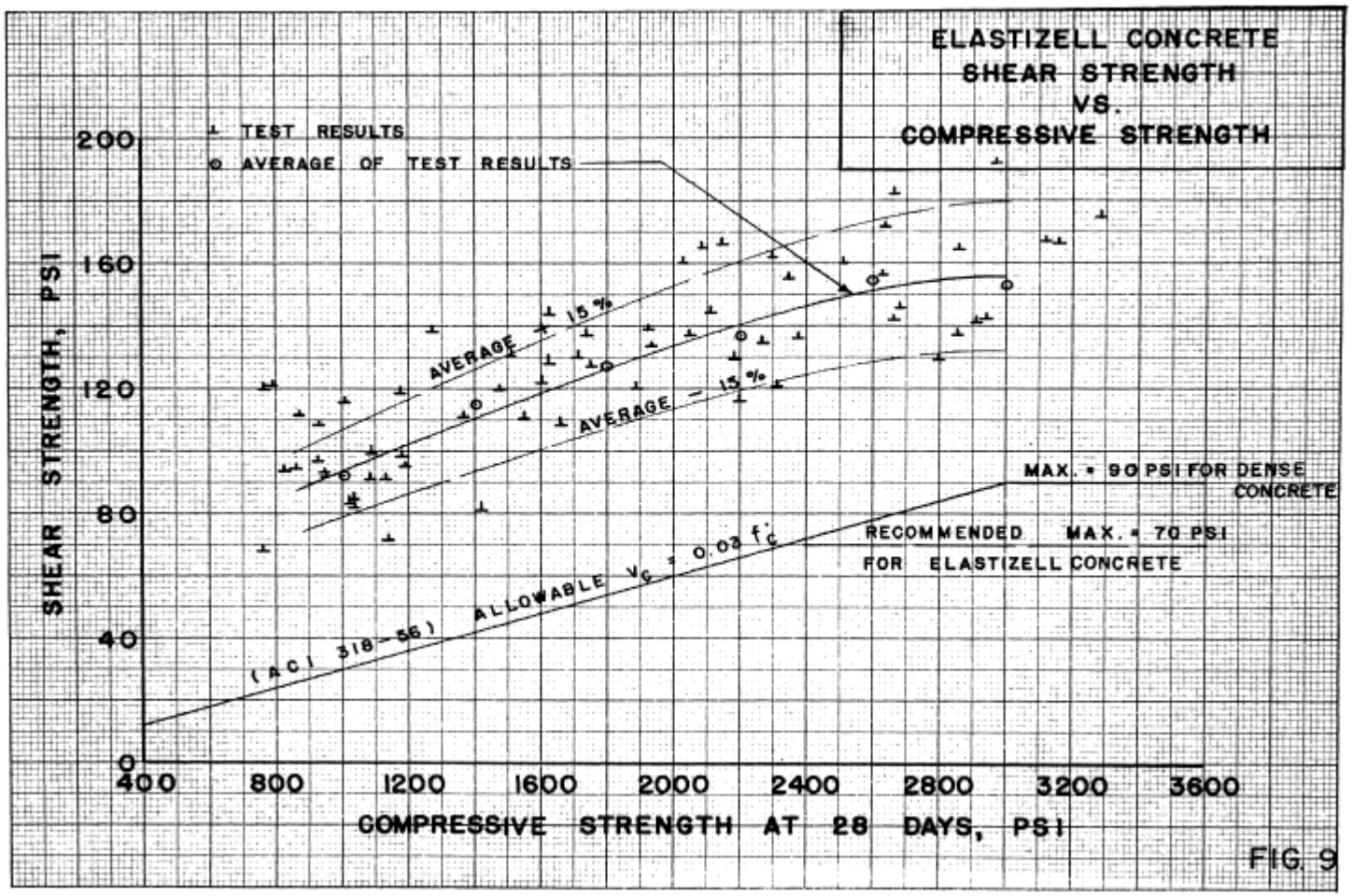

Figure 2-6: Elastizell cellular concrete shear strength vs. compressive strength (Legatski and Mansour 1961).

2.1.1.8 Modulus of Elasticity

The modulus of elasticity is lower for cellular concrete compared to normal concrete. Values range from 145 kip/in.^{2} to 1160 kip/in.^{2} (100 kN/cm^2 to 800 kN/cm^2) for the dry density range of 31.2 pcf to 93.6 pcf (500 kg/m^3 to 1500 kg/m^3). In contrast, the modulus of elasticity for normal concrete is in the range of 3000 kip/in.^{2} to 4000 kip/in.^{2} (2068 kN/cm^2 to 2758 kN/cm^2) for compressive strengths between 2770 psi and 4925 psi (19.1 MPa and 33.0 MPa). Jones and McCarthy (2005) found that the addition of polypropylene fibers could increase the modulus of elasticity by 2 to 4 times. Several equations have been developed to estimate the modulus of elasticity. Equation 2-1 was developed by Tada (1986) for low-density cellular concretes. Equations 2-2 and 2-3 were developed by Jones and McCarthy (2005) for higher strength cellular concretes with sand and fly ash, respectively.

$$E = 5.31 * W - 853 \quad (2\text{-}1)$$

$M = 0.42 f_c^{1.18}$ (sand as fine aggregate), for strengths between 5 and 30 N/mm^2 (2-2)

$M = 0.99 f_c^{0.67}$ (fly ash as fine aggregate), for strengths between 12 and 45 N/mm^2 (2-3)

where:

E = modulus of elasticity in MPa

M = modulus of elasticity in N/mm^2

W = density from 200 to 800 kg/m^3

f_c = compressive strength in N/mm^2

2.1.2 Influence of Fiber Reinforcing on Compressive Strength of Cellular Concrete

Cellular concrete strength can be increased through the addition of polypropylene fibers. After the concrete has cracked, the fiber can impart additional shear strength to the concrete. The

addition of fibers that are 0.47 in. (12 mm) long at a concentration of 0.06-0.19 pcf (1-3 kg/m^3) of cellular concrete can increase the shear strength (Ramamurthy 2009).

Zollo and Hays (1998) also performed compressive strength tests to investigate the effect of fibers on cellular concrete strength. A fiber concentration of 1.0% by total volume in the slurry was used (0.5% in the set concrete). The authors concluded that the fibers were the only source of post-cracking residual strength in the concrete cylinders. The residual strength for the fiber-reinforced cellular concrete was 55% of the peak strength and the cylinder's peak strength ranged between 250 psi and 300 psi (1.7 MPa to 2.1 MPa).

2.1.3 Advantages

Perhaps the greatest benefit to using cellular concrete is its low unit weight. Since cellular concrete is several times lighter than soil, it can be used to reduce the load on a structure or the underlying soil. Applications of cellular concrete include roadway bases, fills above culverts, lightweight levee structures, pipeline fills, and retaining wall fills. Compared to expanded polystyrene (EPS) geofoam blocks, which also have a low unit weight, cellular concrete is more durable, has a higher bearing capacity, and can be more easily placed (EPS blocks must be carefully cut to specified dimensions) (Cellular Concrete Solutions 2009).

Cellular Concrete has several other benefits in addition to its low unit weight. It is recyclable and can be reused. The materials needed to produce cellular concrete can generally be found locally, and the actual mixture can be produced on-site. With cellular concrete the number of truckloads that must be delivered to a project are reduced; a single truckload of slurry for a

low-density mixture will expand to about 3.8 times its original volume after foam has been mixed into the cement slurry. Use of local materials and fewer truckloads give cellular concrete a lower carbon footprint compared to other backfill materials (Cellular Concrete Solutions 2009).

Cellular concrete is easier to place compared to traditional backfill materials. It does not require compaction like other materials. Its flowability characteristics allow it to self-level and fill small areas. Its flowability also makes it an easy material to pump long distances. Low-weight cellular concrete structures do not require deep foundations like their heavy concrete counterparts. This, in turn, reduces the amount of excavation required. All of these factors combine to increase the speed and ease of installation.

2.1.4 Disadvantages

The use of cellular concrete comes with certain drawbacks. Cellular concrete is significantly weaker than normal concrete. Although this is advantageous in situations where future excavation is required, it is a drawback when significant strength is needed. Cellular concrete is also not widely used. Finding a contractor who is familiar with the material and a supplier who is located within a reasonable distance may prove difficult.

Cellular concrete is also more expensive (per cubic yard) than typical backfill materials like sand or gravel. The extra time and effort associated with placing other backfill materials should be considered when comparing costs.

2.2 Passive Force-Displacement Tests for Non-Skewed Abutment Walls

A number of researchers have conducted large-scale field tests to investigate passive force development at bridge abutments. Duncan and Mokwa (2001) performed passive force load tests on native stiff clay and a compacted, well-graded granular backfill. They found that the log-spiral method, with corrections made for 3-D effects, best modeled the measured values. Rollins and Sparks (2002) and Rollins and Cole (2006) performed tests on laterally loaded pile caps and also found that the log-spiral method most correctly predicted the failure geometry. Peak passive pressure was reached at 3-6% of the backwall height in these tests. Lemnitzer et al. (2009) laterally loaded a full-scale model of a bridge abutment and found agreement with the log-spiral method. Peak passive pressure was reached at 3% of the backwall height.

The results of all tests indicate that the log-spiral method best represented the passive force-deflection relationship. Peak passive pressure was reached at a deflection between 3% and 6% of the backwall height. These tests only analyzed conventional granular backfill materials.

Fredrickson (2015) used data compiled by Meyer (2012) to show the relationship between passive resistance and deflection for various backfill materials. A normalized plot for tests with gravel backfills is shown in Figure 2-7, a normalized plot for loose sand is shown in Figure 2-8, and a normalized plot for dense sand is shown in Figure 2-9. All plots show that the maximum passive force is reached between 2% and 5.5% of the wall height. Densely compacted materials have more of a logarithmic shape and are able to reach 80% of the peak passive pressure with about 1% normalized deflection. Loosely compacted materials have a nearly linear shape that reaches the peak passive pressure at much higher deflections.

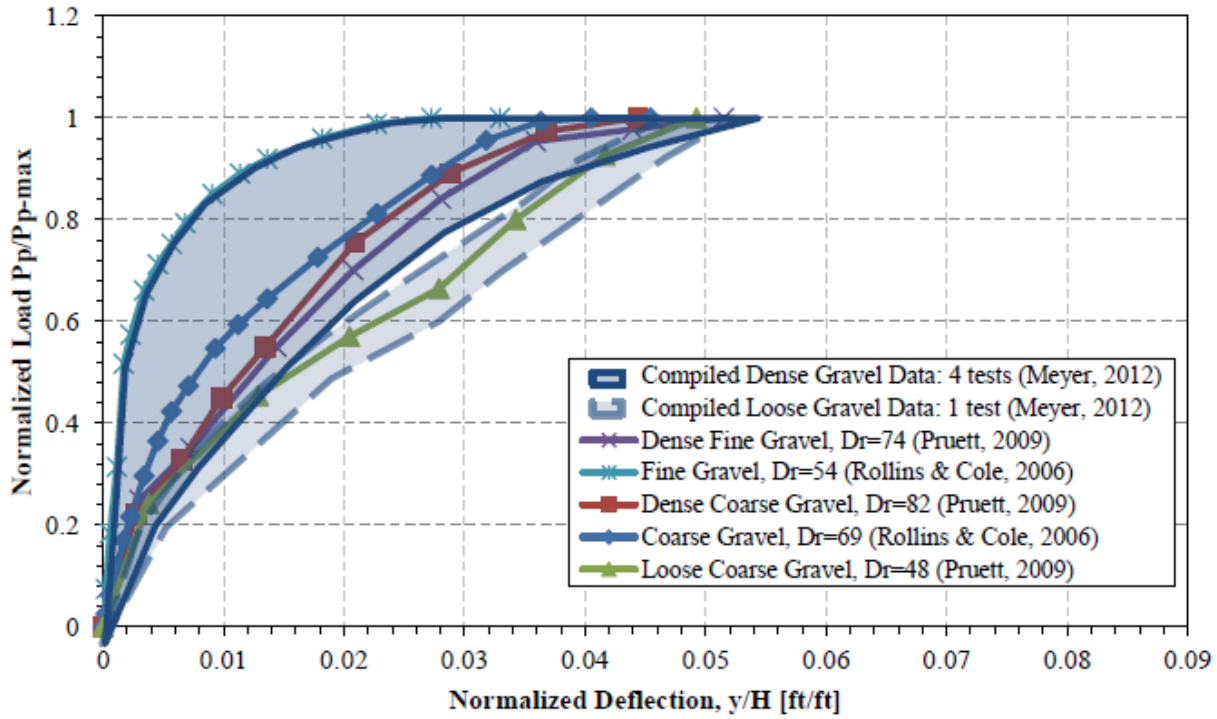

Figure 2-7: Passive force-deflection data from various studies for gravel (Meyer 2012, Fredrickson 2015).

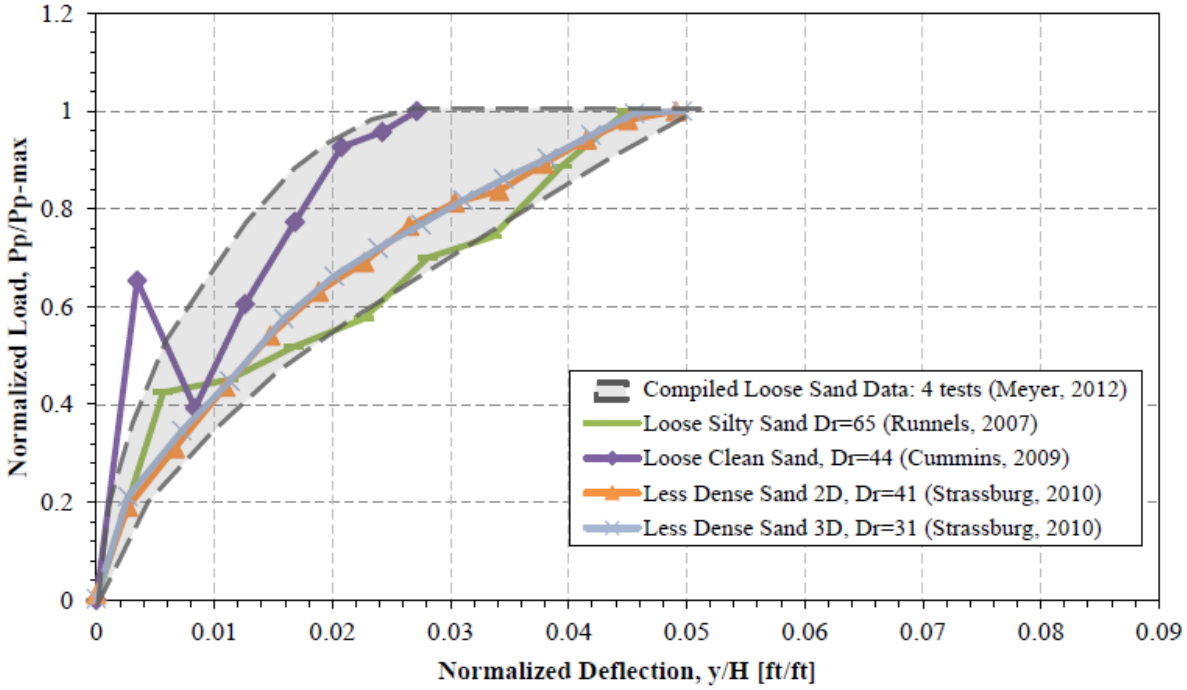

Figure 2-8: Passive force-deflection data from various studies for loose sand (Meyer 2012, Fredrickson 2015).

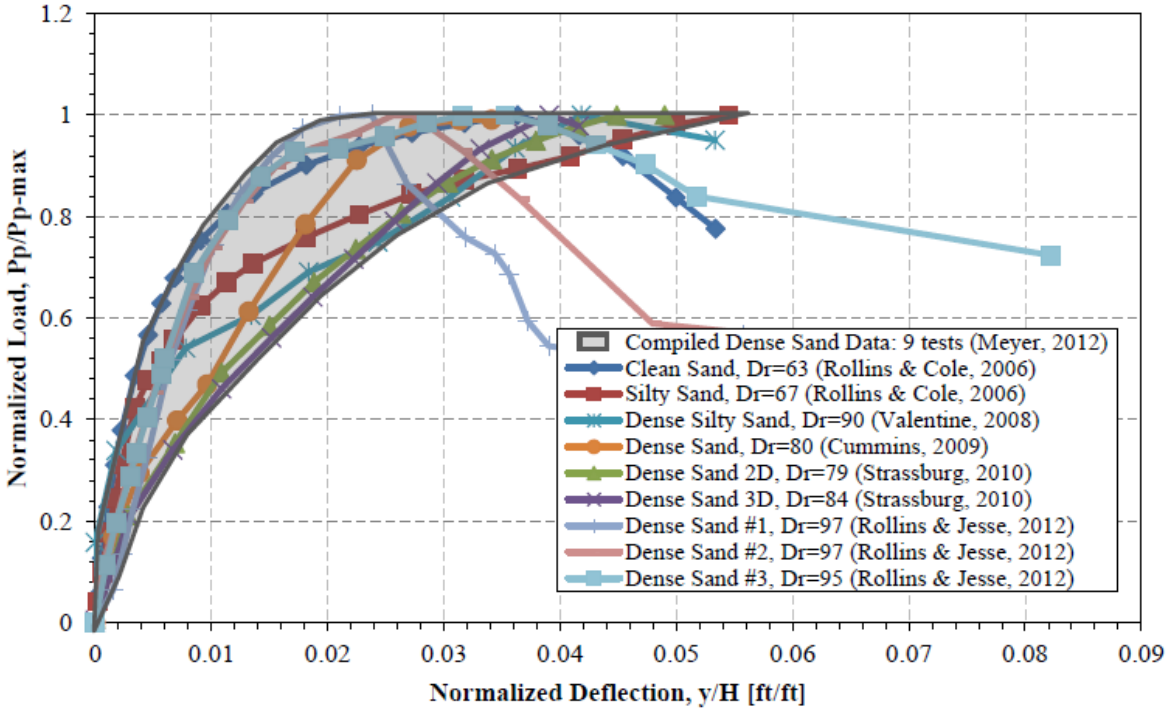

Figure 2-9: Passive force-deflection data from various studies for dense sand (Meyer 2012, Fredrickson 2015).

2.3 Skewed Bridge Earthquake Performance

A large portion of bridges in the U.S. are skewed; Nichols (2012) observed that 41% of the 605,000 bridges in the U.S. bridge database are skewed. The FHWA defines a bridge skew as "the angle between the centerline of a pier and a line normal to the roadway centerline" (FHWA 1995). Figure 2-10 provides a visual reference to the FHWA definition. The Pacific Earthquake Engineering Research Center (Kaviani et al. 2014) found that approximately 60% of the bridges in California had some degree of skew as summarized by the pie chart in Figure 2-11.

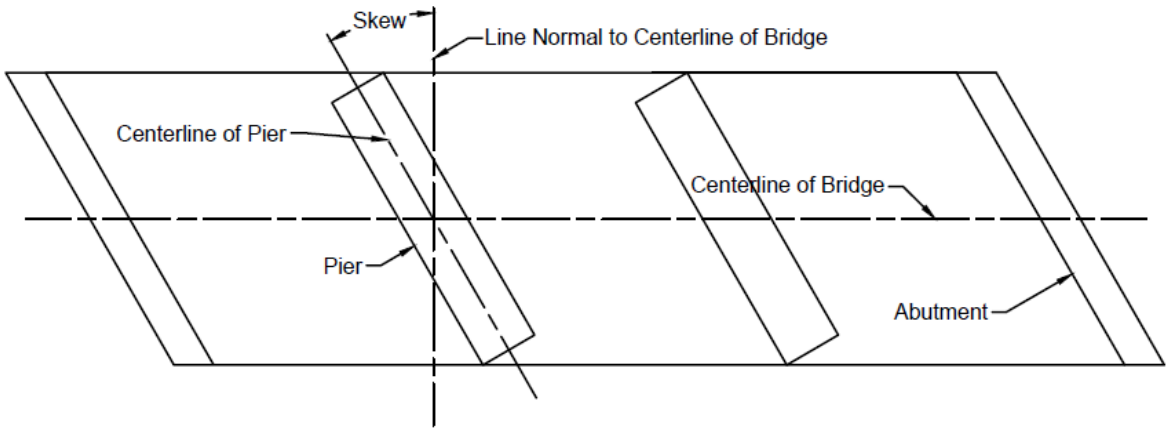

Figure 2-10: FHWA definition of bridge skew angle.

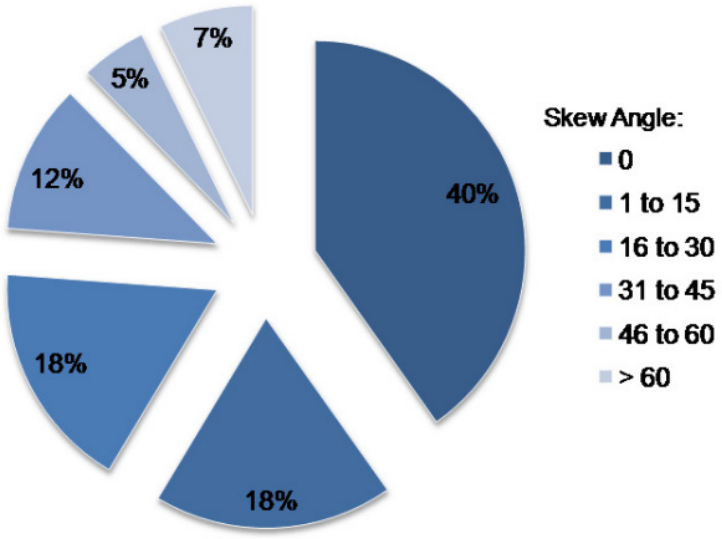

Figure 2-11: Distribution of bridge abutment skew angles in California (Kaviani et al. 2014).

Kaviani et al. (2014) found that bridges with skewed abutments were more likely to fail in the event of an earthquake. The primary cause of failure was excessive rotation, although abutment unseating and column drift ratio demands were also higher (compared to straight bridges). This rotation was evident on a bridge affected by the 2010 Chile earthquake. The shear keys on this bridge failed, allowing the bridge deck to displace as shown in Figure 2-12. Toro et

al. (2013) observed that all of the bridges that collapsed during the 2010 Chile earthquake were skewed bridges (greater than 5° skew).

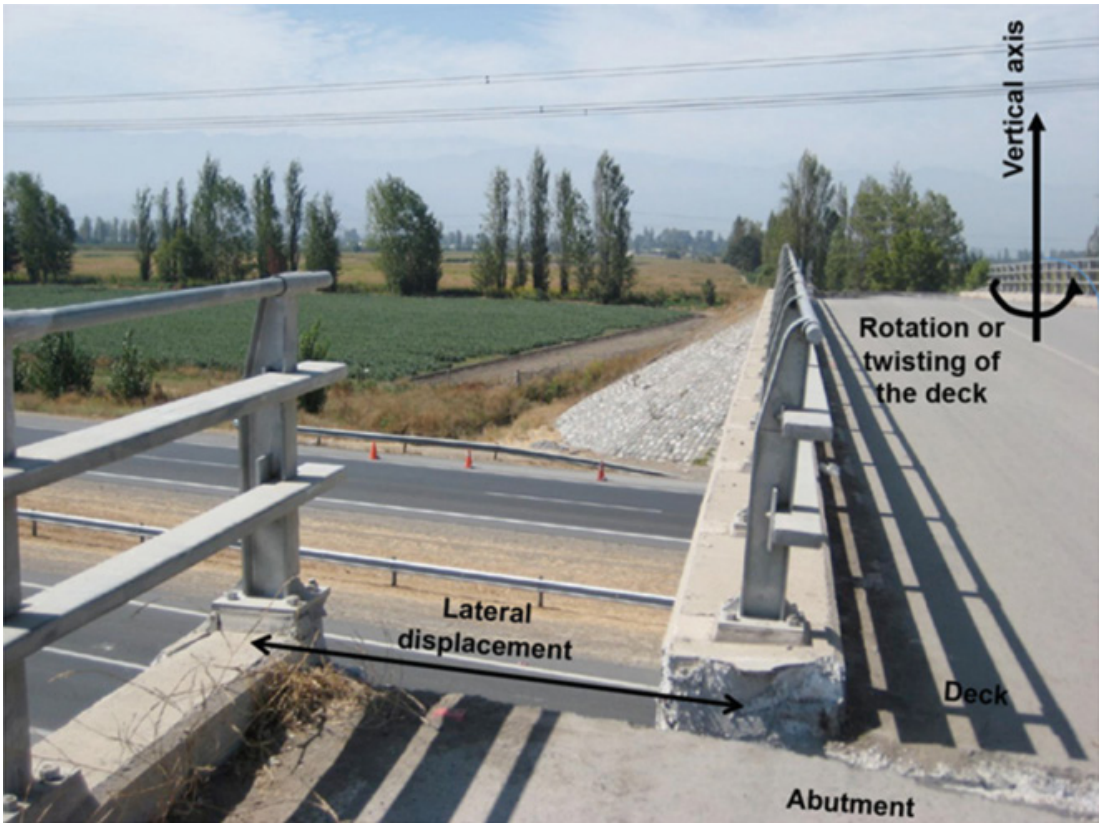

Figure 2-12: Bridge damage from 2010 Chile earthquake (Kaviani et al. 2014).

2.4 Passive Force-Displacement Tests for Skewed Abutment Walls

Because of the poor performance of skewed bridges in the 2010 M_w 8.8 Maule Chile earthquake, several studies have recently been conducted on skewed bridge abutment backfill materials. While skewed geometries are known to produce structural design problems, the geotechnical issues at the abutments had not been previously investigated. Rollins and Jessee (2013) displaced a 4.13-ft- (1.26-m-) wide by 2-ft- (0.61-m-) high abutment wall into a dense sand backfill under plane strain conditions. As shown in Figure 2-13, they found that passive

force decreased significantly as skew angle increased and recommended Equations 2-4 and 2-5 to compute the reduction in passive force based on skew angle.

$$P_{P(skew)} = P_P R_{skew} \tag{2-4}$$

$$R_{skew} = 8.0 \times 10^{-5}\theta^2 - 0.018\theta + 1.0 \tag{2-5}$$

Where $P_{P(skew)}$ is the resulting passive force for the skewed abutment, R_{skew} is the computed skew reduction factor, P_p is the passive force for a non-skewed abutment with similar width and geometry perpendicular to the direction of loading, and θ is the skew angle.

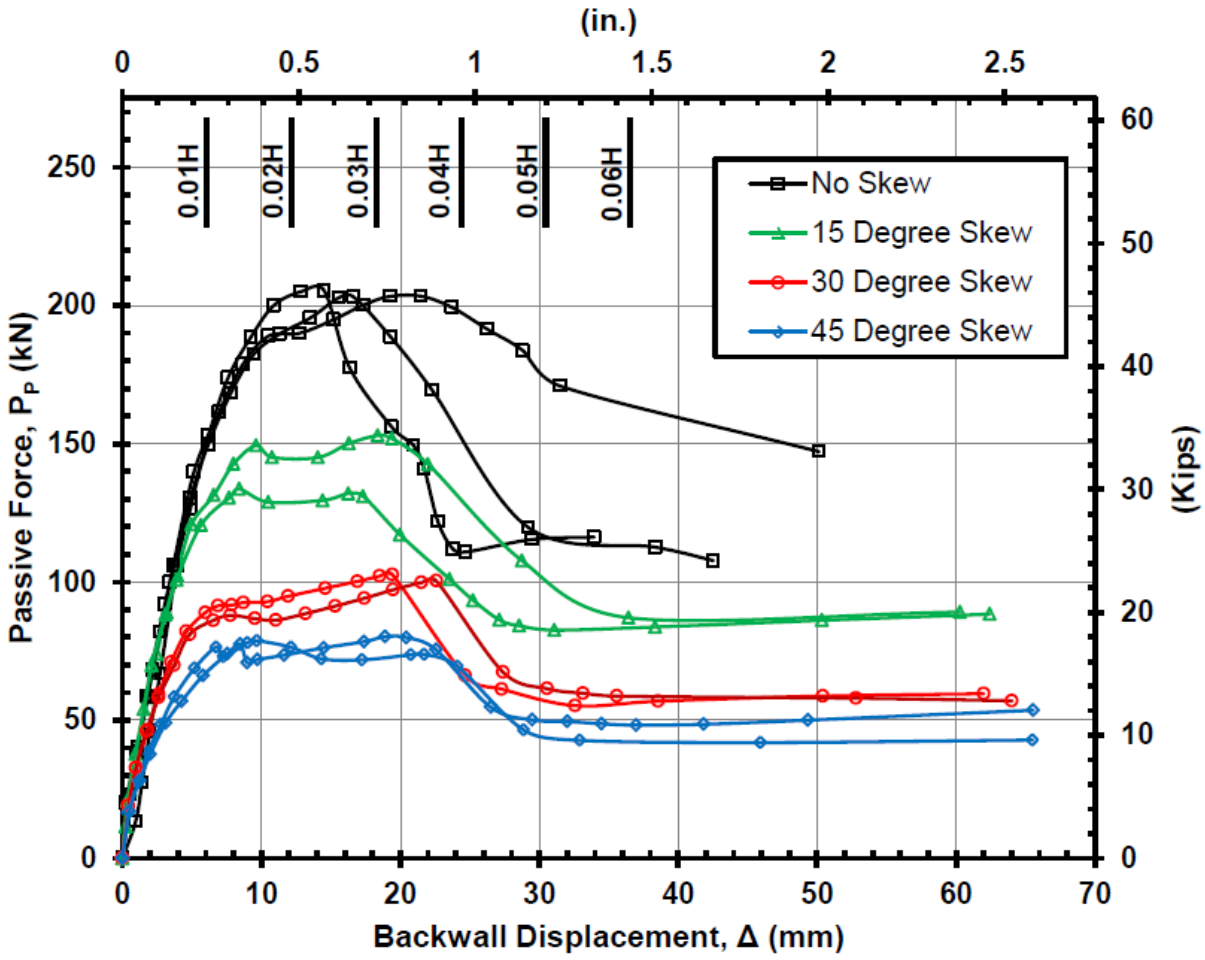

Figure 2-13: Measured passive force-deflection curves for various skew angles (Jessee 2012).

Marsh (2013) conducted field testing on a much larger backwall (5.5-ft-high by 11-ft-wide abutment (1.68-m- by 3.35-m-)) displaced into a compacted sand backfill and found good agreement with the results from Rollins and Jessee (2013) and their reduction factor as shown in Figure 2-14.

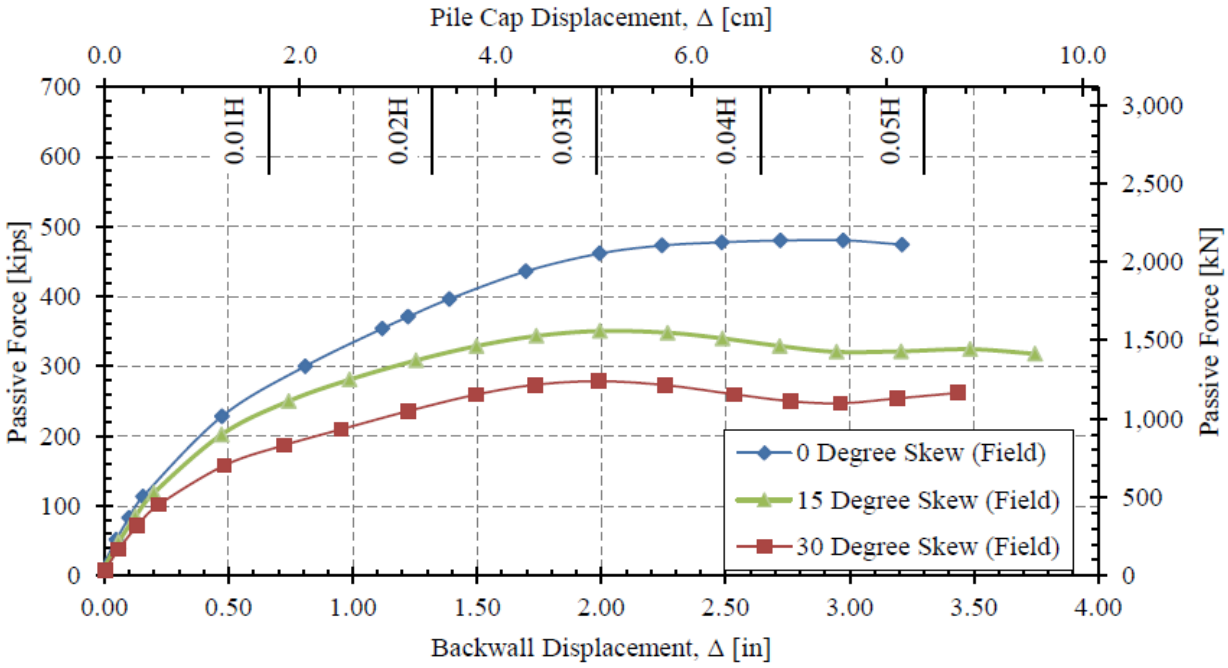

Figure 2-14: Passive force-deflection curves for 0°, 15°, and 30° skew angles (Marsh 2013).

Franke (2013) performed testing at the same site and time as Marsh. The difference in test layout was that mechanically stabilized earth (MSE) wingwalls held the sand backfill in place. Wingwalls were placed parallel to the pile cap sides as shown in Figure 2-15. Franke's results confirmed the equation proposed by Rollins and Jessee (2013) showing a 36% reduction in passive resistance for a 15° angle and a 43% reduction in passive resistance for a 30° angle. The passive-force deflection curves for Franke's tests are shown in Figure 2-16.

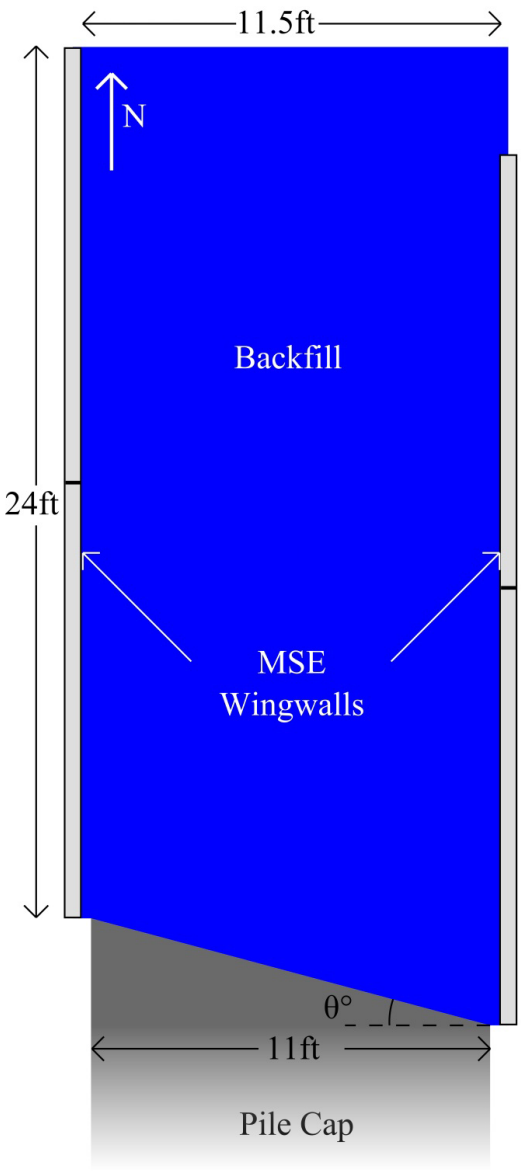

Figure 2-15: MSE wingwall layout for large-scale testing (Franke 2013).

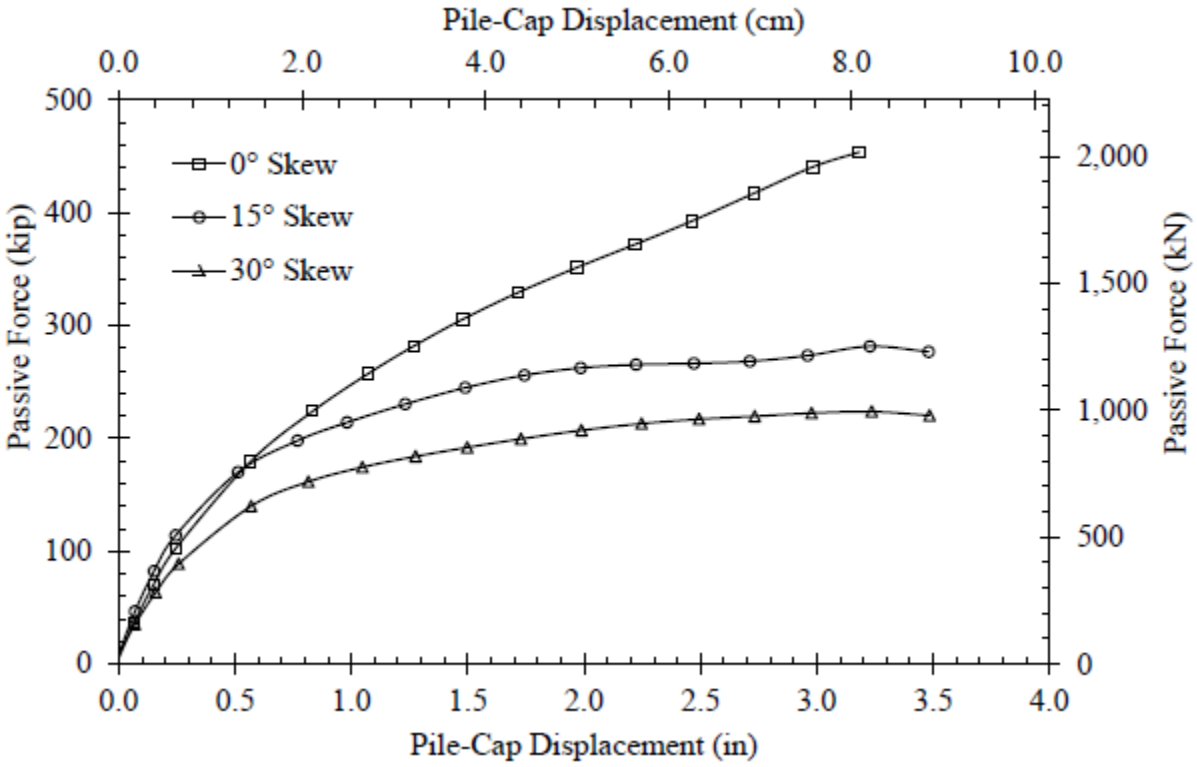

Figure 2-16: Passive force-deflection curves for 0°, 15°, and 30° skew angles (Franke 2013).

Fredrickson (2015) conducted tests on the same 5.5-ft by 11-ft (1.68-m by 3.35-m) abutment used by Marsh. This abutment was displaced into a gravel and a geosynthetic reinforced soil (GRS) backfill. The GRS backfill consisted of the same gravel but incorporated horizontal geosynthetic sheets placed at 1-ft intervals within the backfill. Fredrickson tested each backfill material at 0° and 30° skew angles and found that both gravel and GRS backfills outperformed sand backfills and that the reduction in passive pressure due to a skew angle was somewhat less than that proposed by Rollins and Jessee (2013). This result might be explained by the higher strength of the gravel backfill.

2.4.1 Passive Force Tests on CLSM Backfill

Contractors are increasingly exploring alternative backfill materials to accelerate the construction process behind bridge abutments. One alternative is CLSM, which is also known as flowable fill. Wagstaff (2016) conducted a series of laboratory tests on CLSM consisting of cement, fine aggregate, and water with a unit weight of 127 pcf (2034 kg/m^3). Tests were performed on abutment walls with 0° and 30° skew angles. Walls with plastic sheeting extended from the edge of the abutment backwall to a concrete reaction block at the far end of the backfill. These walls were oriented parallel to the direction of loading to create a 2-D failure geometry, or a plane-strain condition. Plastic sheeting was also placed on the floor to minimize friction and allow the concrete reaction block to be the mechanism driving failure. Figure 2-17 shows the test setup for 30° skew loading.

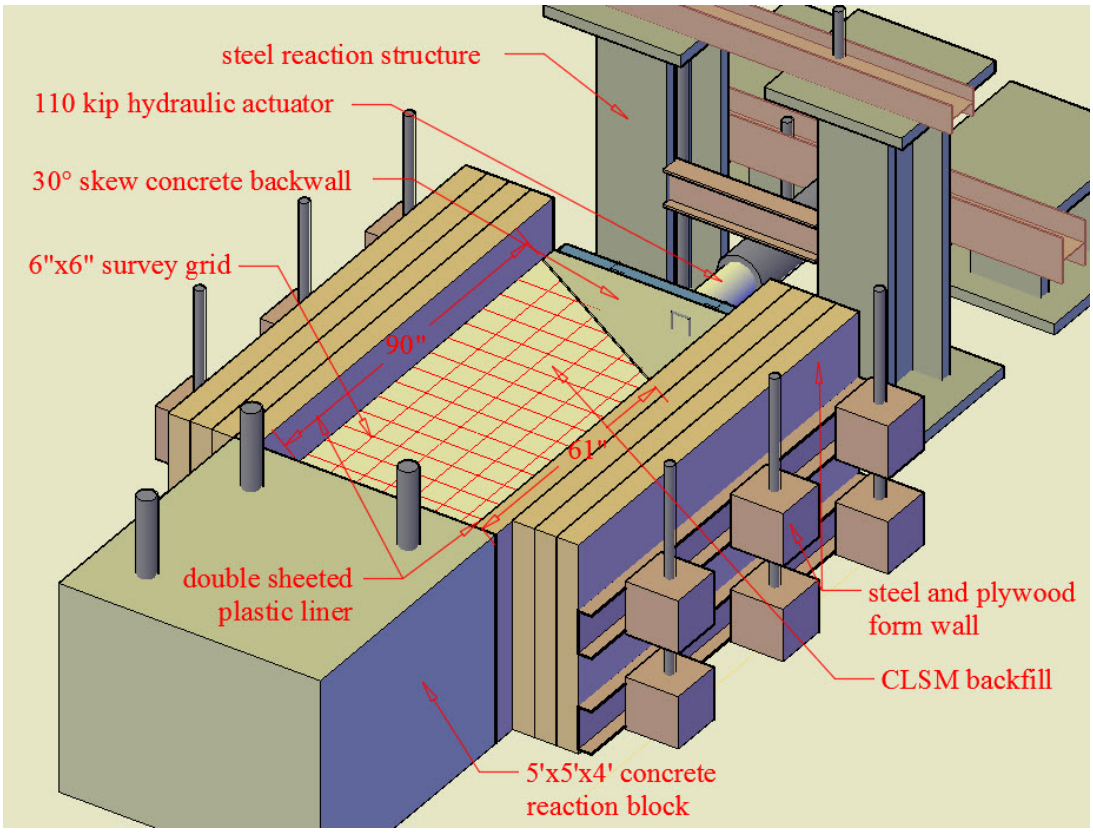

Figure 2-17: Wagstaff 30° skew test setup for CLSM backfill.

Wagstaff found that the use of CLSM allowed the skewed abutment to behave almost as if the abutment was non-skewed. For both the 0° and 30° skew cases, the measured passive force was within about 10 to 15% of the predicted passive force, assuming the shear strength was equal to 50% of the UCS with a friction angle of 0°. Wagstaff observed that the shear resistance along the abutment surface was significantly greater than the shear force, which allowed the CLSM material to behave as if it was part of the abutment itself. In contrast to similar tests with granular backfill where the failure plane daylighted along a skew angle matching the abutment, the failure plane did not change its orientation in the CLSM tests. The failure plane was also observed to exit the surface of the backfill at a distance equal to about three times the abutment height.

The CLSM material behaved differently from conventional backfill material in that the peak passive resistance was reached at 0.75-2% of the abutment wall height, while normal granular backfill reaches the peak passive resistance at a displacement of 3-5% of the wall height (Marsh). In addition, the residual strength also dropped off significantly after the peak passive strength was reached, while the typical drop off for granular backfill is reasonably low (less than 10 to 20%). Wagstaff concluded that the Rankine Method may provide the best estimate of passive resistance for CLSM backfills.

The CLSM material shear behavior was best modeled using the Filz et al. (2015) approach, which uses a friction angle of 0°. For this project, a soil-cement mixture was placed around and primarily above a dam penstock to protect the penstock from additional loads induced by an overlying stability berm. It was concluded that for a 0° friction angle the strength

envelope should follow a line tangent to the compressive and tensile strength envelopes when in the corresponding range of normal stress; Figure 2-18 shows this strength envelope.

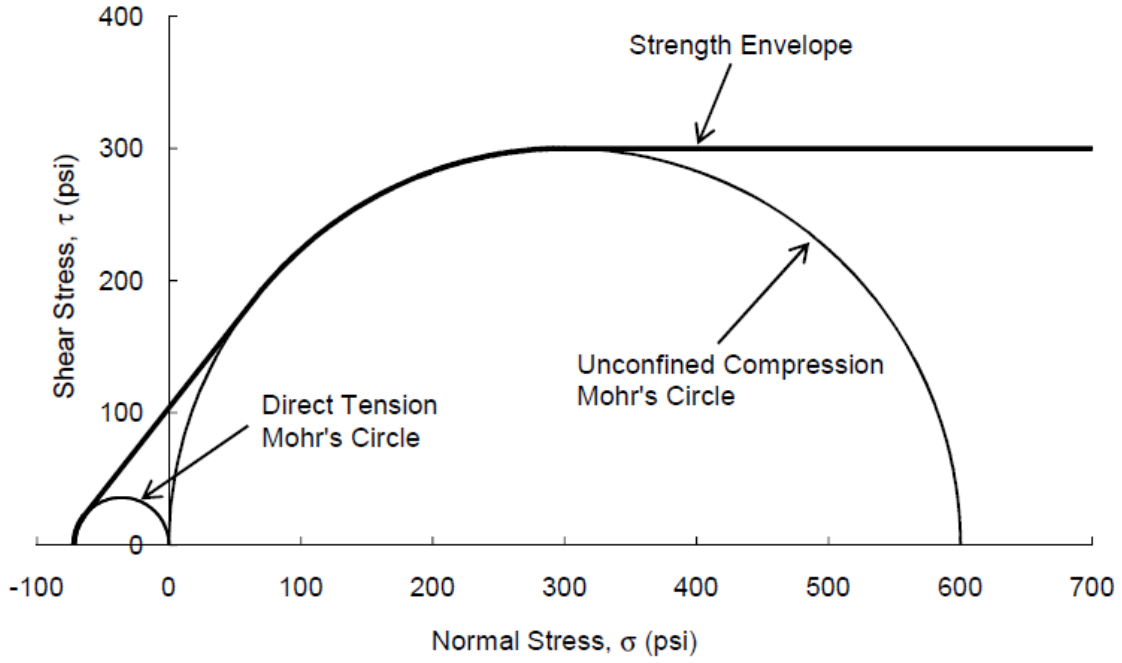

Figure 2-18: Proposed example strength envelope for deep-mixed soil-cement including tension (Filz et al. 2015).

Wagstaff normalized his results for the 30° and 0° skew tests by dividing by the corresponding UCS. He then plotted the results against the shear strength envelope proposed by Filz et al. He found that shear strength envelope compared well with his results as shown in Figure 2-19.

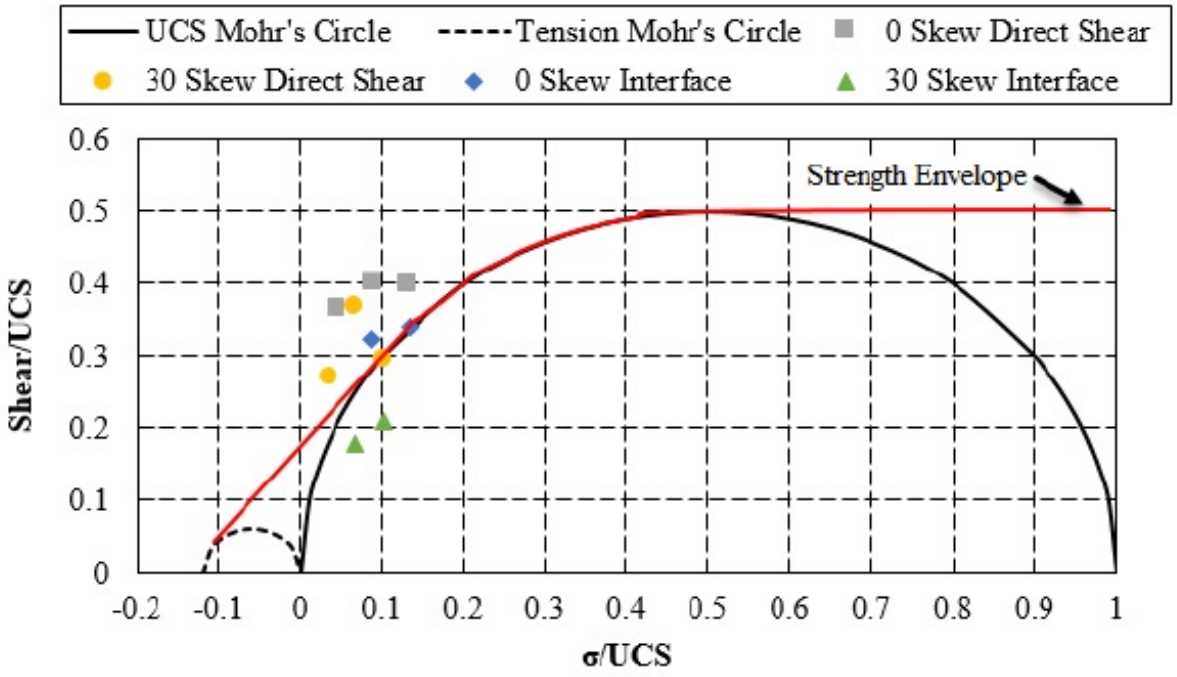

Figure 2-19: Direct and interface shear strengths compared to soil-cement shear strength envelope proposed by Filz et al. (Wagstaff 2016).

2.5 Literature Review Summary

A large amount of research has been conducted to determine the passive resistance of bridge abutment backfill materials. These backfill materials have been limited to sand, gravel, reinforced variants of sand/gravel, and conventional CLSM. For conventional granular backfills, these studies found that (1) passive force is best estimated using the log-spiral method, (2) displacement equal to 3% to 5% of the abutment height is necessary to fully mobilize resistance, (3) the passive force-deflection curve is best approximated by a log-spiral curve, although simpler bi-linear curves are popular for design, and (4) passive force decreases significantly as skew angle increases, providing less restraint for transverse and longitudinal translation as well as deck rotation.

For conventional CLSM, it has been found that (1) passive force is best estimated using a 0° friction angle, (2) a displacement of 0.75-2% of the wall height is necessary to mobilize the peak passive resistance, (3) the passive force-deflection curve was hyperbolic in shape up to a peak resistance, and (4) passive force is only slightly effected by the skew angle.

Low-strength cellular concrete remains a seldom-used material within the U.S but has inherent benefits if used as a backfill material; it is self-consolidating, relatively lightweight, and easy to place. Cellular concrete material is, however, more expensive compared to traditional backfill materials. No research has been performed to evaluate the passive resistance of cellular concrete, the effects of skew angle on passive resistance, the displacement necessary to mobilize peak passive resistance, or how failure theory should be defined for passive resistance. This study seeks to better understand how cellular concrete behaves and determine to what extent it can increase the passive resistance of skewed bridge abutments.

3 SITE LAYOUT

3.1 Overview

All tests were performed at the Salt Lake International Airport (40°47'55.80"N, 111°59'8.89"W). The site had full sun exposure, had almost no plant growth, and consisted of low-plasticity silts and clays. Most of the area immediately around the excavation consisted of a poorly graded sandy gravel due to previous filling. Temperatures ranged from 51˚ to 104˚F (11˚ to 40˚C) during testing. Figure 3-1 shows an aerial view of the site.

Figure 3-1: Salt Lake Airport test site aerial view.

3.2 Geotechnical Characterization

Several geotechnical tests have been previously performed at or near the aforementioned site. These tests include cone penetrometer, dilatometer, standard penetration, vane shear, and shear wave velocity tests. The test site soil profile consists of 5 ft (1.52 m) of sandy gravel underlain by layers of silty clay and sand down to a depth of 100 ft (30.5 m). A portion of the upper 8 ft (2.44 m) was excavated and replaced with clean sand in 2004 in the test site vicinity (Rollins et al 2010). Excavation at the site revealed that the water table was located approximately 5 ft below the surface, which is in agreement with the Rollins et al. 2010 CPT profile.

3.3 Test Layout

All testing was performed using an existing pile cap and reaction frame. This setup has been used for previous tests (Franke 2013, Fredrickson 2015, Marsh 2013). The pile cap was 5.5-ft tall, 11-ft wide, and 15-ft long (1.68-m by 3.35-m by 4.57-m). The cap was held in place by two groups of three piles driven to a depth of approximately 43 ft (13.1 m) (Marsh 2013). The reaction system consisted of two 4-ft- (1.22-m-) diameter concrete shafts along with an AZ 18 sheet pile wall placed against the shafts on the north side. Deep I-beams were placed along the north side of the sheet pile wall and along the south side of the concrete shafts to tie the system together. Plan and profile views of the entire test layout are provided in Figure 3-2.

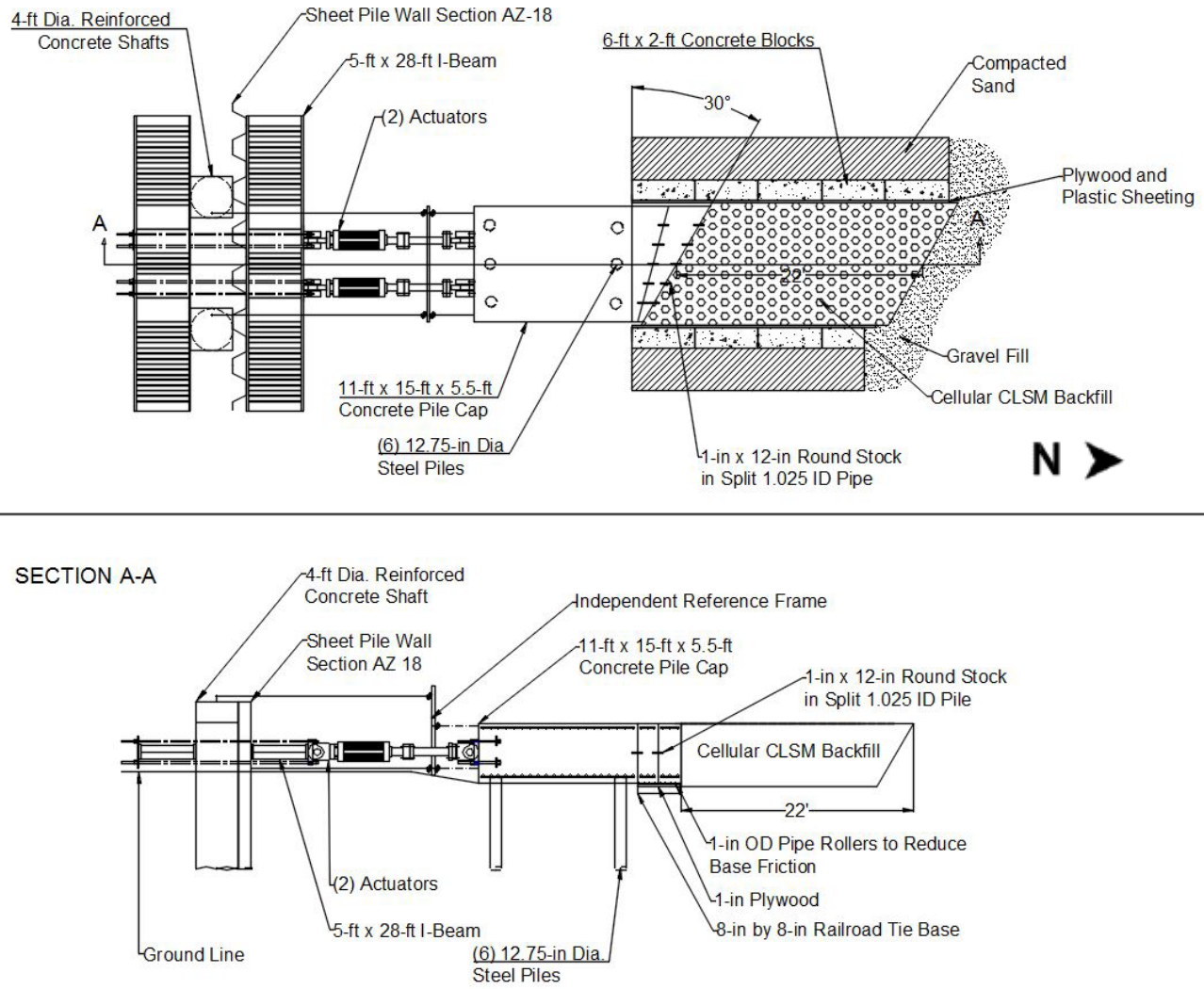

Figure 3-2: Plan and profile view of the site layout at Salt Lake Airport.

Loading was accomplished using two hydraulic actuators placed between the reaction frame and pile cap. Extension pieces were placed on the north side of each actuator to allow the actuator to span the full distance between the reaction frame and pile cap. Each actuator was held in place by four Dyckerhoff and Wildmann AG (DYWIDAG) bars on the north and south ends. The two actuators could apply up to 1,200 kip (5,338 kN) of lateral load to the pile cap. Figure 3-3 depicts the placement of a hydraulic actuator.

Figure 3-3: Hydraulic actuator placement at Salt Lake Airport test site.

Tests were performed for 0° and 30° skew angles. Skew angles were created by adding reinforced concrete block wedges to the simulated abutment. The skew wedges were held in place by dowel rods placed through holes on the center of the skew face and metal plates placed on the top and sides of the pile cap and skew angles. The skew wedges were supported by a railroad tie base overlain by 0.75-in. (1.9-cm) plywood. One-inch- (2.5-cm-) diameter rollers

were placed on the plywood to minimize friction as shown in Figure 3-4. The backfill area was excavated to a depth of 6 in. (15.2 cm) below the simulated abutment base out to a distance of 22 ft (6.71 m) from the abutment and then sloped steeply upward to the ground surface (the slope was later altered as shown in Figure 3-9). Interlocking pre-cast concrete blocks (6 ft x 2 ft x 2 ft (1.83 m x 0.61 m x 0.61 m)) with plywood sheeting were placed along both sides of the cellular concrete backfill to hold it in place and allow the backfill to fail in a 2D fashion as shown in Figure 3-5. Before the concrete placement, two layers of plastic sheeting with grease between them were placed against the plywood sheet facing on each side to reduce friction and better simulate a 2-D geometry typical of a wider abutment wall.

Figure 3-4: Skew wedge base at Salt Lake Airport test site.

Figure 3-5: Backfill area at Salt Lake Airport test site.

Since the water table was located approximately 5 ft (1.52 m) below the ground surface, it had to be lowered below the base of the 6-ft excavation to ensure it did not interfere with the concrete curing process. Dewatering was accomplished with the use of pumps placed in sump boxes on the east and west sides of the pile cap. Perforated conduit was placed from the end of each concrete block wall to a sump box to extend the effective area of each pump. The conduit was sloped at 1.5% to allow the water to flow into the sump boxes. Once the concrete was

placed, a small generator ran continuously to supply power to the two pumps. The two pumps ran frequently to keep the site dewatered.

3.4 Test Layout Alteration

When testing first began on the backfill for the 30˚ skew test, it was found that the gravel fill behind the cellular concrete backfill did not have enough strength to significantly compress the cellular concrete backfill and cause failure. Instead, the entire cellular concrete backfill moved as a unit after just a small pile cap displacement. The slope of the gravel fill also made it so that the cellular concrete backfill could slide upward on the far north side. Therefore, testing was stopped and the far north side of the backfill excavated so an improved reaction block wall could be constructed. The excavation was mainly accomplished with a backhoe with the finer detail work being done with a chainsaw and pickaxe; Figure 3-6 shows the backfill being cut with a chainsaw. A pre-cast concrete block reaction wall was built in the resulting excavation with compacted sand being placed in 6-in. (15-cm) lifts around the reaction wall as shown in Figure 3-7. Flowable fill (CLSM) was then placed to bridge the gap between the reaction block wall and the backfill, as shown in Figure 3-8, as well as to fill the gap between the skew wedge and backfill. The flowable fill was allowed to cure until it reached a strength similar to that of the cellular concrete, at which point testing was resumed. Plan and profile views showing the new test layout are presented in Figure 3-9. This new layout was used for all subsequent testing described in this thesis.

Figure 3-6: Excavation of backfill to alter test layout.

Figure 3-7: Construction of reaction block wall to alter test layout.

Figure 3-8: Flowable fill (CLSM) placed between backfill and reaction block wall to alter test site layout.

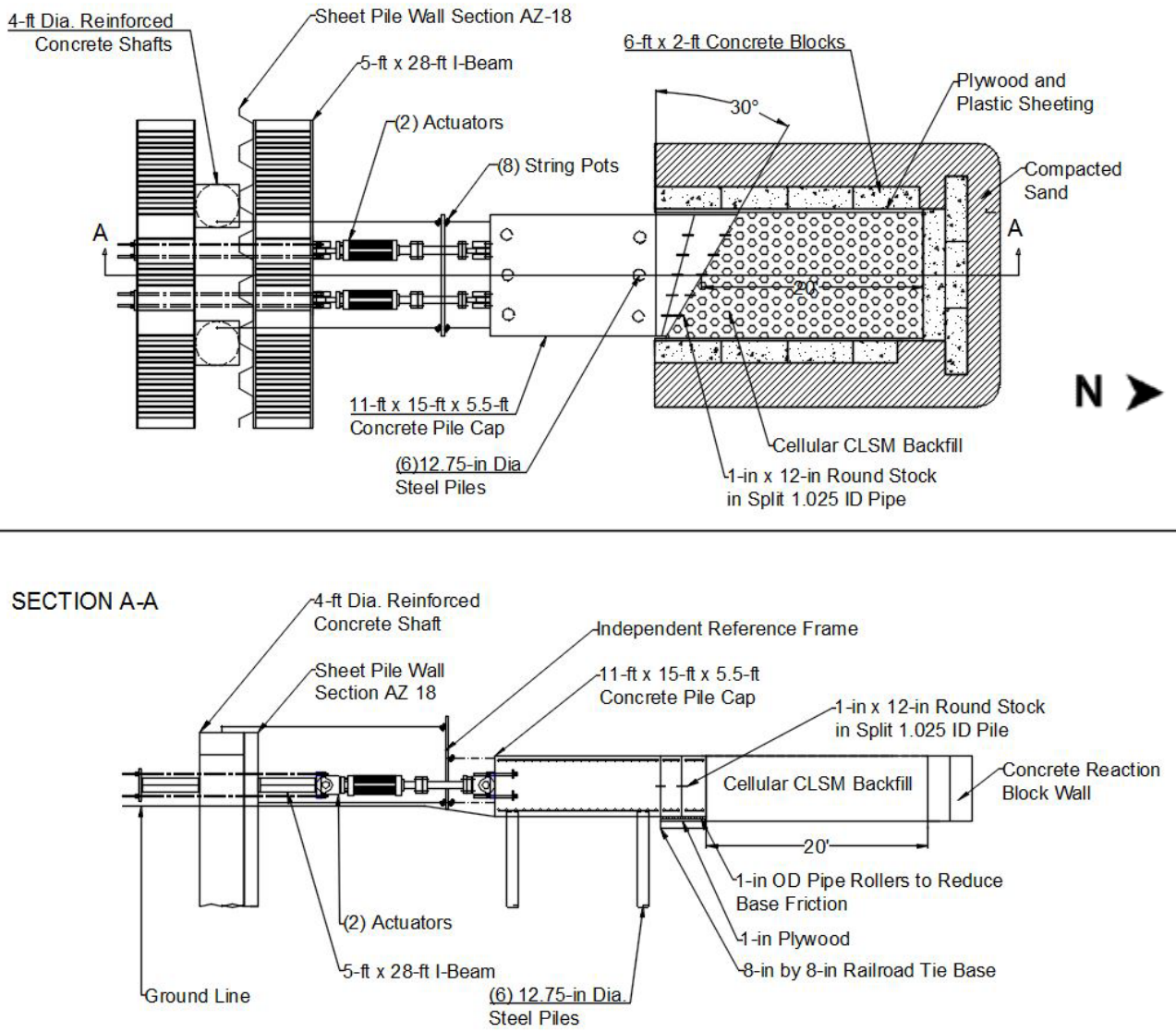

Figure 3-9: Site layout after alteration

3.5 Instrumentation

3.5.1 Longitudinal Load Instrumentation

The hydraulic actuators contained pressure transducers, which measured the applied load. The combined load applied by the two actuators to the south side of the pile cap was recorded continuously during the loading process. The difference between the load applied with no backfill and the load applied with backfill was used to calculate the passive resistance of the cellular concrete backfill.

3.5.2 Longitudinal Displacement Instrumentation

An independent reference frame placed on the south side of the pile cap held eight string potentiometers. Four potentiometers were placed behind each of the four pile cap corners with strings extending to each corner. The other four potentiometers extended to two points on the 28-ft x 5-ft- (8.53-m x 1.52-m-) I-beam and to the top of the two 4-ft- (1.22-m-) diameter concrete shafts. As load was applied to the pile cap, the potentiometers could measure the movement of the I-beam/concrete shafts holding the actuator in place and the longitudinal movement of the pile cap. Potentiometer data allowed adjustments to be made to prevent rotation of the pile cap.

3.5.3 Backfill Compressive Strain Instrumentation

String potentiometers (linear position sensors) were installed near the center of the north side of the pile cap. The strings extended to stakes placed in the backfill at 2-ft (0.61-m) intervals at points near the backfill centerline. A single string potentiometer was placed on the most northern skew wedge to record any compression that might occur between the wedge and pile cap. Figure 3-10 shows the location of these stakes and the corresponding potentiometers.

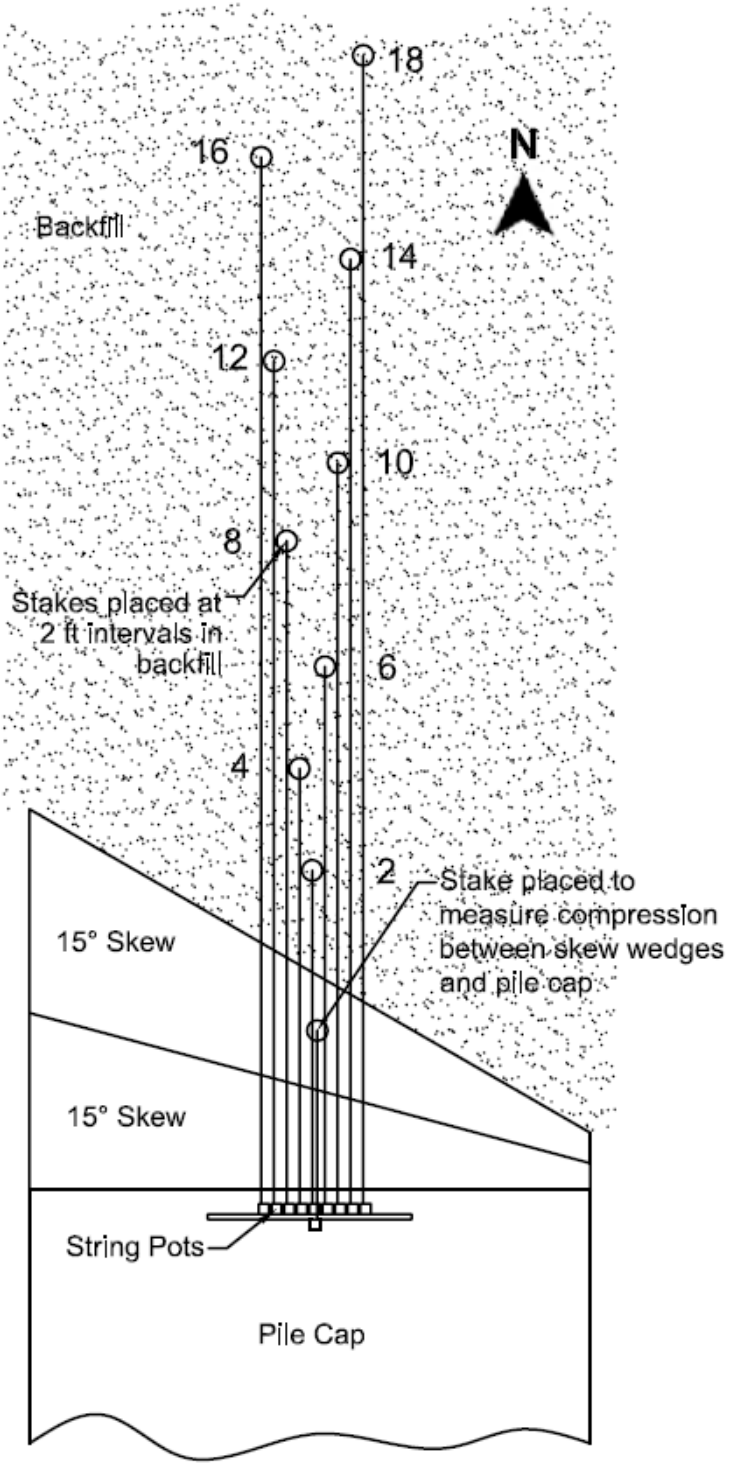

Figure 3-10: String pot layout for compressive strain in backfill.

3.5.4 Backfill Surface Movement

A 1-ft by 2-ft and 2-ft by 2-ft (0.30-m by 0.61-m and 0.61-m by 0.61-m) grid was painted on the surface of the cellular concrete backfill. A survey level was set up close to the site. An elevation rod was used to measure painted intersection points before and after loading. The difference was used as the backfill surface heave measurement. A total station was also used to survey the grid intersection points and track the 3D movement of each point.

A Digital Image Correlation (DIC) camera was set up to monitor the movement of the backfill within a 10-ft (3.05-m) distance from the pile cap. A black and white pattern was painted onto this portion of the backfill to help the camera acquire and track points on the backfill as shown in Figure 3-11. This camera took an image from two different perspectives after each pile cap movement. Instra 4D software then analyzed these images to determine the movement of the backfill. The camera setup during calibration is shown in Figure 3-12.

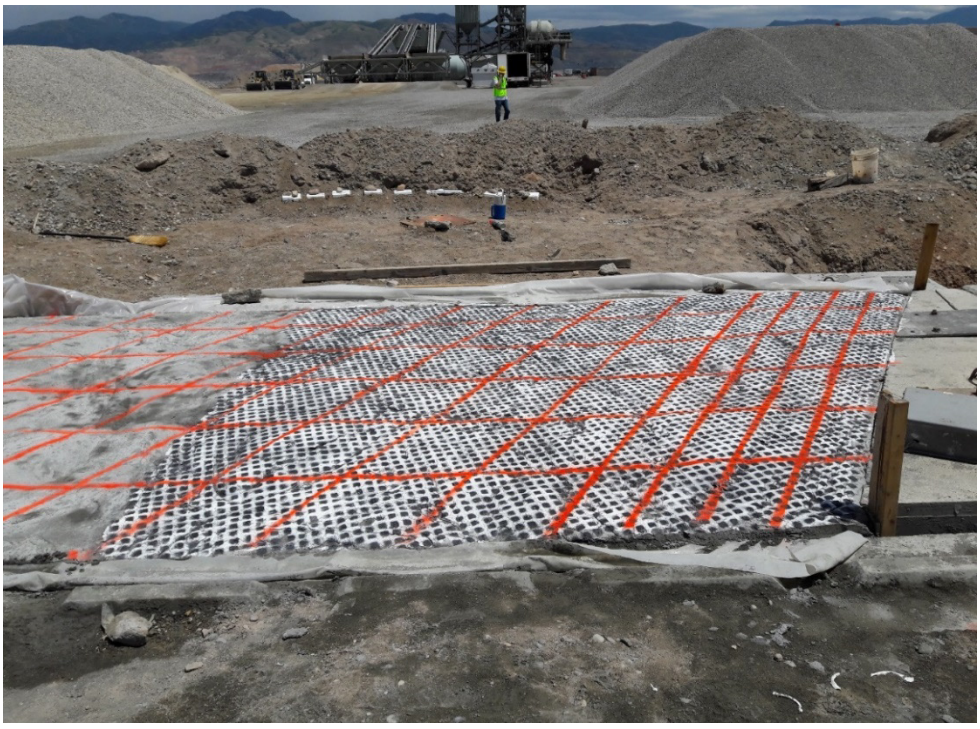

Figure 3-11: 30° skew backfill surface before testing.

Figure 3-12: DIC camera calibration before testing.

3.5.5 Thermocouple Instrumentation

Cellular concrete curing was monitored through the use of a four-channel data recorder. Thermocouple wires were placed at depths of 5.67 ft, 2.25 ft, and 0.50 ft. (1.73 m, 0.69 m, and 0.15 m) from the top of the pile cap as shown in Figure 3-13. Another thermocouple wire was placed at the middle of a 3 x 6 in. cylinder on top of the pile cap. The data recorder logged the temperature at these four locations every hour during the first week of curing.

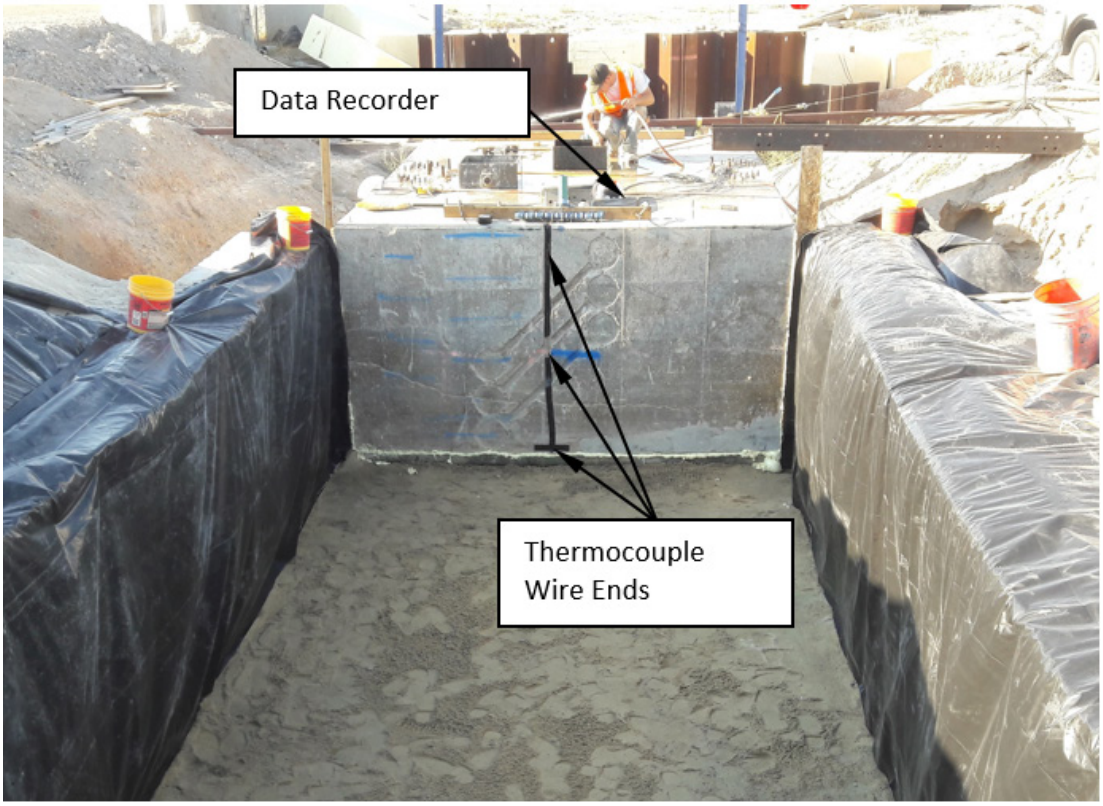

Figure 3-13: Thermocouple instrumentation for backfill area.

3.6 Testing Procedure

3.6.1 Cellular Concrete Placement and Testing

Cellular Concrete poured for the 30˚ skew test was mixed by running a tube from a foam-producing unit to a concrete truck shown in Figure 3-14. Foam was added to the truck in timed intervals with a density test being performed after each interval. The density was measured by placing sampled concrete in a 4-in.- (15.2-cm-) diameter by 8-in.- (20.3-cm-) tall cylinder and weighing the cylinder empty and full. Once the desired density was achieved, the material was poured into the excavation. This approach is used for small projects when it is not practical or

cost-effective to mobilize a dedicated mixing unit; however, it is more time-consuming and has the potential to produce a less uniform product.

Cellular concrete for the 0˚ skew test was produced by a unit that mixed specified volumes of foam and cement slurry to the desired density, then pumped the mixed material to the excavation. Density was also measured by filling and weighing a cylinder, although the density could be adjusted by simply turning a knob that controlled the rate at which foam was added to the mixture. Figure 3-15 shows cement slurry being produced and mixed with foam. Figure 3-16 shows the mixture being pumped to the excavation. This operation allowed cellular concrete to be placed almost continuously and is more typical of cellular concrete construction.

Figure 3-14: Addition of foam to cement slurry in cement truck for the 30˚ skew test backfill.

Figure 3-15: Production of cement slurry (truck on left) and the mixing with a specified amount of foam (unit on right) for the 0˚ skew backfill.

Figure 3-16: Cellular concrete placement by pumping unit for the 0˚ skew backfill.

In accordance with Caltrans specifications, the cellular concrete was poured into the backfill area in two 3-ft (0.91-m) lifts. The first lift was allowed to cure for 24 hrs before the second lift was placed. The first lift was left uncovered, as this would result in better bonding with the second layer (Legatski 2016). After placement of the second lift, the concrete was allowed to cure. As discussed in Chapter 2, concrete tends to gain 70% of its 28-day strength within the first seven days, and there is suggestive evidence that cellular concrete gains strength even quicker. To allow for the availability of personnel and equipment, the concrete for the 30˚ skew test cured for 24 days while the concrete for the 0˚ skew test cured for 14 days. Compressive strength testing was performed over time to document the strength at the time of testing as discussed in Section 4.3.1.

Efforts were made to sample the cellular concrete in a way that would best represent the material in the excavation. For the 30˚ skew test, a sample was taken in the middle of each concrete truck load. For the 0˚ skew test, a sample was taken every 30 minutes and/or when the mixing operation had to stop and restart. Concrete was placed in Styrofoam molds for UCS testing; flowability, air content, and density measurements were also taken. These tests, as well as their results, are discussed in Section 4.3.

3.6.2 Loading Procedure

Two 600-kip (2669-kN) actuators applied the load to displace the concrete backwall until the cellular concrete backfill reached failure. These actuators were set to displace 0.25 in. (6 mm) within 1 minute, hold the position for at least 2 minutes, and then displace another 0.25 in. (6 mm). The hold in displacement allowed incremental measurements to be taken as well as the

reduction in load over time to be observed. This procedure continued until an abutment displacement of 3.0 in. to 3.5 in. (7.6 cm to 8.9 cm) was reached.

4 CELLULAR CONCRETE PROPERTIES

4.1 Mixture Design

For the 30˚ and 0˚ skew tests, a cement slurry with a water-cement ratio of 0.55 was mixed with foam until the desired density was achieved. The specified mixture design is shown in Table 4-1. Although the mixture design specified a cast density of 27 pcf (432 kg/m^3), the actual density varied considerably; Figures 4-1 and 4-2 show the ranges in wet density measurements taken for the 30° and 0° skew tests, respectively.

Table 4-1: Cellular Concrete Mixture Design

Mixture Design Designation:	CCC 27-55
Cast Density (pcf):	27.00
Water-Cement Ratio:	0.55
Foam Type & Lot #:	JLE
Foam Density (pcf):	3.50
Foam Rate (cfm):	32.00
Quantity of Cement (#):	422.64
Design Strength (psi):	50+

Mixture Component	lb/CY	Specific Gravity	Density (pcf)	Absolute Vol. (ft^3)
Potable Water	232.45	1.00	62.40	3.73
Portland Cement (ASTM C150)	422.64	3.15	196.50	2.15
Foam (ASTM 796-97, 869)	73.91	0.05	3.50	21.12
Total	729.00		27.00	27.00

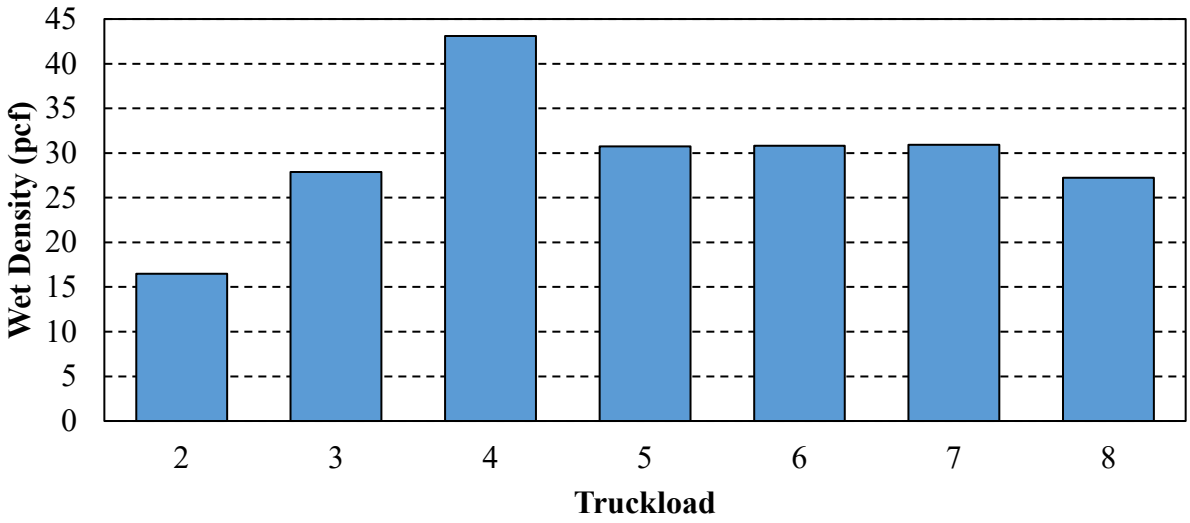

Figure 4-1: Wet density by truckload for 30° skew test (manual mixing in each cement truck).

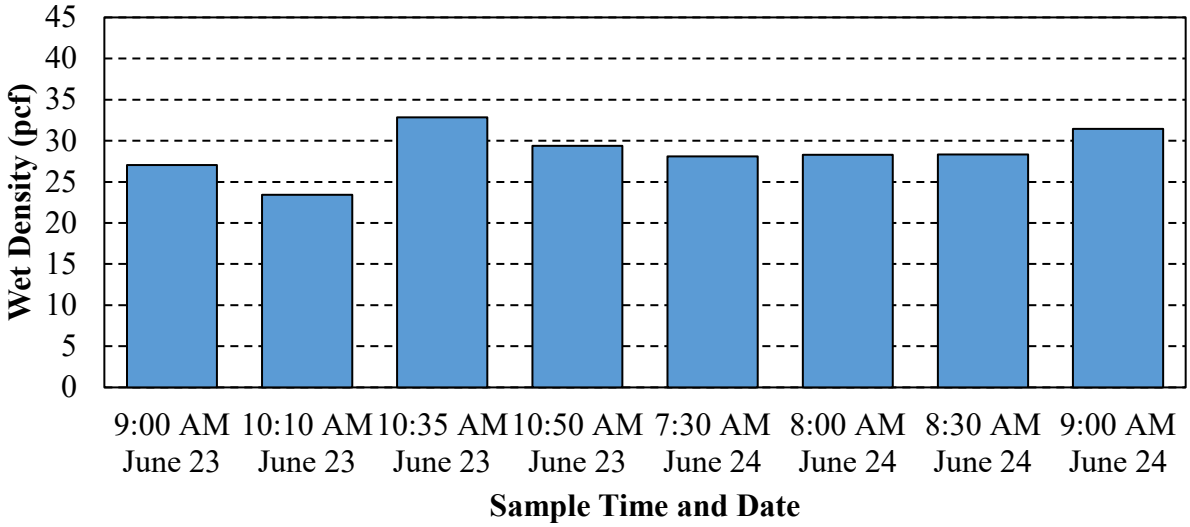

Figure 4-2: Wet density by time and date for 0° skew test (continuous placement).

4.2 Field and Laboratory Testing

A flow diameter test was conducted in general accordance with ASTM D6103 (Standard Test Method for Flow Consistency of Controlled Low Strength Material) to determine the

fluidity of the mixture, a wet density measurement was taken using a 4 x 8 in. (10.2 x 20.3 cm) plastic cylinder and scale, and a pressuremeter test was taken in general agreement with ASTM C231 (Standard Test Method for Air Content of Freshly Mixed Concrete by the Pressure Method) as explained in Section 4.3.4. Concrete was also poured into direct shear boxes and 3-in. x 6-in. (7.6-cm x 15.2-cm) Styrofoam cylinder molds for shear strength and compressive strength testing, respectively. Cylinder casting was done in accordance with ASTM C495 and the modifications made in Caltrans Standard Specifications Section 19-10. Laboratory curing of the cylinders was accomplished using the aforementioned procedure, while field curing of the cylinders was accomplished using the procedure described in Section 4.3.1.

4.3 Engineering Properties

4.3.1 Unconfined Compressive Strength

As explained in Section 4.1, concrete cylinders were cast and cured according to ASTM C495 with some modifications made in accordance with Caltrans Standard Specifications Section 19-10. Half of the cylinders were given at least 24 hours of field curing on site, 48 hours of curing at room temperature, and, lastly, moist curing in a laboratory fog room at 84˚F (28.9°C). The other half of the cylinders were left in the field to cure on site to investigate potential differences in strength between the two curing methods. The cylinders left on site remained in Styrofoam molds. Soil was placed around these molds as shown in Figure 4-3 in an attempt to better replicate on-site curing conditions.

Figure 4-3: Cellular concrete cylinders left to cure on site.

Before concrete cylinders could be placed in the fog room or tested, they had to be removed from the Styrofoam molds. The removal was accomplished using the recommendations of the Styrofoam mold manufacturer. The box was first cut into four pieces as shown in Figure 4-4. The lower 0.5 in. (1.27 cm) of each piece was then sawn off, and vertical cuts extending to the cylinder were made on all four sides of each piece. The Styrofoam was then carefully removed by hand, with special care being taken to minimize damage to the cylinder. The cylinders were then each given a unique number for identification.

Figure 4-4: Cylinder removal from Styrofoam box.

Concrete cylinders were tested at weekly intervals until the cylinders had cured for at least 28 days. Cylinders cured in the fog room were allowed to dry at room temperature for 24 to 48 hours prior to testing. Cylinders cured on site were removed from the site (and their molds) on the day of the test. Tests were ordered using a randomized complete block design. This method allowed testing of field and laboratory cylinders of varying density at each time interval. Cylinders were capped using gypsum cement and then placed in an unconfined compression test machine with a linear variable differential transformer (LVDT) to measure the deformation of the cylinder as shown in Figure 4-5. Since the LVDT measured displacement on only one side of

the concrete cylinder, it is possible that non-uniform deflection of the cylinder occurred and was not accounted for; however, the relatively low strength of the cylinders appeared to allow fairly uniform compression of the cylinder, and no differential strain was visually observed. Unlike typical concrete cylinders, the cellular concrete cylinders often did not reach a recognizable peak strength followed by a rapid drop in resistance. Instead, in many cases the strength remained relatively constant or gradually increased with strain. Tests were conducted in which the cylinders had deformed over 1 in. (2.54 cm), had numerous cracks, and were still gaining strength. For this reason, the load was recorded at 0.01 in. (0.0254 cm) intervals (with reference to the LVDT data) so the cylinder strength could later be classified using several different methods.

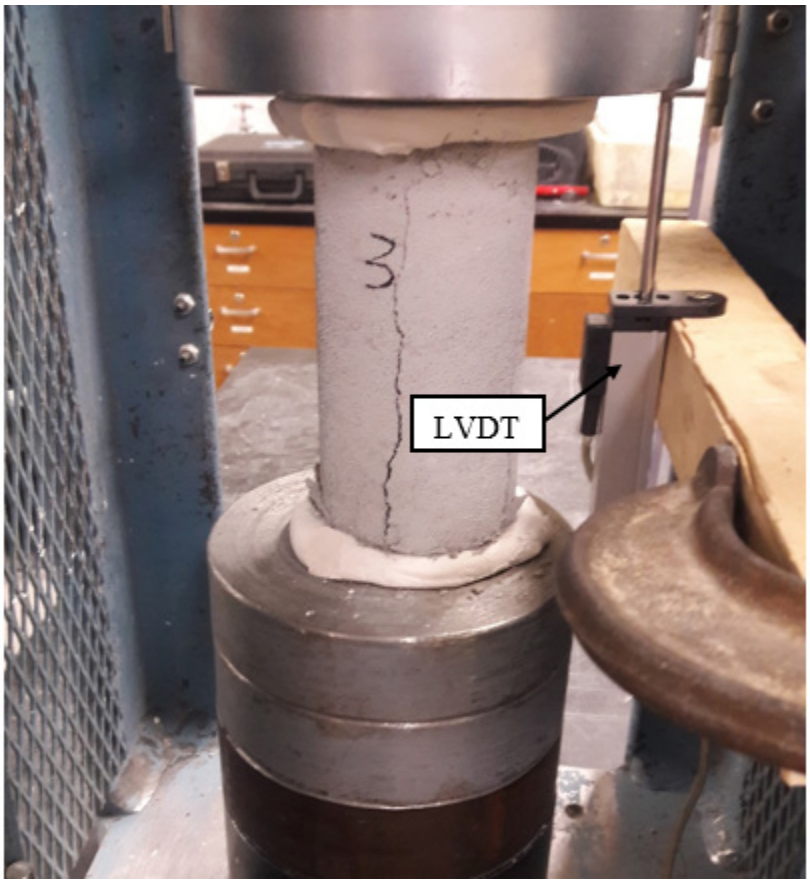

Figure 4-5: Cellular concrete cylinder after failure in UCS testing.

The testing procedure for the cylinders involved setting the strain rate to be 0.08 in./min (2.03 mm/min) until the change in load per 0.01 in. (0.25 mm) of deflection was less than or equal to 10 lb (4.54 kg). At this point the strain rate was increased to 0.20 in./min (5.08 mm/min) to expedite the testing process. The loading process continued until the cylinder had clearly hit a peak strength or until the cylinder had deflected at least 0.5 in. (1.27 cm). Nearly all of the cylinders exhibited a high residual strength similar to the cylinder shown in Figure 4-6.

Strength was classified using the 0.2% offset method. This method was chosen because it provided a consistent way to classify strength for both skew tests: The 30º skew test cylinders tended to reach what appeared to be a peak strength with very little deflection, while the 0º skew test cylinders required more deflection to reach the similar "peak" strength. The 0.2% offset method accounted for these differences, with the 30º skew cylinders reaching a 0.2% offset strength at 0.63% average strain and 0º skew cylinders reaching a 0.2% offset strength at 1.21% average strain. The 0.2% offset method was also chosen because little strength gain or loss generally occurred after this strength was reached, as shown by the stress-strain curve in Figure 4-6.

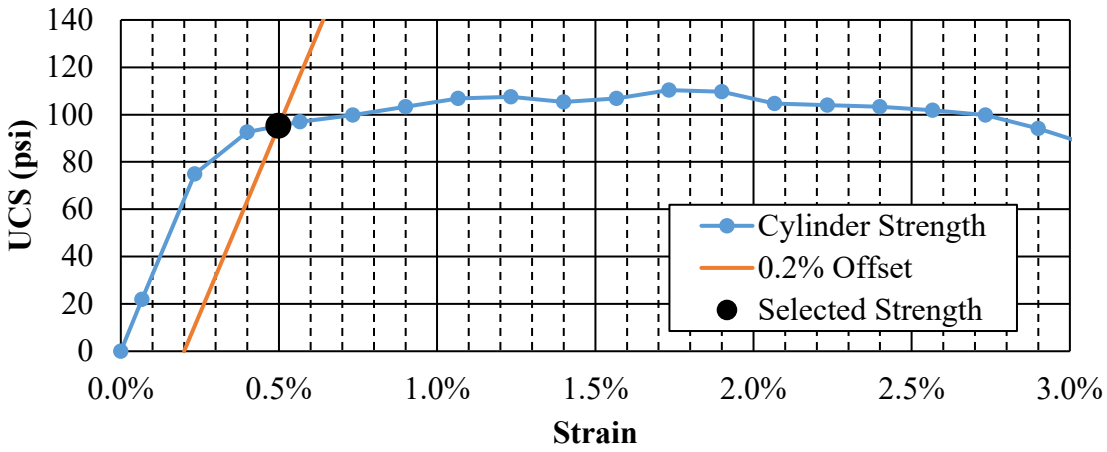

Figure 4-6: Stress-strain curve for cylinder collected during 30° skew pour.

4.3.1.1 30˚ Skew Test UCS Results

A total of 62 UCS tests were performed on cylinders cast during cellular concrete placement for the 30° skew test. As explained in the previous section, approximately half of the cylinders (29) were cured in the laboratory, and half (33) were cured on site in the field. UCS is plotted as a function of time after curing in Figure 4-7. Age did not have a statistically significant effect on strength (i.e., the null hypothesis that the true slope of the line is equal to zero could not be rejected with a *p*-value = 0.391 at the $p = 0.05$ significance level) for the curing times evaluated in this research. The low R^2 value of 0.012 shows that almost no variation in strength can be explained by variation in age. In fact, UCS results for the 30° skew test show that the only factor with a statistically significant correlation to cylinder strength is the wet density (i.e., the null hypothesis that the true slope of the line is equal to zero is rejected with a *p*-value < 0.001 at the $p = 0.05$ significance level). UCS is plotted as a function of wet density in Figure 4-8, and the exponential best-fit relationship for UCS in psi is given by Equation 4-1.

$$UCS = 3.101e^{0.091d} \quad (4\text{-}1)$$

where:

d = density in pcf

UCS = unconfined compressive strength in psi

This equation has a reasonable correlation (R^2) of 0.690 and a *p*-value < 0.001, indicating statistical significance although the data are clearly scattered around the trend line.

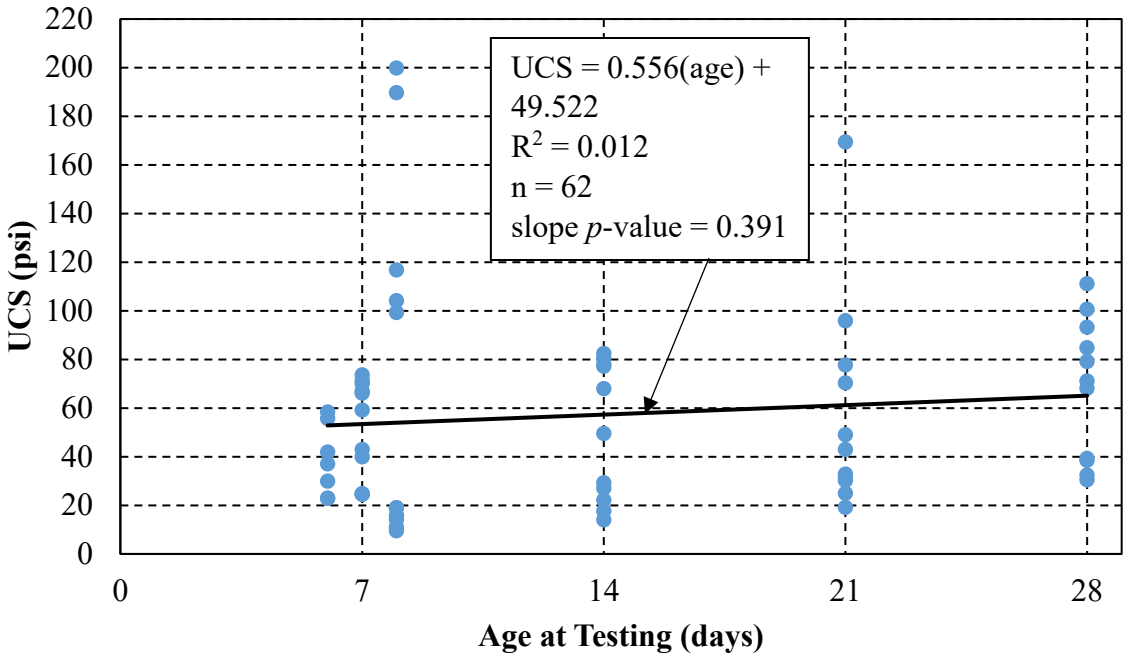

Figure 4-7: 30º skew UCS by age.

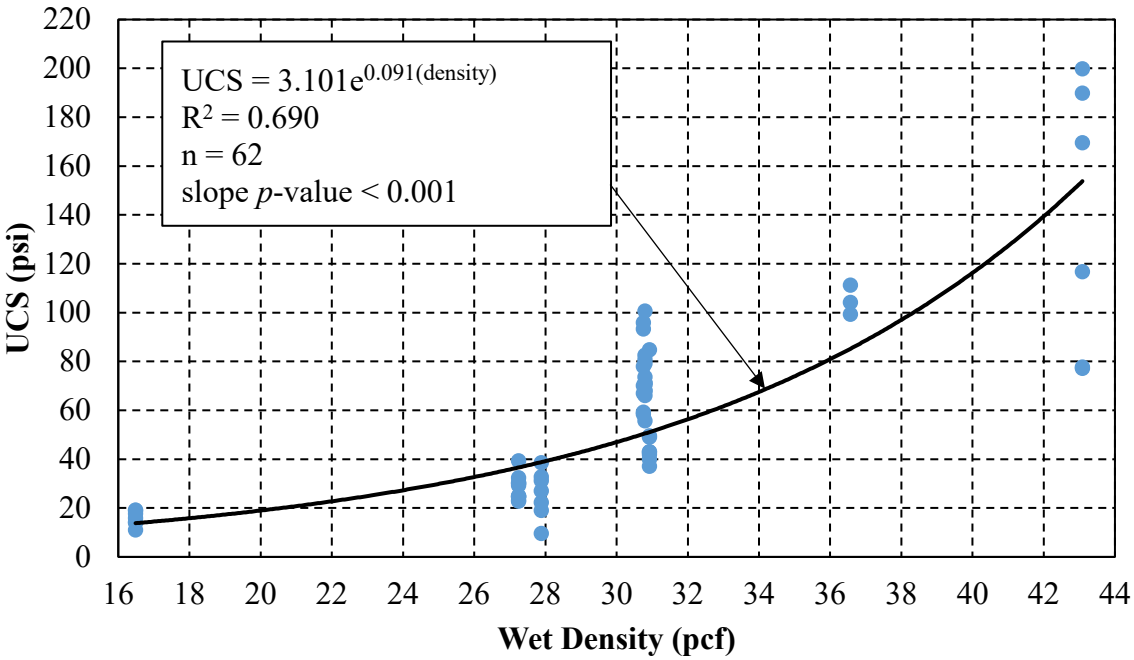

Figure 4-8: 30º skew UCS by wet density.

A two-sample *t*-test used to analyze the difference in strength between the cylinders cured in the laboratory and those cured in the field found no significant difference between the two curing methods (i.e., the null hypothesis that there is no difference between curing method means could not be rejected with a *p*-value = 0.939 at a $p = 0.05$ significance level). A box and whisker plot of the two curing methods is shown in Figure 4-9. Although the two curing methods have different median values (represented by the middle line), they have similar average values (represented by the X) due to the presence of outlier points. The outlier values were examined and determined to be accurate points.

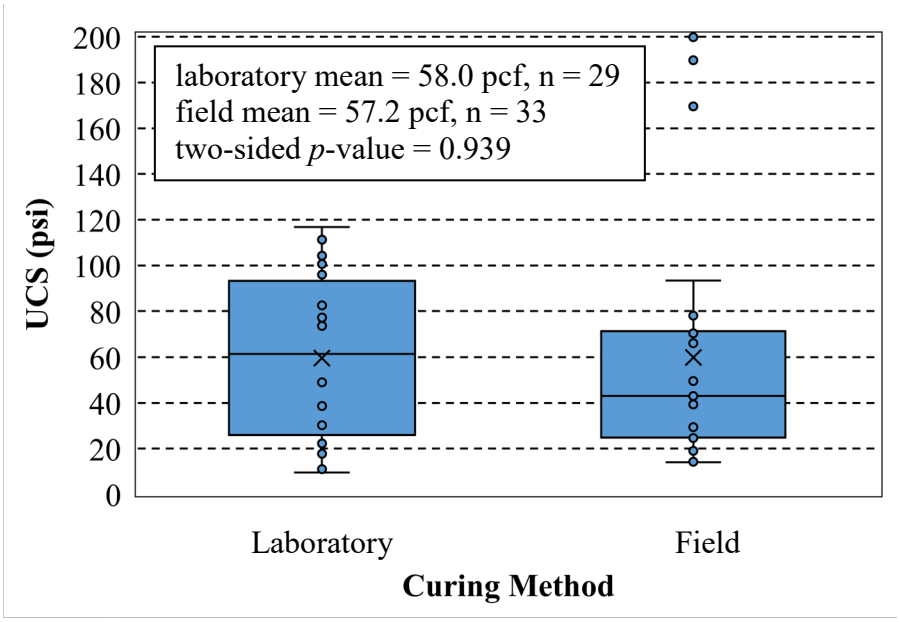

Figure 4-9: 30º skew UCS by curing method.

The backfill strength at the time of the 30º skew test was determined by taking the average of all cylinder strengths. This method was chosen due to the absence of any correlation between cylinder strength and age. The average strength of all cylinders was determined to be 57.6 psi (0.397 MPa).

4.3.1.2 0˚ Skew Test UCS Results

A total of 56 cylinders were tested from the 0° skew backfill, with exactly half of the cylinders cured in the laboratory and the other half cured in the field. UCS behavior for the 0˚ skew test was similar to that observed for the 30˚ skew test with the exception that age had a significant effect as shown in Figure 4-10. Although the best-fit line was able to explain only a small portion of the variation ($R^2 = 0.218$), the *p*-value for this line indicates that age had a statistically significant effect over the time period tested. (i.e., the null hypothesis that the true slope of the line is equal to zero is rejected with a *p*-value < 0.001 at the $p = 0.05$ significance level)

Figure 4-11 shows that wet density once again had a statistically significant effect on cylinder strength (i.e., the null hypothesis that the true slope of the line is equal to zero is rejected with a *p*-value < 0.001 at the $p = 0.05$ significance level), with an exponential line being the best fit to the data. The R^2 value of 0.555 was somewhat lower than what was observed for the 30° skew test; this may be due to the effect of age on strength and the significant interaction between both variables, which is explained subsequently.

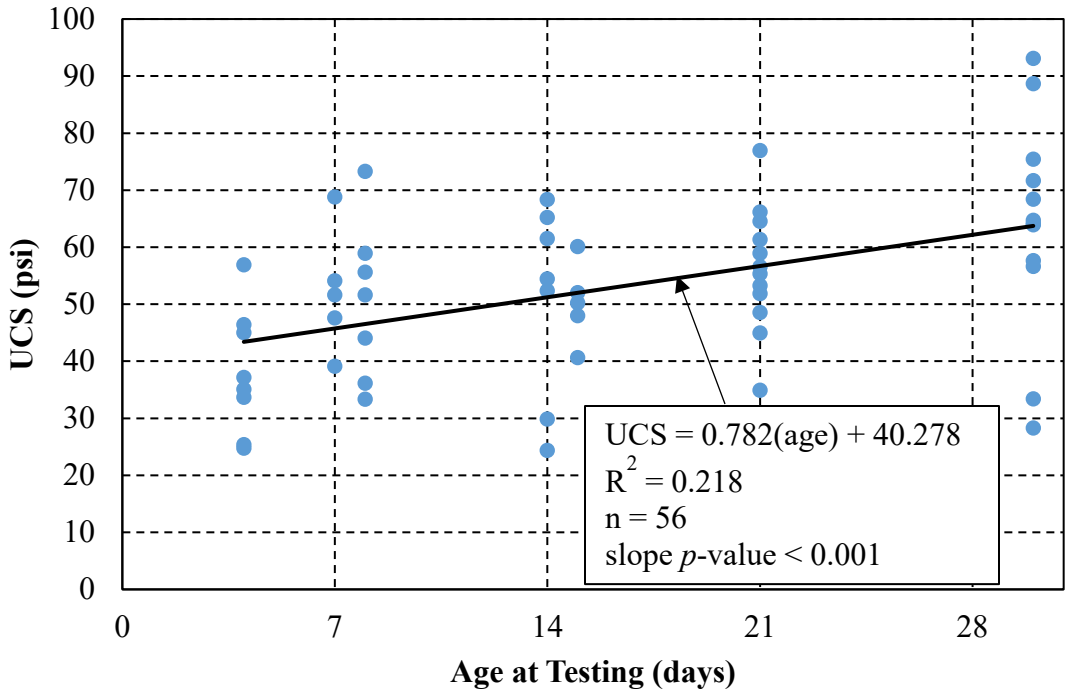

Figure 4-10: 0º skew UCS by age.

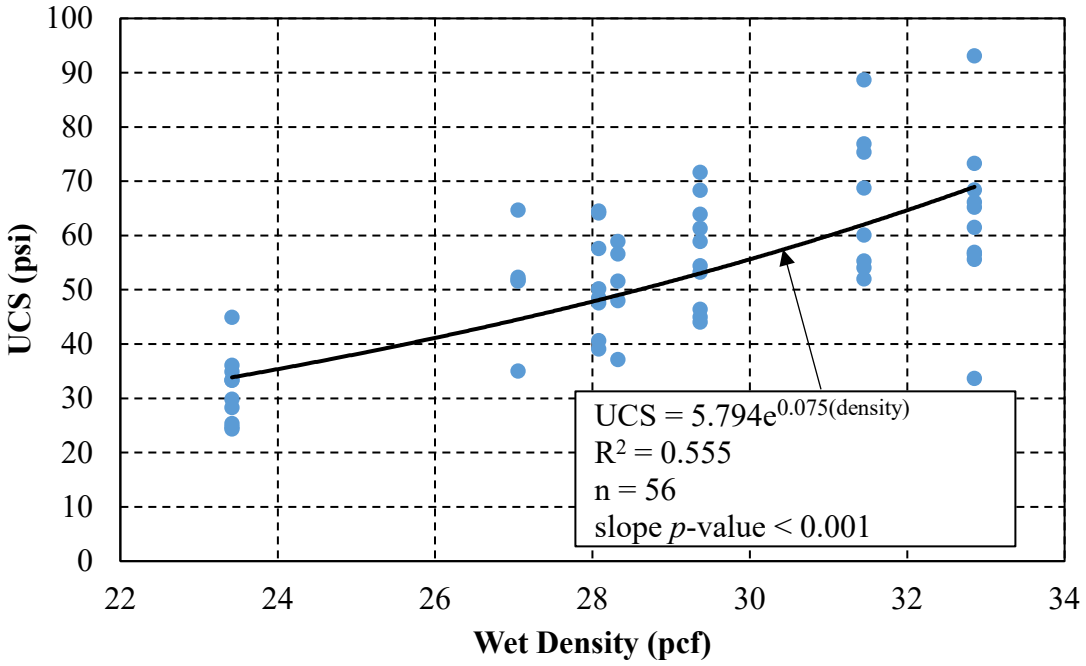

Figure 4-11: 0º skew UCS by wet density.

Both the age at testing and the wet density remained highly significant when used together to predict cylinder strength (i.e., the null hypotheses that partial slopes are equal to zero for density, age, and their interaction in a multiple regression model was rejected with a p-value < 0.001 at a $p = 0.05$ significance level). The resulting R^2 value of 0.736 was also much higher, showing that both variables were able to explain a large part of the variation. This relationship is presented in Figure 4-12, where each curved line represents a 4 psi (6.89 kPa) increase in cylinder strength. This relationship was obtained by using a linear relationship for both wet density and the age at the time of testing. The corresponding equation is Equation 4-2. This equation is only valid for cellular concrete cylinders produced and cured in a manner similar to those previously discussed for the 30° skew test (explained in Sections 3.6.1 and 4.1) and for cylinders with an age and wet density within the ranges shown in Figure 4-12.

$$UCS = -60.82 + 0.7502A + 3.533D + 0.08347(A - 16.21)(D - 28.74) \quad (4\text{-}2)$$

where:

UCS = unconfined compressive strength in psi

A = age at testing in days

D = wet density in pcf

A two-sample t test showed that curing method once again had no effect (i.e., the null hypothesis that there is no difference between curing method means could not be rejected with a p-value = 0.943 at a $p = 0.05$ significance level), as shown in Figure 4-13. Unlike the 30° skew test cylinders, the median and average values (represented by the X and the middle line, respectively) are nearly identical for both curing methods.

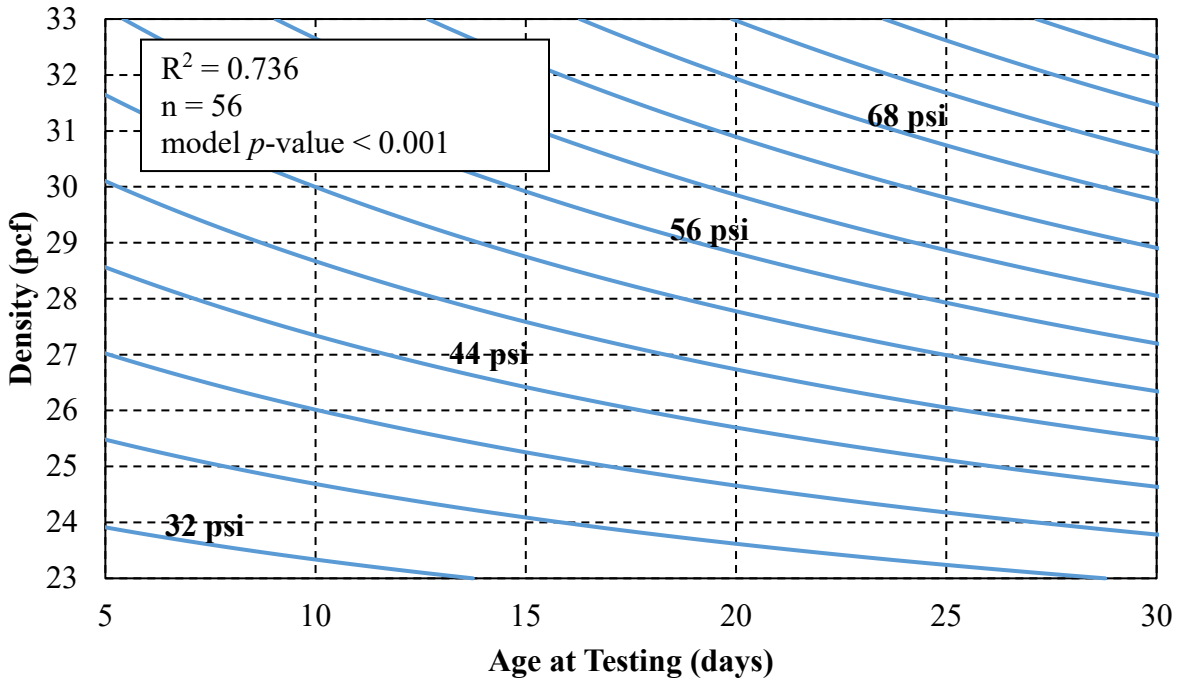

Figure 4-12: Interaction between age and wet density for 0° skew cylinders.

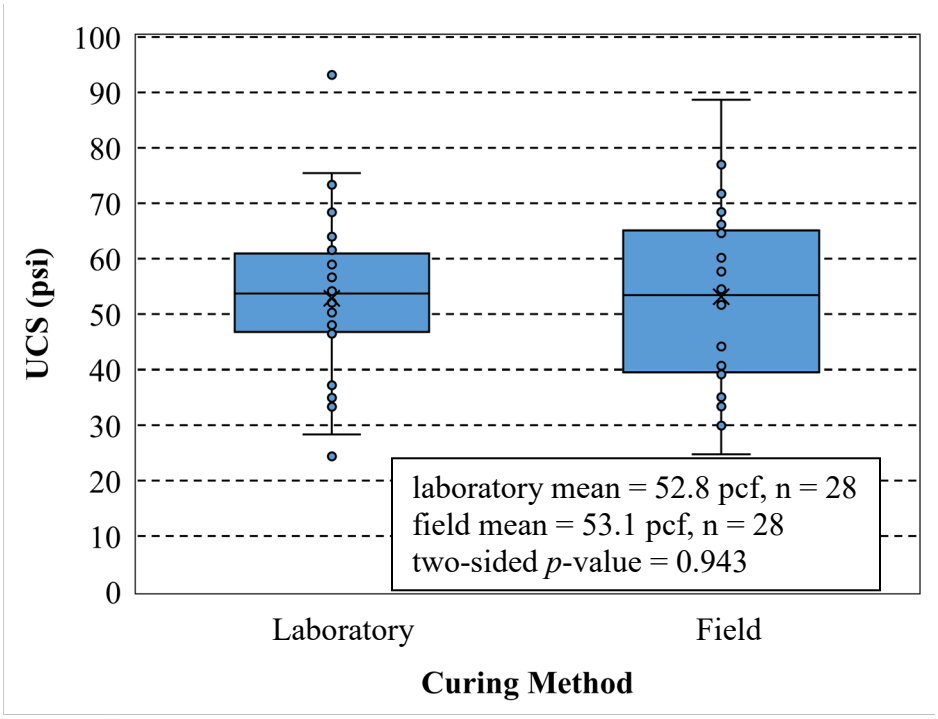

Figure 4-13: 0º skew UCS by curing method.

The strength of the backfill at the time of the test was estimated by plotting the cylinder strength against the age of the backfill, as shown in Figure 4-14. This figure is very similar to Figure 4-10, with the only difference being that all cylinders were assumed to be cast on the first day of concrete placement; because the age of the backfill was defined as starting on the first day of concrete placement, the cylinders cast on the second day of concrete placement were effectively assumed to have been cast one day earlier than they were actually cast. The strength of the cylinders relative to the backfill age was then plotted to estimate the average backfill strength at a given time. The backfill strength at the time of the 30º skew test was determined to be 50.9 psi (350.9 kPa) by finding the point on the trend line that corresponded to the time the full-scale test was conducted.

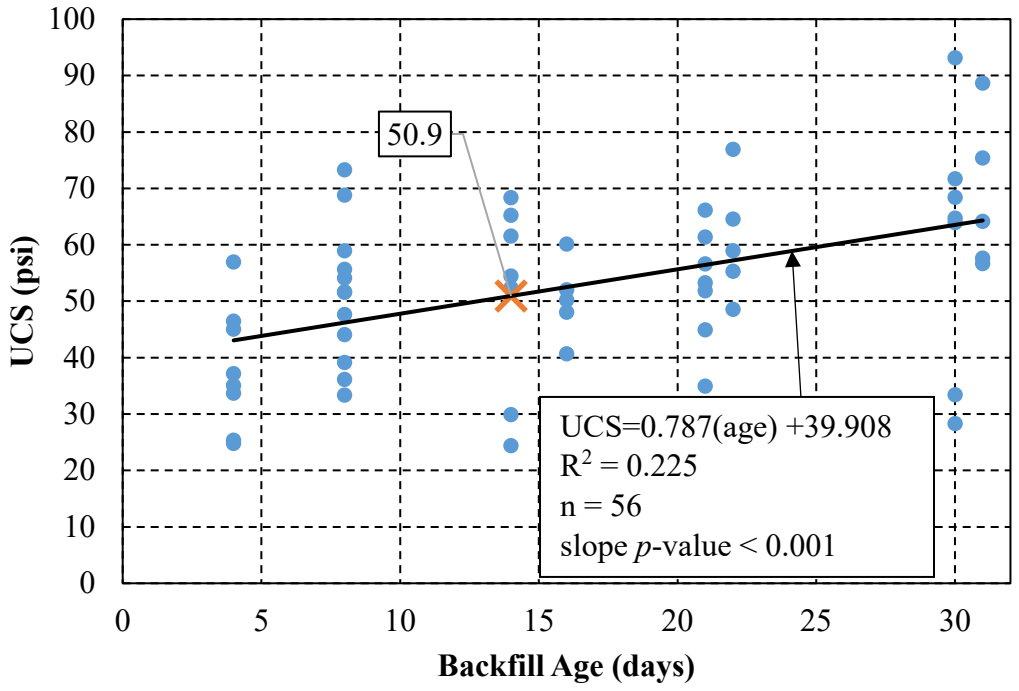

Figure 4-14: 0º skew UCS by backfill age (days).

4.3.2 Triaxial Testing

Gerhart-Cole, an independent geotechnical consulting firm, conducted triaxial testing on three cylinders, which were left to cure in the field (Maw and Cole 2015). These cylinders were placed in a Styrofoam mold, which was left exposed on top of the pile cap. The cylinders were tested at confining pressures of 2.5 psi, 12.5 psi, and 30 psi (17.2 kPa, 86.2 kPa, 207 kPa) to evaluate confining pressure effects. As shown in Figure 4-15, confining pressure appeared to have very little effect on shear strength. The maximum shear strength was between 35.5 psi and 32.0 psi (245 kPa and 221 kPa), with an average value of 33.9 psi (234 kPa).

Deviator stress versus strain plots for each of the triaxial tests at different confining pressures are plotted in Figures 4-16, 4-17, and 4-18. In contrast with conventional flowable fill where strength decreases rapidly after reaching the peak compressive strength, these test cylinders generally exhibited a high residual strength that was relatively constant with strain. These results are similar to what was observed during UCS testing.

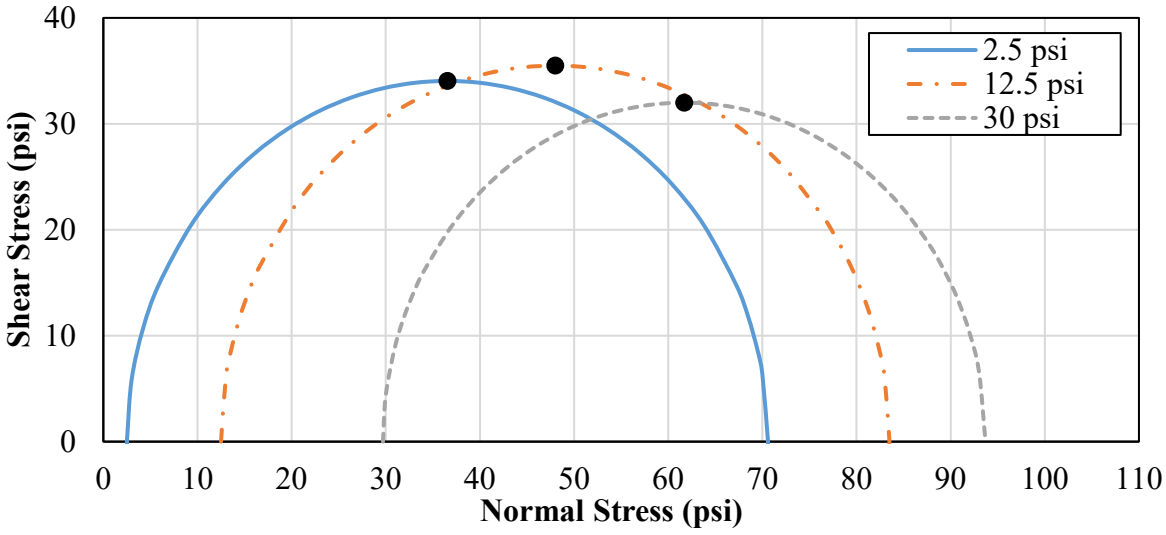

Figure 4-15: Shear strength based on confining pressure for three cylinders cured on site.

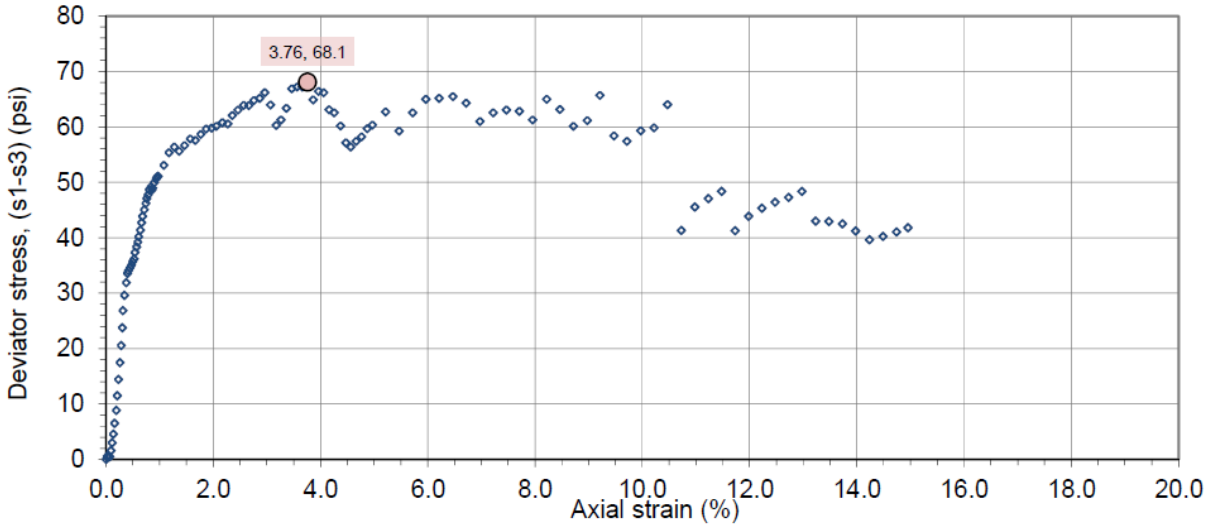

Figure 4-16: Stress vs. strain for cylinder cured on site at 2.5 psi confining pressure.

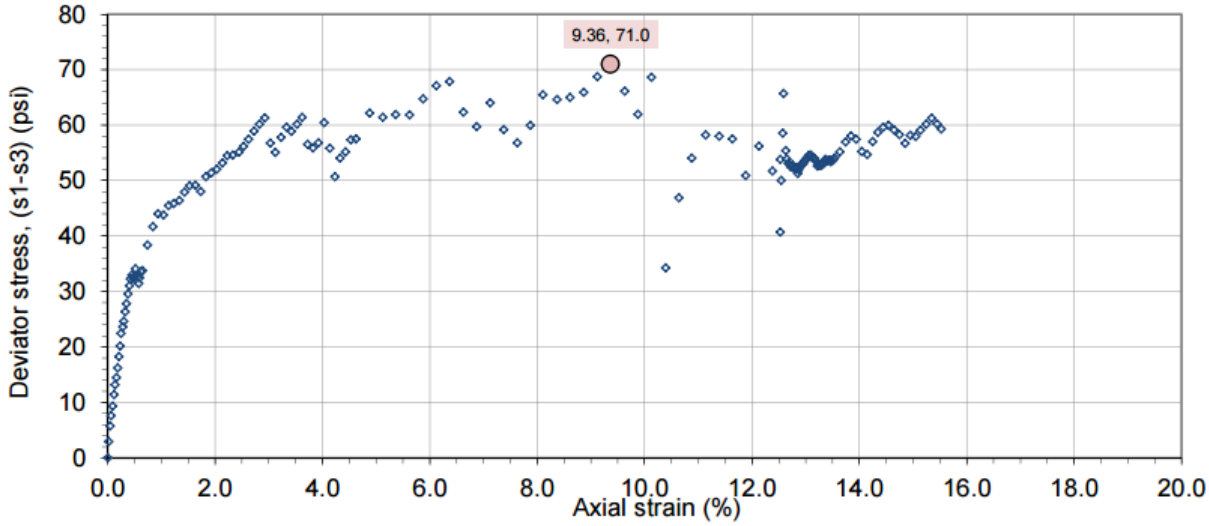

Figure 4-17: Stress vs. strain for cylinder cured on site at 12.5 psi confining pressure.

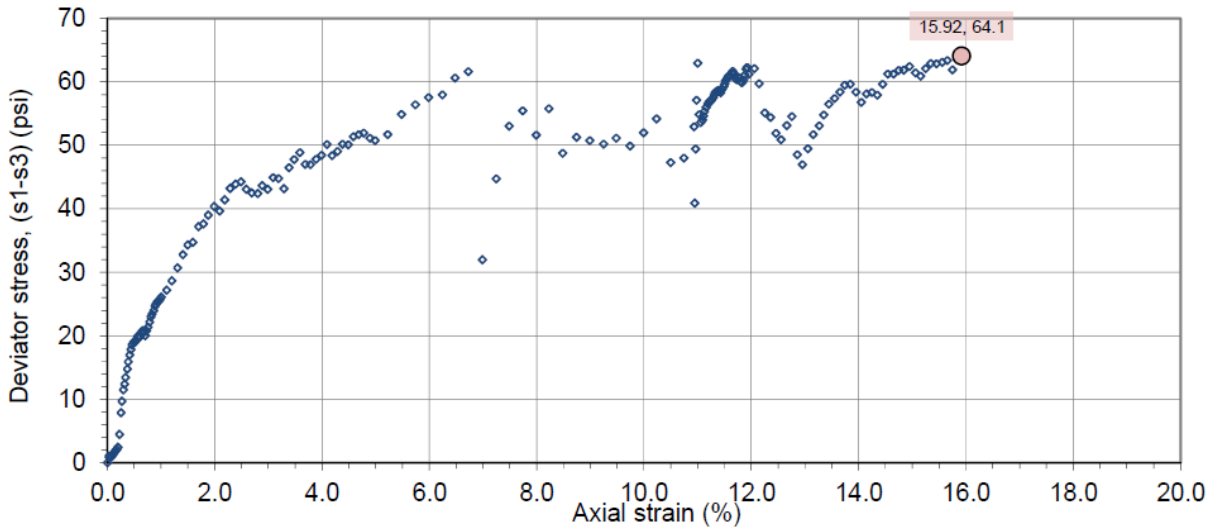

Figure 4-18: Stress vs. strain for cylinder cured on site at 30 psi confining pressure.

4.3.3 Shear Strength Testing

A total of five direct shear boxes were used to determine the relationship between effective normal stress and shear strength. All of the shear boxes were cast during the first day of concrete placement for the 0˚ skew test. Two 18-in. x 18-in. (45.7-cm x 45.7-cm) boxes were placed on the pile cap to determine the shear strength between the cellular concrete and pile cap interface; Figure 4-19 shows both shear boxes shortly after the concrete was placed. The other three 12-in. x 12-in. (30.5-cm x 30.5-cm) boxes were split through the middle and held together with tack welds shown in Figure 4-20 during concrete placement. The tack welds were ground off on the day of testing so the cellular concrete could be sheared through the middle to define its shear strength.

Figure 4-19: Direct shear test between cellular concrete and pile cap.

Figure 4-20: Direct shear test for cellular concrete with normal load of 1,799 lb (816 kg).

Direct shear tests were conducted the day after the passive force-displacement test. A 0.50-in.- (1.27-cm-) thick steel plate cut to match the inside dimensions of each shear box was first placed over the cellular concrete. This was done to evenly distribute the weights, which were then stacked on top. The first 12-in. x 12-in. (30.5-cm x 30.5-cm) box, shown in Figure 4-20, had a normal load of 1,799 lb (816 kg). The other two 12-in. x 12-in. (30.5-cm x 30.5-cm)

boxes had weights placed to represent two thirds and one third of the first test's load. The corresponding normal stresses were 12.49 psi (86.13 kPa), 8.33 psi (57.43 kPa), and 4.16 psi (28.68 kPa). The two 18-in. x 18-in. (45.7-cm x 45.7-cm) boxes used to determine the interface friction between the pile cap and the cellular concrete had normal loads of 1,799 lb (816 kg) and 899 lb (408 kg) placed on top of the cellular concrete. The corresponding normal stresses for the 18-in. x 18-in. (45.7-cm x 45.7-cm) boxes were 5.55 psi (38.28 kPa) and 2.78 psi (19.14 kPa). Normal loads do not include the weight of the steel plate or shear box placed above the friction interface.

A string potentiometer was placed on each of the left and right sides of the shear box at the height of loading. These two potentiometers measured the movement and lateral rotation of the shear box that occurred during loading. A load cell was also placed between a hand-pumped hydraulic jack and the shear box to measure the applied load. The hydraulic jack was slowly pumped so that the peak load was reached after at least one minute of loading. Very little movement, less than 0.018 in. (0.46 mm) of movement for all but one shear test, occurred before the peak load was reached. The 12-in. x 12-in.- (30.5-cm x 30.5-cm-) shear box with 1799 lb (816 kg) of weight took 0.165 in. (4.19 mm) of movement to reach a peak load.

It is important to note that, due to the existing configuration of the shear boxes, the load was applied above the shear interface. This resulted in a moment being applied to the shear box that caused it to rotate. The result was an induced tensile stress, which most likely caused the cellular concrete to fail at a lower shear strength. This effect was noticeable for lower confining pressures as is shown in Figure 4-21.

Figure 4-21: Rotation of upper box owing to applied moment during shear test.

Figures 4-22 and 4-23 show that the shear strength is generally unaffected by the normal stress. This is in agreement with a 0° friction angle and the assumption that the shear strength is equal to half of the UCS. The average shear strength for the direct shear test was 17.65 psi (121.7 kPa) or 35% of the UCS, and the average shear strength for the interface test was 6.60 psi (45.5 kPa), or 13% of the UCS. Although 50% of the UCS would be expected, these lower values can be attributed to several factors. The applied moment on the shear box placed the concrete in tension for the direct shear and interface tests. Since cellular concrete is extremely weak in tension, the applied moment would have reduced the shear strength. The concrete poured on top of the pile cap for the interface test also may have formed a cold joint, which did not allow a strong bond between the cellular concrete and the pile cap. Although the pile cap was cleaned before concrete placement, any debris that remained in place would further weaken the bond to

the pile cap. A weaker cellular concrete-pile cap interface could explain why the shear strength against the pile cap was significantly lower than the shear strength in the direct shear tests.

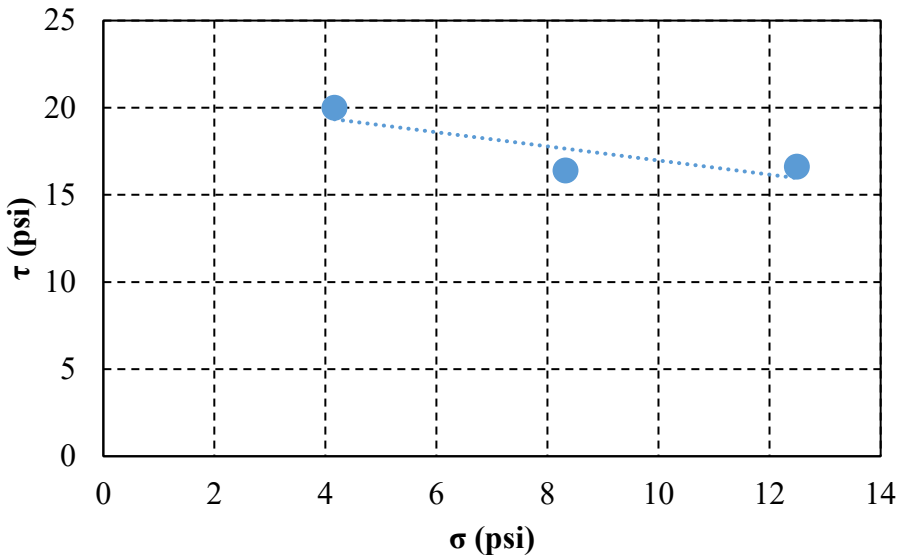

Figure 4-22: Normal vs. peak shear stress for cellular concrete.

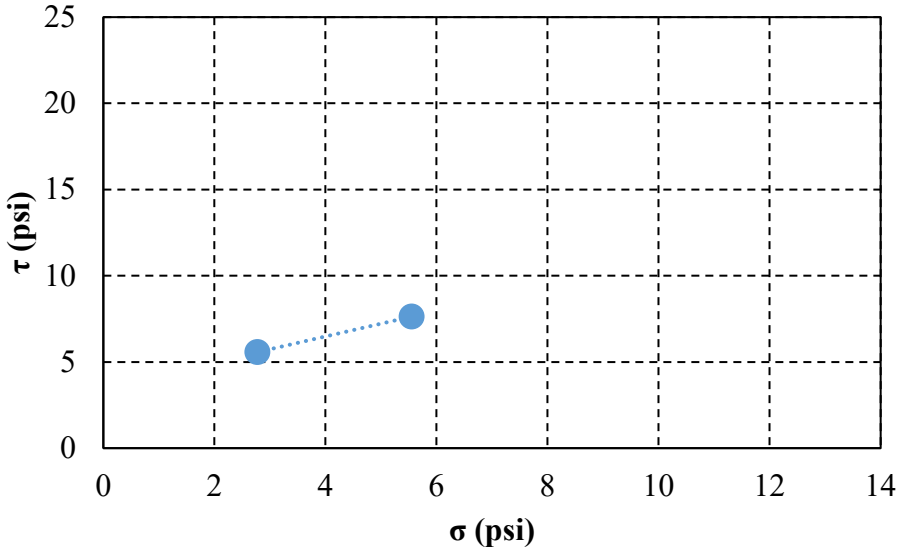

Figure 4-23: Normal vs. peak shear stress for cellular concrete and pile cap interface.

Figure 4-24 plots the shear strength results against the strength envelope presented by Filz (2015). The shear test results compare reasonably well with the strength envelope for the range of normal stresses tested. Filz recommended reducing the shear strength of the material by 70% due to variation in soil-cement properties, but this was not taken into account due to the fairly uniform nature of cellular concrete.

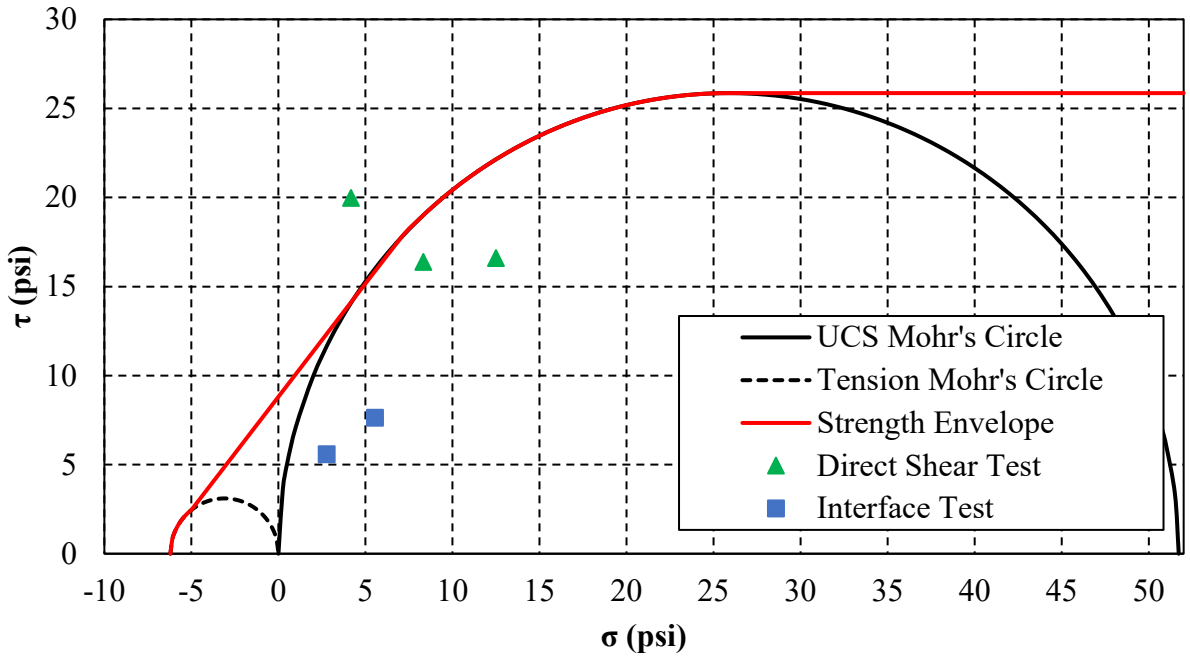

Figure 4-24: Direct and interface shear strengths compared to strength envelope for soil-cement proposed by Filz et al. (2015).

4.3.4 Air Content

A pressuremeter was used to determine the air content of the wet cellular concrete during placement in general accordance with ASTM C231. One modification to the procedure that was necessary was that both petcocks remained closed throughout the procedure, as the water that would otherwise be added through an open petcock would sink into the material due to its porosity. Another modification was that the operator lightly tapped the outside of the

pressuremeter a few times with his hand to consolidate the material, which was placed in two equal lifts, to a representative density after observing that any rodding or vibration would excessively consolidate the material. Since this test is generally used for normal-weight concrete mixtures (~150 pcf (2403 kg/m^3)), it is assumed that there is a degree of error when using this test to evaluate a very lightweight mixture (~30 pcf (481 kg/m^3)). Despite this limitation the pressuremeter appeared to give fairly consistent and accurate results when the specified procedure was followed. The pressuremeter test was conducted once per day during each concrete pour. Air content ranged from 65% to 78% as summarized in Table 4-2. Using the mixture design data and assuming the foam liquid has the same density as water (the Elastizell mixing procedure indicates that the foam liquid is 98% water (Elastizell Corporation of America 2016)), the design air content is 74%. Therefore, the measured air content is in good agreement with the expected design value.

Table 4-2: Air Content

Date	Test	Air Content (%)
23-Jun	30 degree skew	70
24-Jun		65
9-Aug	0 degree skew	78
10-Aug		72

4.3.5 Flowability

A flow consistency test was performed in general accordance with ASTM D6103. This test indicates how well the material will flow and self-level during placement. All spread diameters were above 8 in. (20.3 cm), which indicates good flowability (NRMCA 2000). Results are shown in Table 4-3.

Table 4-3: Flow Consistency Measurements

Cellular Concrete Test	Batch/ Interval	Flow Diameter (in.)
0˚ Skew	2	8.0
	3	8.0
	4	9.5
	5	8.5
	6	9.0
	7	8.5
	8	8.0
30˚ Skew	1	10.0
	3	9.0
	4	8.5
	5	8.5
	6	8.0
	7	9.0
	8	8.0

4.3.6 Curing Rate

As explained in Section 3.5.5, concrete temperature data were collected using a four-channel concrete maturity meter. The thermocouple lead wires were placed at the bottom, middle, and top of the backfill. The fourth thermocouple wire went to the center of a cellular concrete cylinder encased in its Styrofoam mold. The concrete maturity meter recorded the temperature as measured at the end of each thermocouple wire every hour.

Thermocouple data recording concluded after 8 days (192 hours) for the 30˚ skew test and 2 weeks (336 hours) for the 0˚ skew test. Time vs. temperature data for these two tests are plotted in Figures 4-25 and 4-26. The two plots are one day short of the entire time the thermocouple data were being recorded. This is due to the fact that the concrete was placed on two separate days; the thermocouple wires placed at the middle and top of the backfill started recording on the second day and have 24 hours less data than the other thermocouple wire locations.

Figures 4-25 and 4-26 both show the backfill reaching the highest temperature after approximately 12 hours of curing. The variation in temperature observed for the top of the backfill and the cylinder are presumably due to daily ambient temperature changes; the middle and bottom of the backfill were better insulated and as a result do not show these fluctuations.

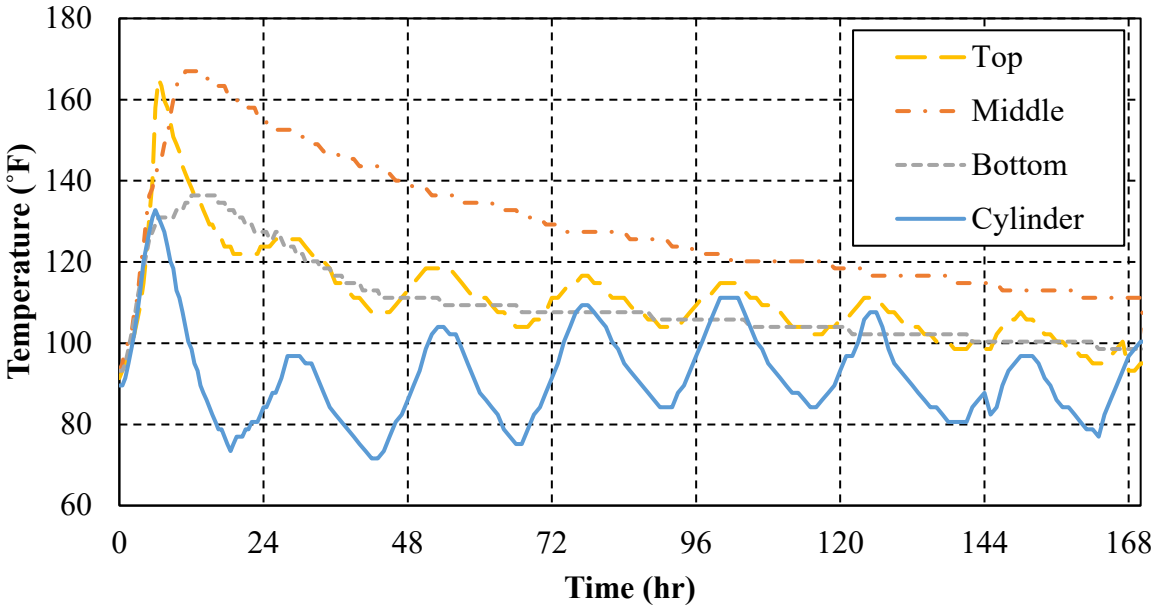

Figure 4-25: Temperature vs. time for 30° skew test backfill.

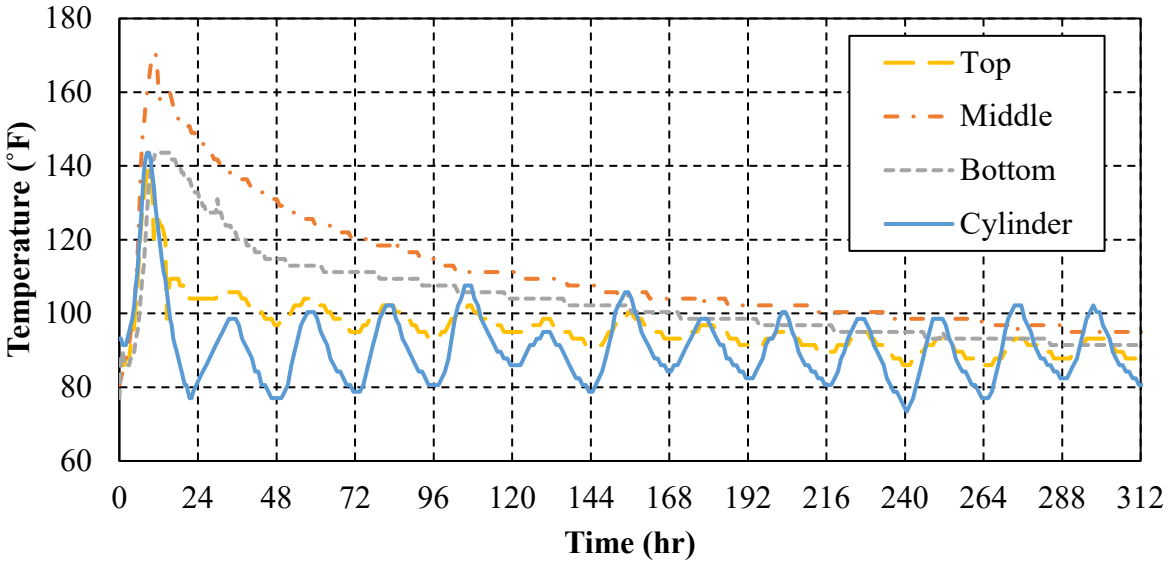

Figure 4-26: Temperature vs. time for 0° skew test backfill.

Figures 4-27 and 4-28 provide plots of curing temperature vs. depth in backfill for different time periods during the 30° and 0° skew tests, respectively. Both tests yielded similar results indicating that the temperature changed the most in the first 50 hrs but substantially stabilized thereafter. This is typical of cement hydration reaction rates, which decrease over time. After 10 days of curing, the backfill temperature was 95°F to 122°F (35° to 50°C) hotter than ambient temperature, but this difference decreased to about 59°F (15°C) after 150 hrs (6.25 days). The curing heat was similar for both backfill materials. The top and bottom of the backfill cooled considerably faster than the middle section; this is presumably due to heat being absorbed by the underlying soil and air above the backfill. Although the difference in temperature from the center to the edges was up to 64°F (18˚C) at 10 hrs, the maximum difference in temperature by the time the concrete had been curing for 150 hrs was only 12.6°F (7˚C).

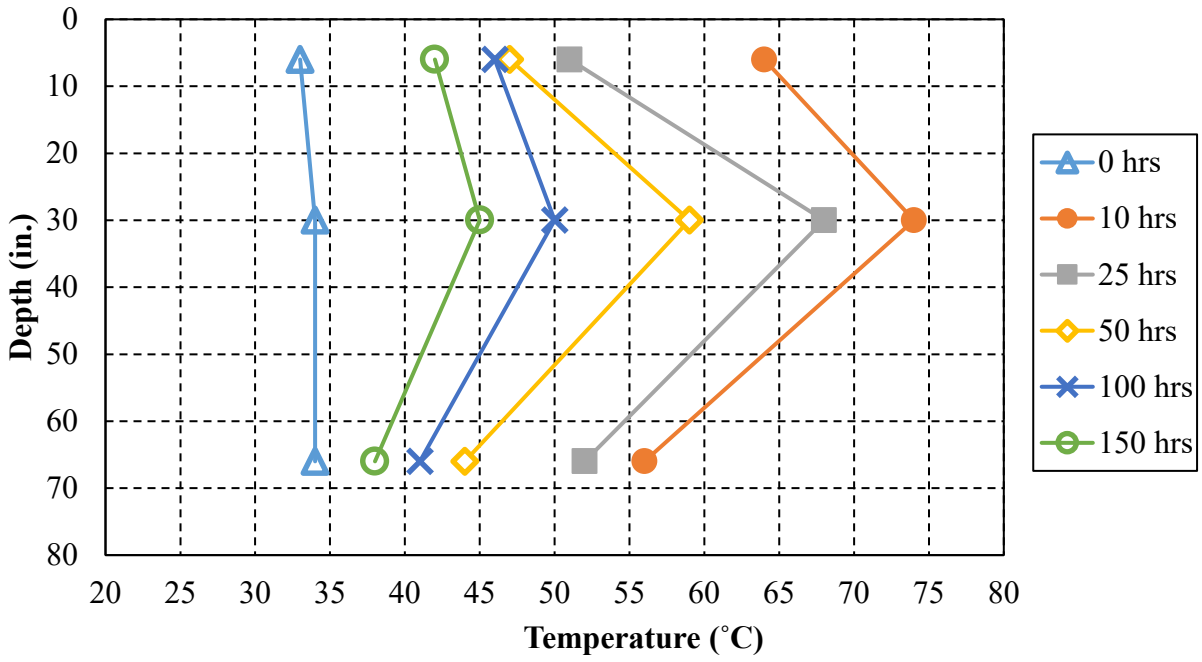

Figure 4-27: Change in temperature by depth and time for 30˚ skew test backfill.

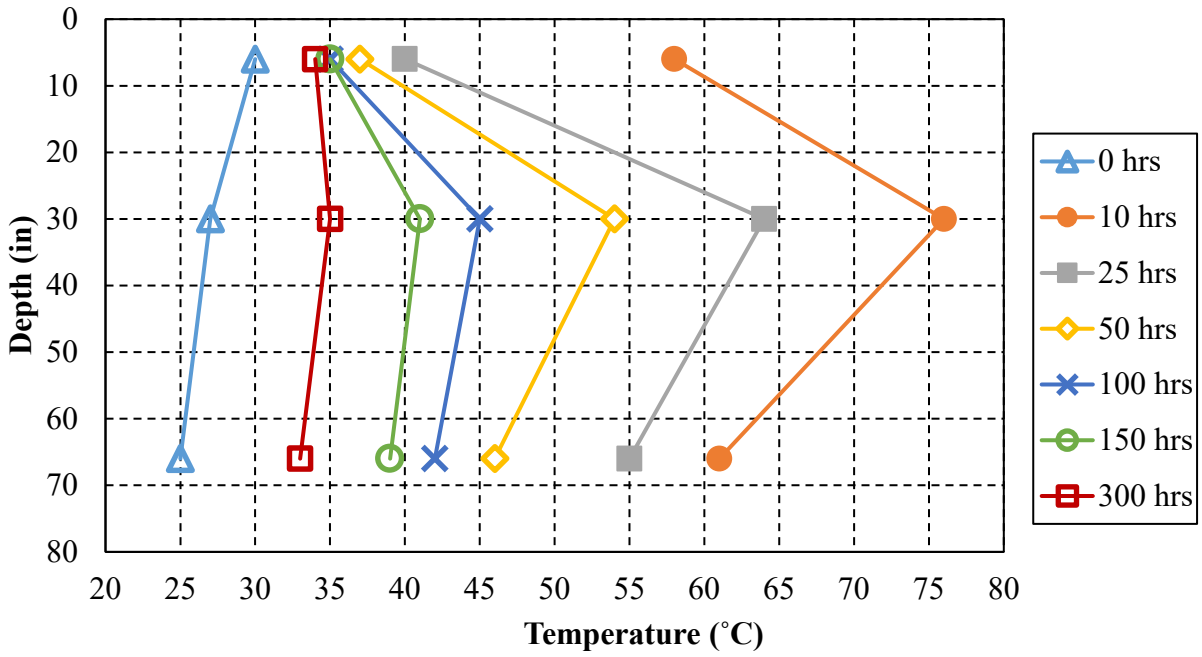

Figure 4-28: Change in temperature by depth and time for 0˚ skew test backfill.

5 PASSIVE FORCE TEST RESULTS

5.1 Force-Deflection Relationship

To determine the passive force provided by the backfill, a "baseline" load test was first conducted. This test consisted of pushing the pile cap forward with no backfill present to measure the lateral resistance of the pile cap, the piles, the skew wedge, etc. The baseline curves shown in Figures 5-1 and 5-2 represent the lateral resistance before the placement of backfill for the 30° and 0° skew tests. Total force was measured by adding the two actuator loads together. Deflection was calculated by averaging the displacement measured by the four string pots placed on each corner of the back (southern) side of the pile cap (the string pot layout is shown in Figure 3-9). Since small gaps were present between the two 15° skew wedges and the pile cap, a single string pot measured the compression of these gaps; this reading was subtracted from the average pile cap movement to get the true movement at the backwall face. The force-deflection data were reduced by finding the maximum load and corresponding deflection for each interval (these intervals are explained in Section 3.6.2).

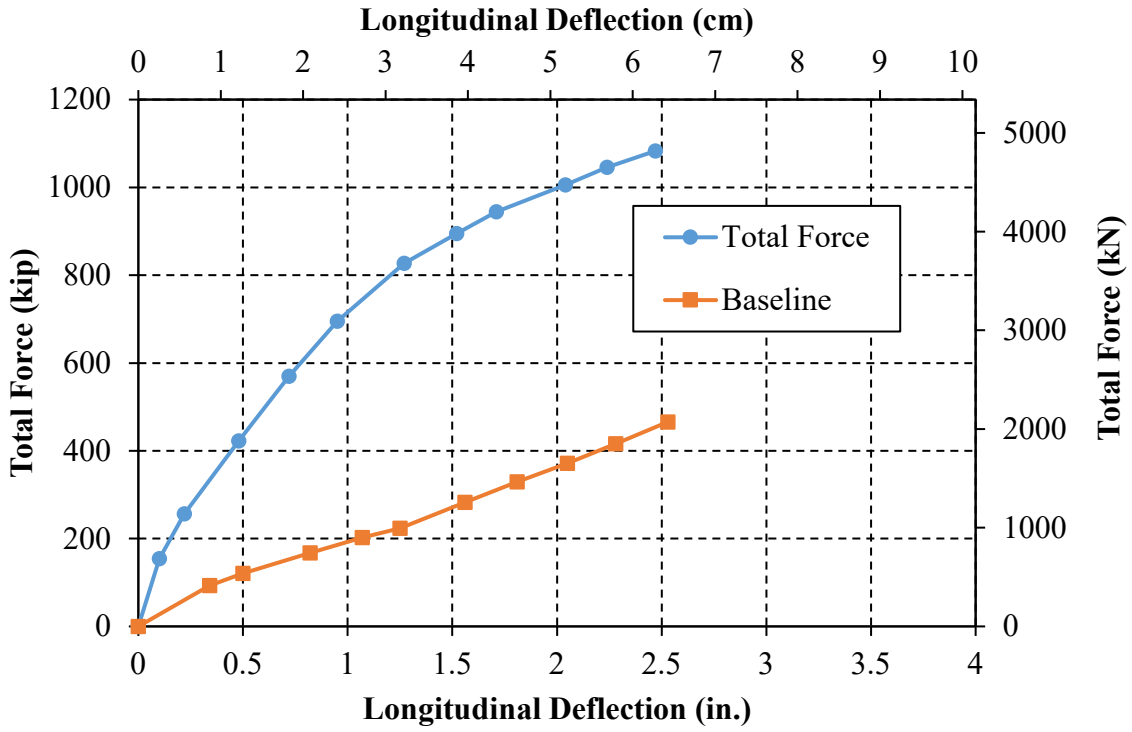

Figure 5-1: Total applied force and baseline curve for 30° skew test.

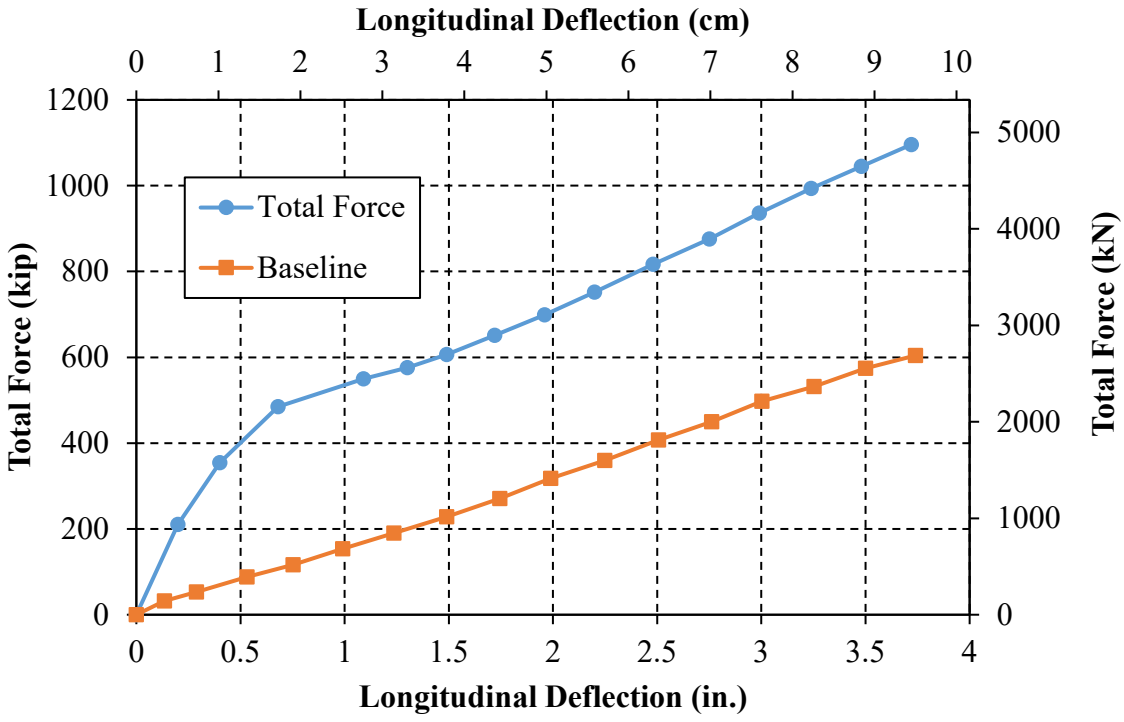

Figure 5-2: Total applied force and baseline curve for 0° skew test.

Passive force was calculated by subtracting the baseline resistance from the total measured force to compute the 0° skew curve shown in Figure 5-3. To facilitate this calculation, the baseline curve was approximated with a 6th order polynomial equation. The passive force for the 30° skew case was calculated by using the following Equation 5-1.

$$P_P = P_L cos\theta \quad (5\text{-}1)$$

where:

P_p = passive force

P_L = longitudinal force (total force – baseline)

Θ = skew angle

Figure 5-3 shows the 30° and 0° skew passive resistance vs. deflection. Contrary to the behavior of granular backfill, the 30° skew angle did not result in a decrease in passive resistance of the cellular concrete backfill. In fact, the initial passive force for the 30° skew test was about 33% higher than that for the 0° skew (with initial passive force being defined as the highest resistance before any drop in resistance occurs). Some of this increase could be explained by the fact that the UCS for the 30° backfill was about 13% higher than that for the 0° skew backfill.

Although the 30° skew backfill reached a higher initial passive resistance, in part due to the higher UCS, it required more deflection to do so. This resulted in a stiffness value around 60% of the 0° skew backfill stiffness. The stiffness of the 30° and 0° skew tests is surprising as the cellular concrete cylinders behaved opposite to what was observed; namely, the cylinders from the 30° skew backfill were noticeably stiffer than those from the 0° skew backfill. Some possible explanations for this behavior are subsequently discussed in Section 5.4.

Both skew tests showed the backfill retaining nearly 100% of the initial peak passive resistance past the deflection required to reach initial peak resistance. This observation was

replicated numerous times in UCS and triaxial cylinder testing. The 100% residual strength is very different than what has been observed for other backfill materials. Wagstaff (2016) observed the residual strength of CLSM or "flowable fill" to be between 20 and 40%, Rollins and Jessee (2013) observed the residual strength of compacted sand to be 55 to 65% in small-scale testing, and Marsh (2013) observed the residual strength of compacted sand to be 89-92% in full-scale testing.

The 0° skew backfill continued to gain strength at 1.49 in. (3.78 cm) of deflection up until the maximum pile cap displacement. This is similar to the behavior that has been observed for geofoam (Leo et al. 2008), which continues to gain strength at high deflections. It is also representative of the majority of laboratory cylinders tested for this thesis, which exhibited strength gain at strain levels exceeding 0.2%.

The passive force versus the normalized wall displacement (based on the height of the backwall) is shown in Figure 5-4. The initial peak passive force was developed at a displacement equal to 1.7 and 2.6% of the wall height for the 0º and 30º skew tests, respectively. These displacements are slightly higher than the peak passive force displacements for flowable fill reported by Wagstaff (2016), where the UCS of the backfill was comparable. The displacements are lower than the values of 3 to 5% typically reported for dense compacted granular backfill (Rollins and Cole 2005).

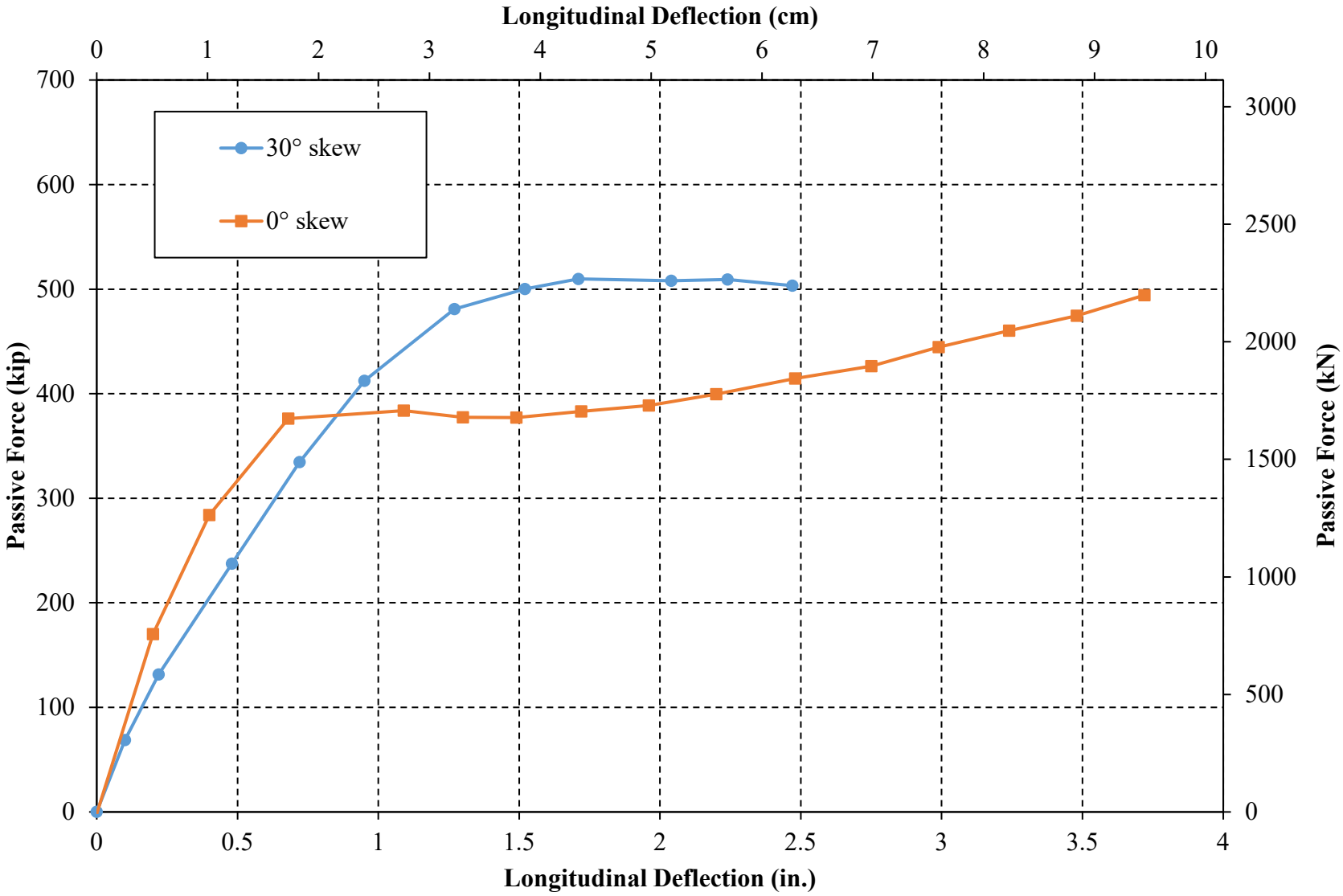

Figure 5-3: Passive force-deflection curves for 30° and 0° skew field tests.

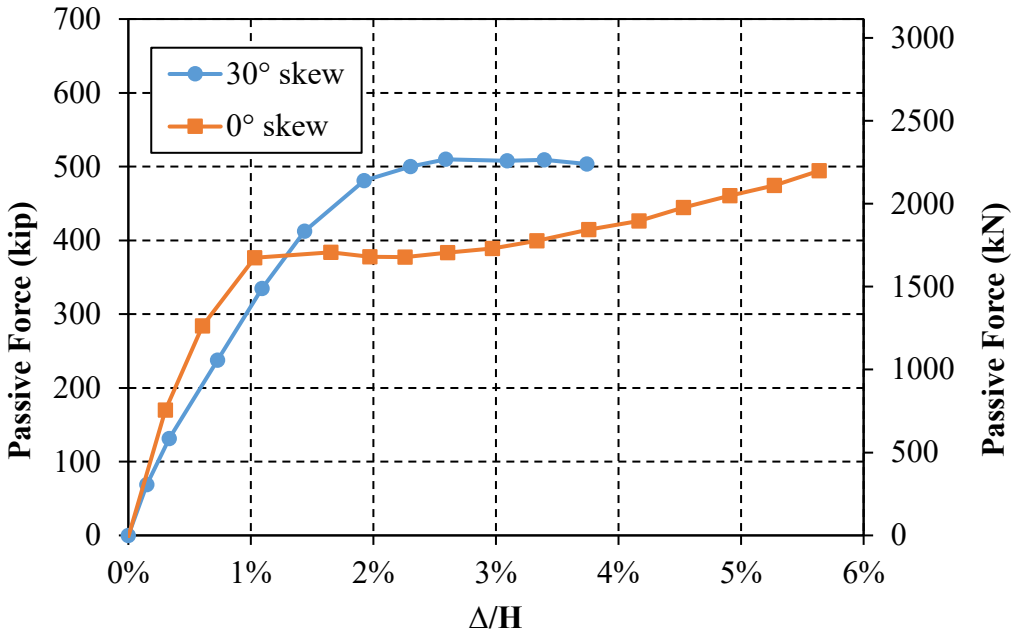

Figure 5-4: Passive force vs. normalized displacement for 30° and 0° skew field tests.

The results from the passive force-deflection test are summarized in Table 5-1. The peak resistance was determined as the highest measured resistance before any drop in resistance occurred. Stiffness was calculated by determining the passive force-deflection slope in the linear portion of the curve.

Table 5-1: Force-Deflection Results for 30° and 0° Skew Tests

Test	Measured Resistance	Measured Displacement to Peak Resistance	Measured Stiffness
30° Skew	509.8 kip (2268 kN)	1.71 in. (4.34 cm)	434 kip/in. (760 kN/cm)
0° Skew	383.7 kip (1707 kN)	1.09 in. (2.77 cm)	710 kip/in. (1243 kN/cm)

5.2 Surface Heave

Before the testing began, a 2-ft x 2-ft (0.61-m x 0.61-m) grid was painted onto the surface of the cellular concrete. Additional grid lines were placed in the first 4 ft (1.2 m) behind the pile

cap to create 1-ft by 2-ft grids (0.30-m by 0.61-m), as more movement was expected in this area. The grid points were surveyed using an automatic level before and after the passive force test was conducted. The difference in grid point elevations was then input into ArcMap to create heave contours using the inverse distance weighted method. Heave contours for the 30° and 0° skew tests are presented in Figures 5-5 and 5-6, respectively. These figures use the same heave intervals so they can be compared against each other.

For the 30° skew test, Figure 5-5 shows that the most heave occurred at the back end of the backfill area. There was a small zone near the center of the pile cap that appeared to settle, while the rest of the zone in front of the pile cap remained relatively stable. For the 0° skew test, Figure 5-6 shows the most heave occurring 3-6 ft (0.91-1.83 m) from the pile cap with almost no heave occurring near the reaction block wall. These figures clearly show that a greater amount of heave occurred during the 0° skew test. In the 30° skew test, the backfill had almost no heave in the half closest to the pile cap, while the backfill in the 0° skew test had most of the heave occurring in the section closest to the pile cap.

In the 0° skew test, the backfill appeared to develop a crust in certain areas that behaved independently from the rest of the backfill. This observation was most prominent in the area where the greatest amount of heave occurred. It is possible that a gap existed under this area, which caused the heave to appear greater than what actually occurred. This observation is shown in Figure 5-7.

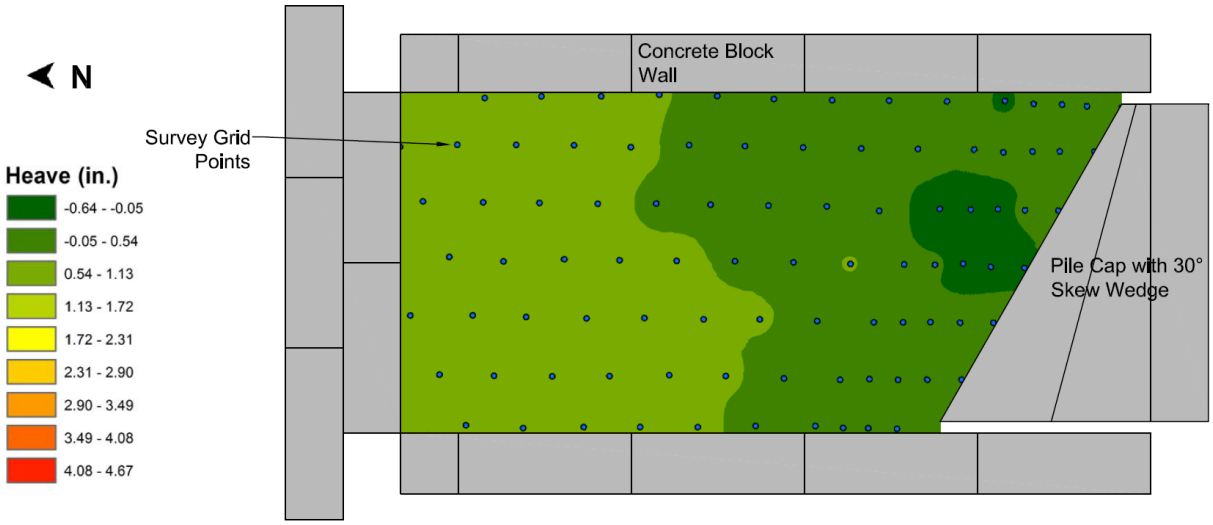

Figure 5-5: 30˚ skew test heave using equal intervals.

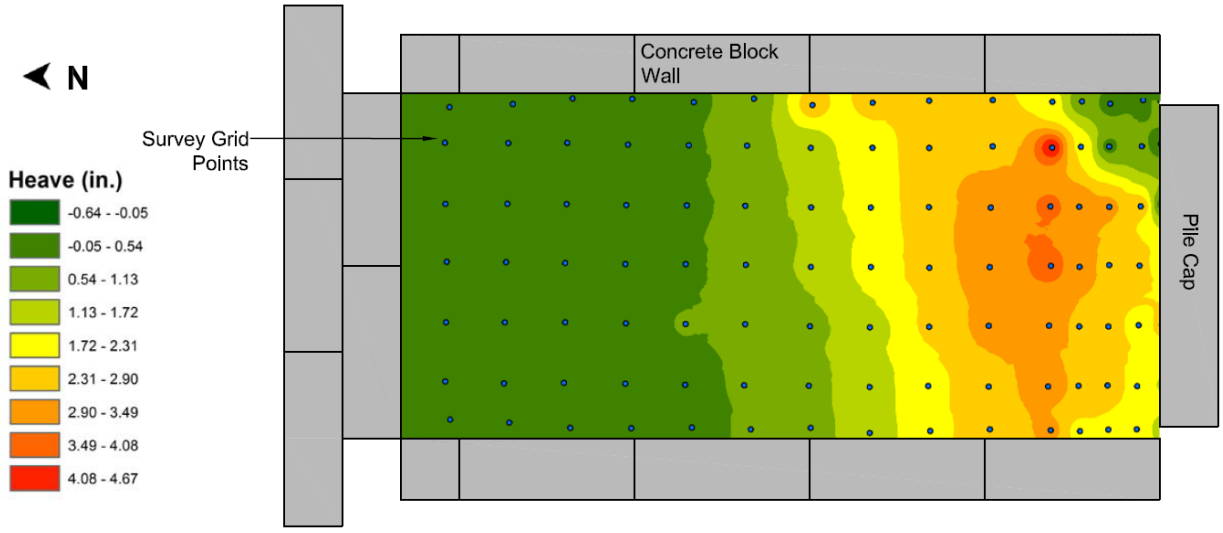

Figure 5-6: 0˚ skew test heave using equal intervals.

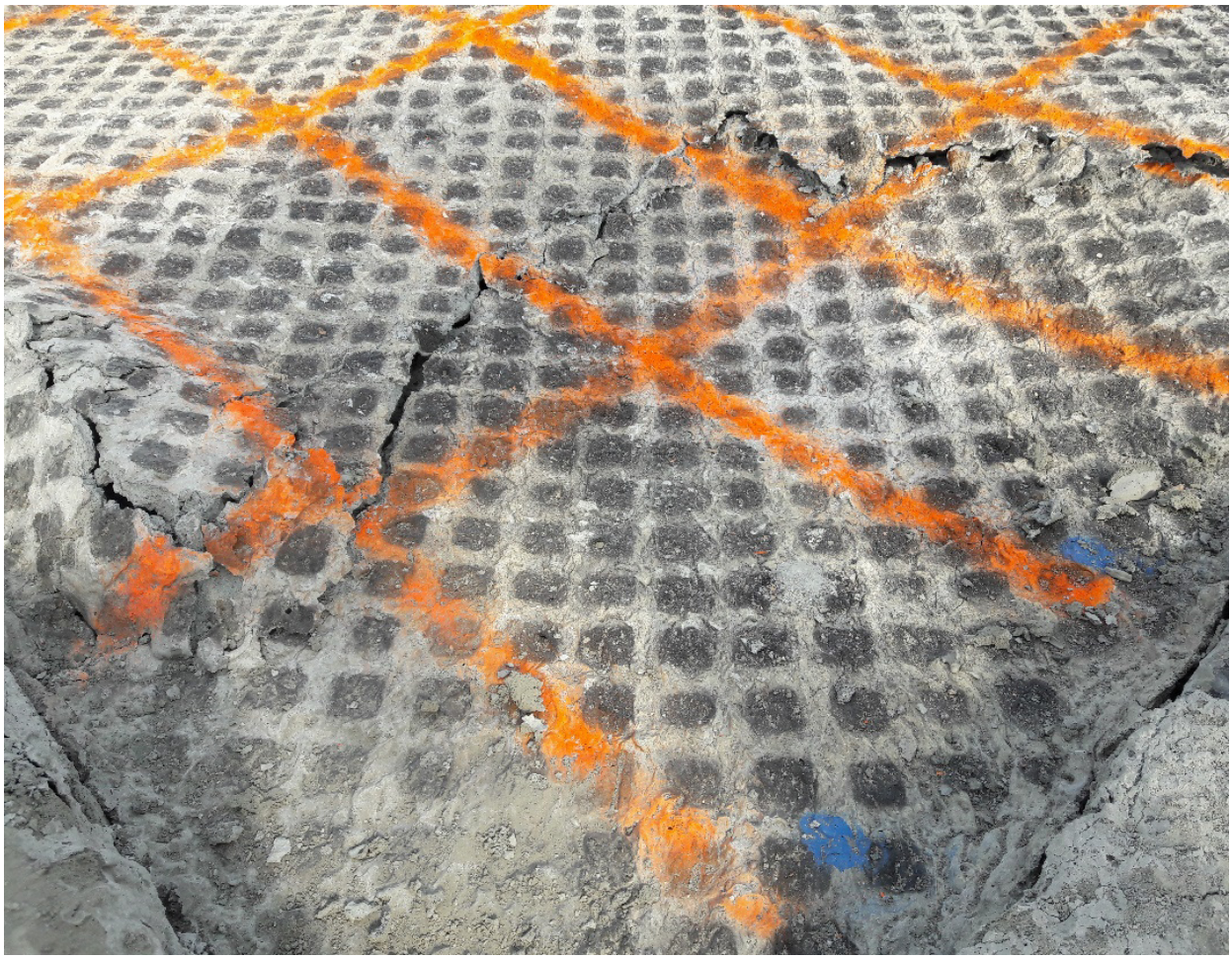

Figure 5-7: Development of crust layer on 0° skew backfill after testing (southeast corner).

The heave data relates to the surface movement presented subsequently in Sections 5.3 and 5.4. The 0° skew test showed the most backfill compression taking place near the pile cap, which is also where the greatest amount of heave was observed. In contrast, the 30° skew test shows more even compression taking place over the entire backfill, which may be represented by the gradual increase in heave moving from the pile cap to the reaction block wall.

Although there appears to be a correlation between surface movement and heave, it is difficult to explain the sources of heave for both tests. Section 5.4 clearly shows that the backfill

compressed as would be expected of geofoam; however, a geofoam backfill would have a negligible amount of heave. In comparison, a CLSM backfill would heave (due to the development of a failure surface) but would not compress in the manner observed for the 0° skew test. Although a failure surface in the cellular concrete is possible, it is unclear whether a failure surface developed as explained in Section 5.5.

5.3 Lateral Surface Movement

Lateral surface movement was tracked by surveying the grid before and after the backfill was loaded (explained in Section 3.5.4). The vector plots in Figures 5-8 and 5-10 were created by scaling the surveyed movements by 12. These movements were then divided in four equal-interval classes, which are represented by the four colors shown in these figures. The DIC camera data were not used to track lateral surface movement as the results were determined to be unreliable.

Surface movement for the 30° skew test is shown in Figure 5-8. The vectors show the most movement near the pile cap with progressively less movement towards the reaction block wall. The slow change in vector magnitude suggests that the entire backfill compressed almost uniformly. This conclusion is generally supported by the data presented subsequently in Section 5.4, where the string pots did not detect the backfill near the pile cap compressing any more than backfill farther back from the pile cap.

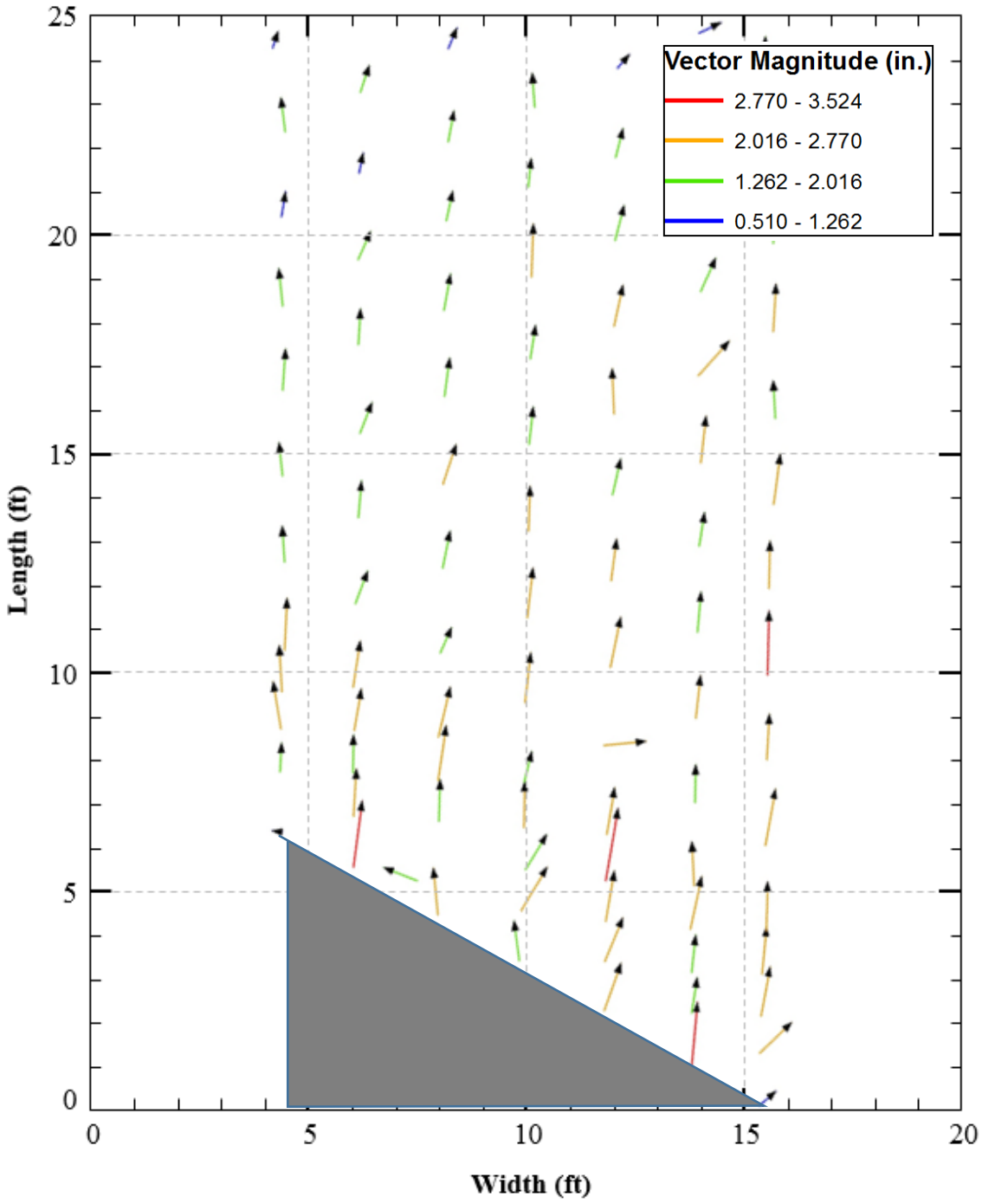

Figure 5-8: 30° skew test lateral surface movement (6:1 scaling).

Surface movement for the 0° skew test was more difficult to capture due to multiple reasons. After the first 1 ft (0.30 m) of backfill behind the wall, the movements were generally less than 1 in. (2.54 cm), which made measurement errors more noticeable on the magnified plot. The reference point, which was shot before and after each set of measurements were taken, also revealed that the total station moved while recording the location of each grid point. These two sources of errors are presumed to be the reason why the displacement vectors shown in Figure 5-10 are somewhat erratic.

Despite these measurement errors, Figure 5-9 makes it clear that most of the displacement occurred at the pile cap and that very little displacement occurred past the 1-ft (0.30-m) mark in the backfill. This expands upon the data for the 0° skew wedge in Section 5.4 by showing that nearly all of the compression occurred in the first 1 ft of backfill and that the compressive strain over the interval of 0-6 ft (0-1.83 m) would be several times higher had it been measured over the interval of 0-1 ft. This information is also similar to what Scott (2015) observed while testing geofoam. Scott placed geofoam blocks against the pile cap and compacted sand behind the blocks. Scott observed that the geofoam blocks compressed the most in the first 1 ft closest to the pile cap with a smaller spike in strain where the blocks met the sand backfill. Figure 5-10 shows the compressive behavior of the geofoam blocks.

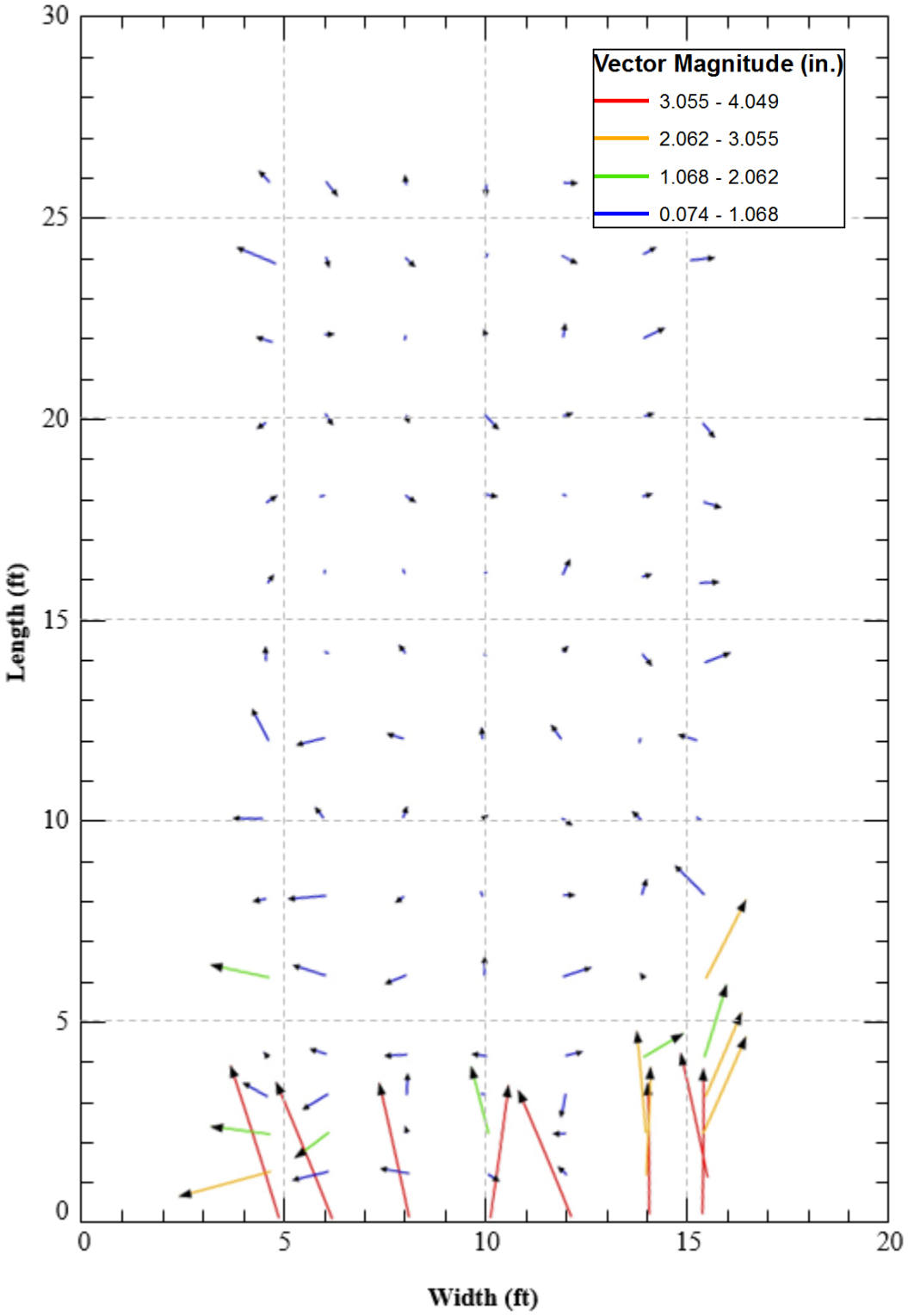

Figure 5-9: 0° skew test lateral surface movement (12:1 scaling).

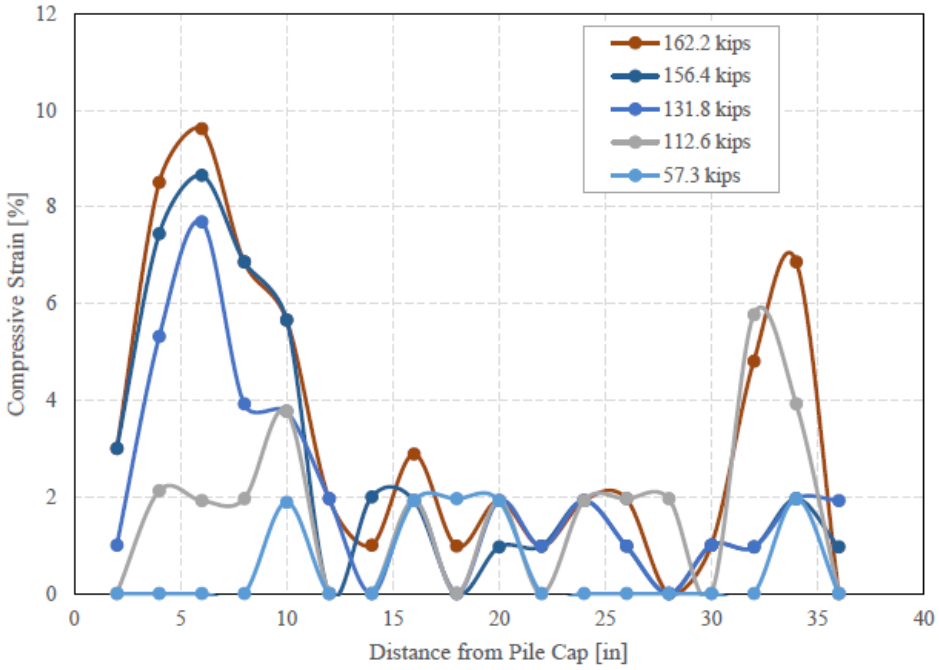

Figure 5-10: Compressive strain in geofoam blocks (Scott 2015).

5.4 Surface Displacement and Strain

Figures 5-11 and 5-12 show the backfill displacement measured as a function of distance from the backwall based on string pot measurements for a series of wall displacements for the 30° and 0° skew tests, respectively. String pot data shows the backfill material performing differently in the 30° skew and 0° skew tests. These differences are possibly due to differences in the cellular concrete placement and testing (explained in Section 3.4 and 3.6.1), rather than differences due to the skew angle. The 30° skew test backfill appeared to displace the concrete reaction block wall farther than the 0° skew test. Since this was the first test with the reaction wall in place it likely required more displacement to mobilize the peak passive resistance of the soil behind the reaction wall than the subsequent 30° skew test. This difference can be seen in

comparing the 18-ft (5.49-m) interval in Figures 5-11 and 5-12. Figure 5-11 shows that the backfill compressed fairly evenly over the 18 ft that the string pots were placed, with more compression taking place at the higher displacements. Figure 5-12 shows nearly all of the compression taking place within the first 6 ft (1.83 m) of backfill and almost no displacement occurring at 18 ft (5.49 m) after the first 1.12 in. (2.84 cm) of movement at the pile cap.

Wagstaff (2016) had string pot instrumentation set up similar to the instrumentation in this study. He found that very little compression occurred in the failure wedge and that the displacement past the failure wedge was nearly zero. This behavior was not observed for the 30° or 0° skew test. This supports the conclusion that a failure plane did not reach the surface of the backfill during testing.

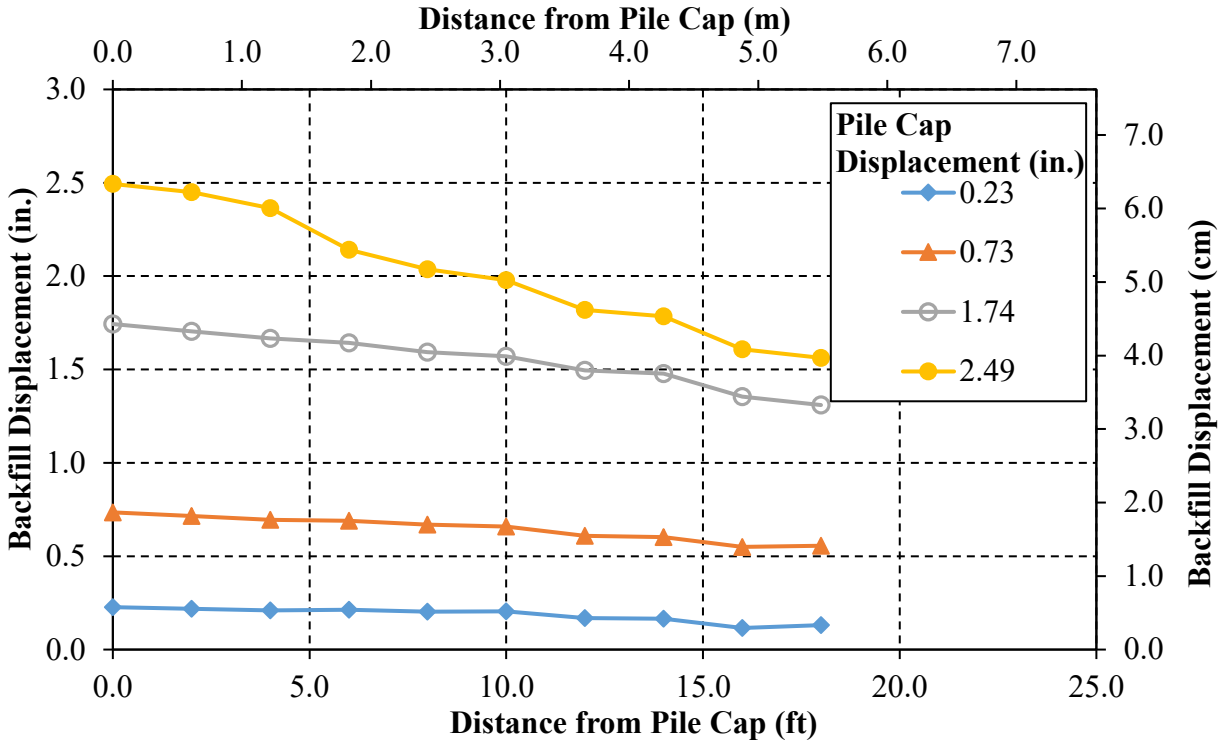

Figure 5-11: 30° skew backfill displacement at selected pile cap displacement intervals.

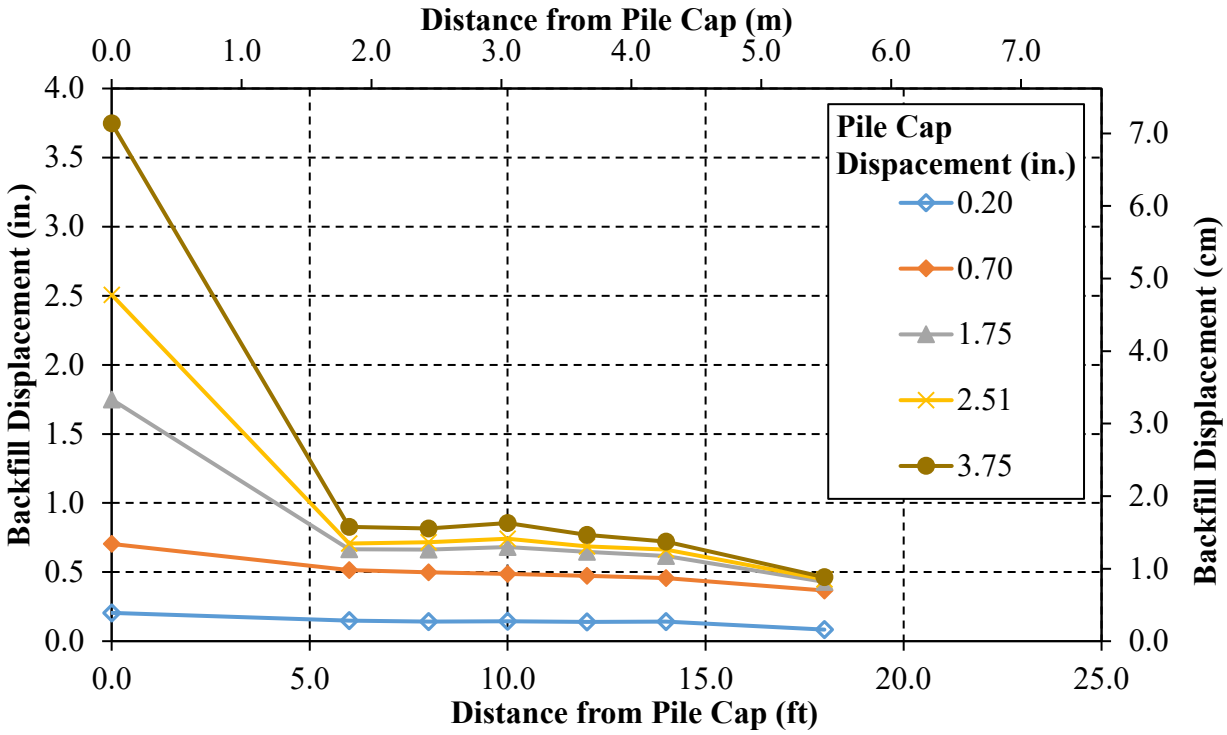

Figure 5-12: 0º skew backfill displacement at selected pile cap displacement intervals.

Figure 5-13 was created by calculating the maximum compressive strain occurring in each string pot segment. For example, the difference in displacement between the string pots located at 6 ft (1.82 m) and 8 ft (2.44 m) was divided by the initial 2 ft (0.6 m) interval between the string pots to obtain strain. This strain is then plotted as a constant value from 6 ft to 8 ft (1.83 m to 2.44 m). The backfill in the 30° skew test developed relatively low amounts of strain, typically below 1% throughout the length of the backfill. In contrast, the backfill for the 0° skew test had the highest strain within the first 6 ft (1.83 m) of backfill and very little strain in the following segments. The string pots for the 0° test placed at the 2-ft, 4-ft, and 16-ft (0.61-m, 1.22-m, and 4.88-m) intervals appeared to malfunction, so the associated data were removed from the results. This made it impossible to determine whether most of the 0° skew strain occurred in the first 1 ft (0.30 m) of backfill or the first 6 ft (1.83 m) of backfill. However, the lateral surface movement

for this test suggests that most of the strain occurred in the first 1 ft (0.30 m) of backfill as depicted in Figure 5-10.

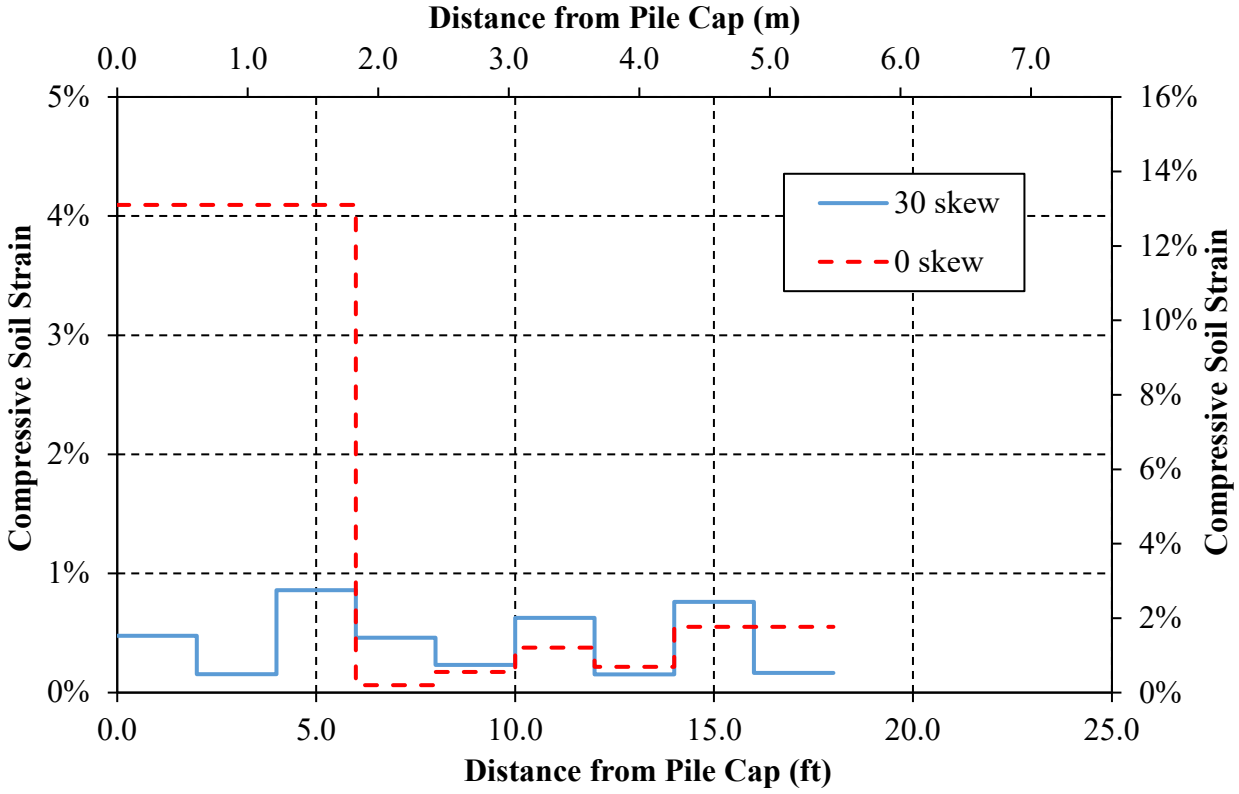

Figure 5-13: Compressive backfill strain for 30° and 0° skew tests.

The compressive behavior of both skew tests appears to mimic that of the concrete cylinders in some respects. Although the 30° skew cylinders had a higher computed stiffness compared to the 0° skew cylinders, the 30° skew backfill likely required more displacement to mobilize the resistance of the reaction block wall, thus resulting in a low stiffness value compared to the 0° skew backfill. Figure 5-13 also provides evidence that the 30° skew backfill was more rigid than the 0° skew backfill; the 30° skew backfill had a peak strain well below the peak strain of the 0° skew backfill.

5.5 Failure Surface Discussion

During the excavation of the 0° skew backfill, it was observed that the cellular concrete below the base of the pile cap appeared to be one solid piece and that mud had collected on the surface of the cellular concrete. After the 0° skew test was performed, the groundwater pumps were turned off, and the excavation filled with water. It is hypothesized that sediment from this water settled on the shear surface of the cellular concrete as shown in Figure 5-14 and that the cellular concrete did, in fact, shear rather than move as one block. Up to this point, the space between the backfill and pile cap was too small to directly observe the shear surface.

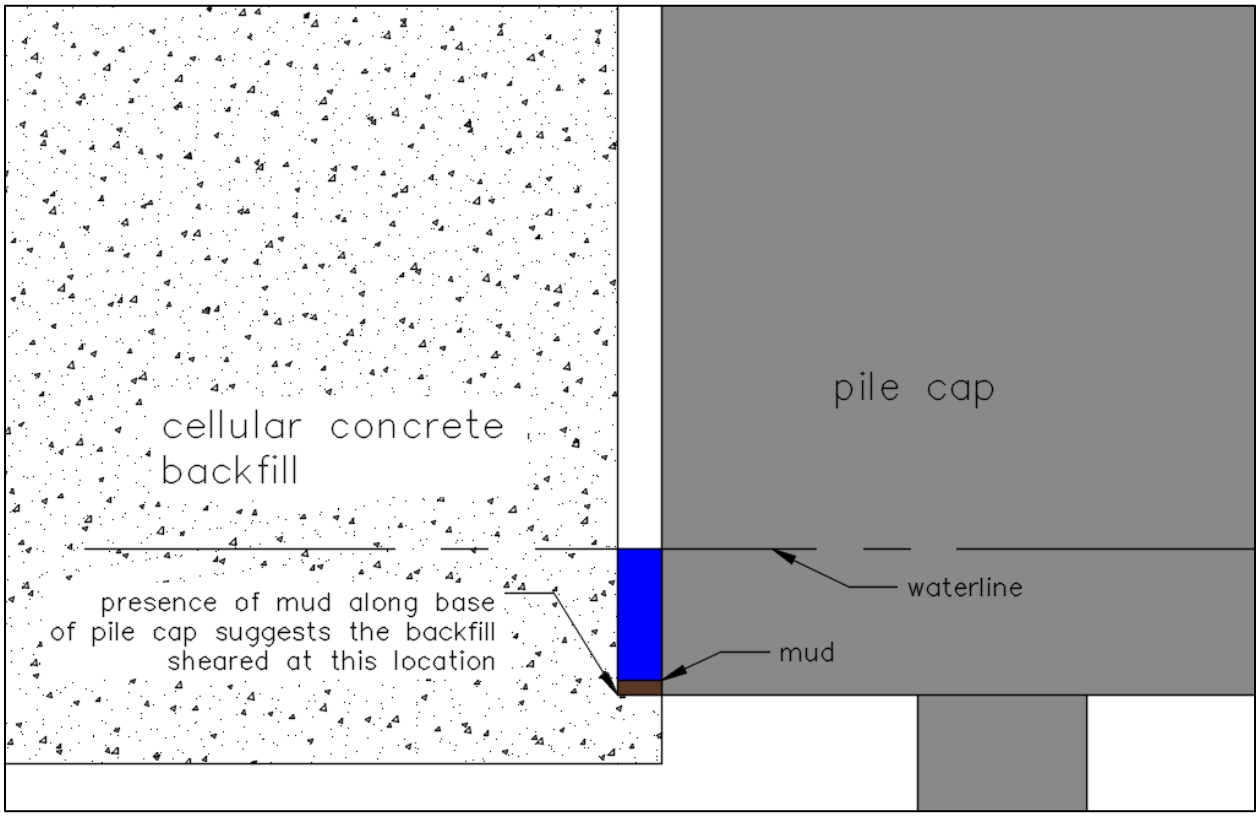

Figure 5-14: Backfill shear behavior observation at base of pile cap.

Although it appears that the cellular concrete sheared at the base of the pile cap, it is unclear whether this shear surface extended farther into the backfill. No shear surface could be observed

at the surface of the backfill or within the backfill itself. The cellular concrete cylinders tested for UCS generally failed in overall compression and did not develop clear failure surfaces as explained in Section 4.3.1.

6 ANALYSIS OF RESULTS

The force- deflection results are analyzed in this section to provide design guidance on the use of cellular concrete for bridge abutments. The PYCAP program developed by Duncan and Mokwa (2001) is used to model the field results. This program uses the Log-Spiral, Rankine, and Coulomb methods to predict the passive resistance of the backfill. Since a 0º friction angle is assumed, all of these methods predict the same passive earth pressure coefficient, K_p, and thus the same passive resistance. The passive resistance predicted using the Rankine method is shown in Equation 6-1.

$$P_p = 0.5\gamma H^2 B K_P + 2c'HB \quad (6\text{-}1)$$

where:

P_p = passive resistance

γ = unit weight of backfill

H = height of backwall

B = width of backwall

c' = cohesion

K_p = passive earth pressure coefficient

All of these methods assume a failure surface, which may or may not have occurred during field testing as it was not possible to identify the surface in the field. The PYCAP model was used as it provides a reasonable strength model nonetheless. Since the 0º skew and 30º skew tests

differed in the method of placement, caution should be taken when comparing the results of the two tests against each other.

6.1 PYCAP Input Parameters

The PYCAP input parameters are summarized in Table 6-1. Cap width, height, embedment depth, and surcharge were all known values. Cohesion was calculated as 50% of the UCS. The UCS was based on the average of all samples for the 30° skew test and by the point corresponding to the age at backfill testing for the best-fit line of age vs. strength for the 0° skew test. The basis for these UCS values is explained in Section 4.3.1. Soil friction angle was assumed to be 0° based on the observed results in Section 4.3.2 but was entered as 0.00001 to prevent the program from using the $\phi = 0°$ sliding wedge method. The sliding wedge method factors in the vertical component of the passive resistance. The wall friction was assumed to be zero based on the 0° soil friction angle. Soil modulus, E, and failure displacement were altered through a trial and error process to best match the measured curve. Poisson's ratio was entered as 0.13 based on the Poisson's ratio measured for a 60 pcf (961 kg/m^3) cellular concrete reported by Lee, Bronowski, and Hardy (2004). Backfill unit weight was entered as the average wet density of the cellular concrete samples. The wall adhesion factor was entered as zero to obtain the horizontal passive resistance only.

The cap width and height were determined based on the behavior observed during testing. In both the 30° and 0° skew tests, the entire width of the backfill moved rather than shear at the sides of the pile cap. The backfill did shear at the base of the pile cap, however. Due to these observations, the cap width was entered as 11.7 ft (3.57 m), which was the entire width of the

backfill, and the height of the backfill was entered as 5.5 ft (1.68 m), which was the height of the pile cap.

Table 6-1: PYCAP Input Parameters

Input Parameters		30° Skew	0° Skew
cap width,	**b (ft)**	11.7	11.7
cap height,	**H (ft)**	5.5	5.5
embedment depth,	**z (ft)**	0	0
surcharge,	**q_s (psf)**	0	0
cohesion,	**c (psf)**	4147 (28.80 psi)	3667 (25.47 psi)
CLSM friction angle,	**ϕ (deg.)**	0.00001	0.00001
wall friction,	**δ (deg.)**	0	0
initial soil modulus,	**E_i (kip/ft^2)**	450	750
poisson's ratio,	**ν**	0.13	0.13
CLSM unit weight,	**γ_m (pcf)**	29.6	28.6
adhesion factor,	**α**	0	0
Displacement,	**Δ_{max}/H**	0.024	0.017

6.2 PYCAP Results

The passive force vs. deflection curves generated by PYCAP and the measured results are compared in Figure 6-1. For the 30º skew test, the measured peak passive force was about 5% lower than the computed peak force, while for the 0º skew test the measured peak force was about 20% lower. Table 6-2 compares the field and PYCAP results. Considering the simplicity of the strength model employed, the agreement between measured and computed responses is very good. Although PYCAP tends to over-predict the peak passive resistance, it does model the high residual strength of the backfill fairly well. The trial-and-error process for displacement and soil modulus allowed PYCAP to closely match the initial slope of the observed passive resistance for the 30° and 0° skew tests. The 0° skew test had the greatest difference between

measured and computed peak values (93.3 kip (415 kN)), while the 30° skew test was quite similar to the PYCAP curve with a 29.2 kip (130 kN) difference. The differences between the two tests are summarized in Table 6-2. The error for both tests was calculated by comparing the measured value to the predicted design value as shown in Equation 6-2.

$$E = 100(P - M)/P \quad (6\text{-}2)$$

where:

E = error (%)

M = measured peak value

P = predicted peak value

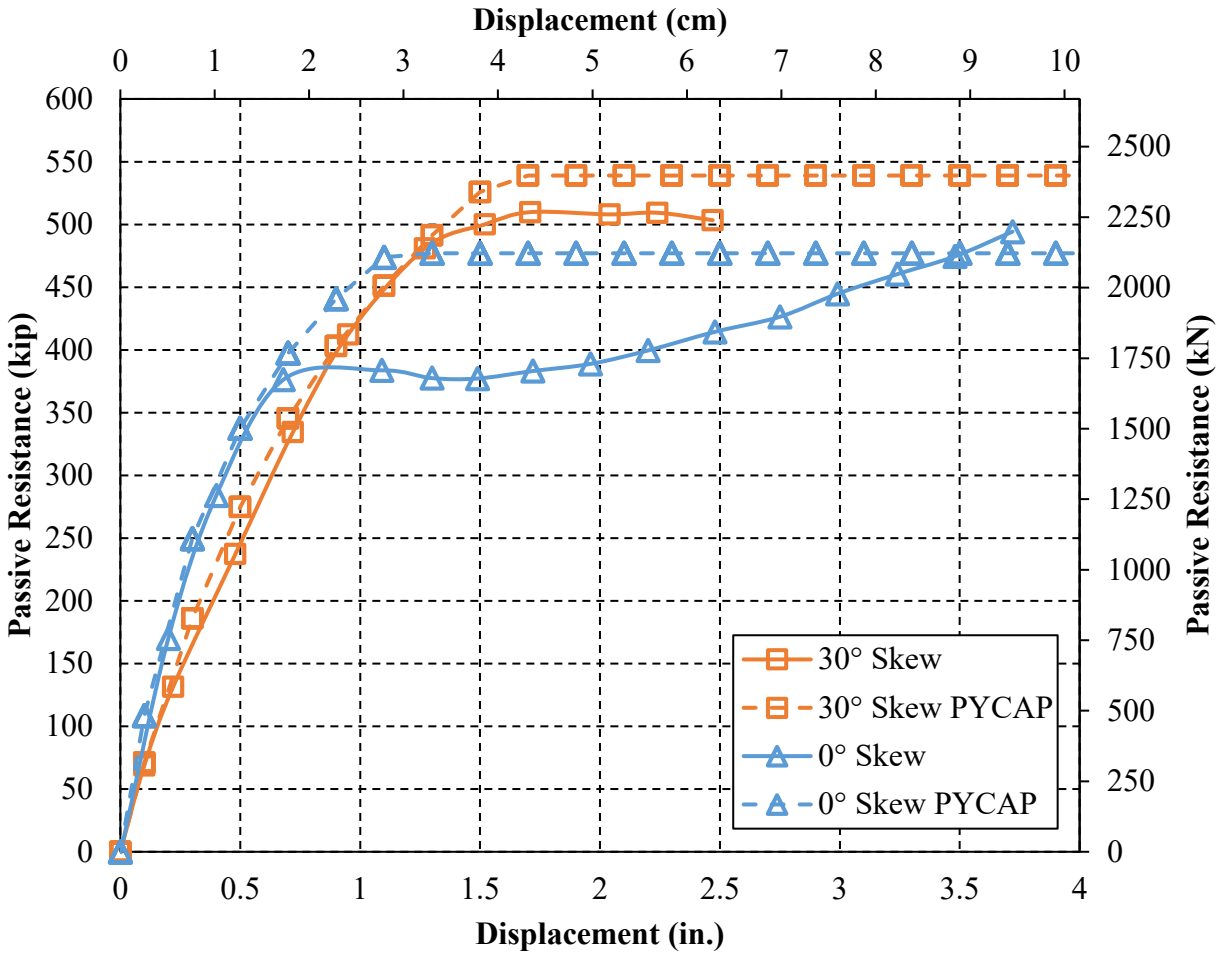

Figure 6-1: PYCAP computed passive resistance vs. measured passive resistance.

Table 6-2: Computed and Measured Ultimate Resistance for 30° and 0° Skew Tests

Test	Computed Resistance	Measured Resistance	Error
30° Skew	539.0 kip (2398 kN)	509.8 kip (2268 kN)	-5%
0° Skew	477.0 kip (2122 kN)	383.7 kip (1706.8 kN)	-20%

The computed and measured maximum stiffness values were similar for the 30° skew test and fairly different for the 0° skew test. The computed maximum stiffness for the 30° and 0° skew tests were 711 kip/in. (1245 kN/cm). and 1085 kip/in. (1900 kN/cm), respectively. The measured maximum values were 689 kip/in. (1207 kN/cm) for the 30° skew test and 850 kip/in. (1488 kN/cm) for the 0° skew test. The ratio of UCS to modulus was almost twice as high for the 30° skew test as for the 0° skew test; the 30° skew test had a ratio of 0.018, and the 0° skew test had a ratio of 0.0098.

6.3 Granular Backfill Comparison

The Caltrans procedure for estimating the passive resistance of granular backfill materials is described in this section, and the results are compared to the measured results although the cementitious materials in this study are not within the Caltrans material specification. Caltrans recommends using Equation 6-3 to estimate the abutment stiffness, K_{abut}, and Equation 6-4 to estimate the passive resistance of the granular backfill, P_{bw}. Initial stiffness was entered as 50 kip/in./ft, backwall width as 11 ft, and backwall height as 5.5 ft.

$$K_{abut} = K_i * w * \left[\frac{h}{5.5ft}\right] \quad (6\text{-}3)$$

where:

K_i = initial stiffness, ≈ 50 kip/in./ft for embankment fill meeting Caltrans requirements and ≈ 25 kip/in./ft for embankment fill not meeting Caltrans requirements

w = projected width of the backwall (ft)

h = height of backwall (ft)

$$P_{bw} = A_e * 5.0ksf * \left[\frac{h_{bw}}{5.5}\right] \quad (6\text{-}4)$$

where:

A_e = effective abutment wall area (ft^2)

h_{bw} = height of backwall (ft)

The measured and computed passive force and stiffness values are presented in Figure 6-2 and summarized in Table 6-3. The Caltrans procedure under-predicted the passive resistance for both tests with an error of about 19% and 58% for the 0º and 30º skew tests, respectively. Nevertheless, the resistance provided by the cellular concrete with compressive strength between 50.9 psi and 57.6 psi (351 kPa and 397 kPa) was comparable to that expected for dense granular backfill according to Caltrans design procedures. The Caltrans method provided a stiffness estimate that is between the observed values for both tests and that is very close to the average measured value. Based on the results of this study, the Caltrans procedure could be used to provide a reasonable estimate of stiffness and a somewhat conservative estimate of passive resistance for Class II cellular concrete.

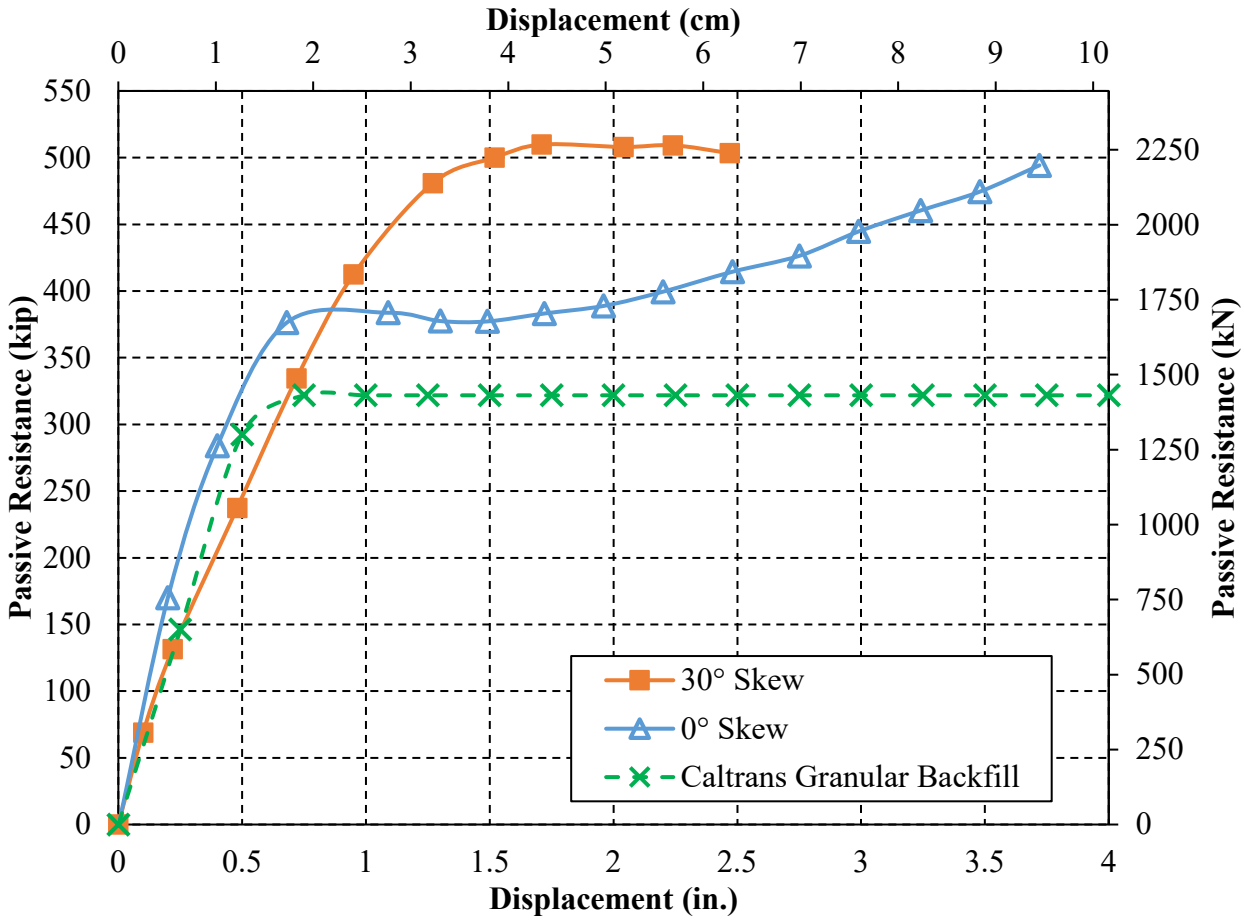

Figure 6-2: Measured passive resistance and Caltrans granular backfill estimate vs. displacement.

Table 6-3: Cellular Concrete Results vs. Caltrans Granular Fill Estimates

	30° Skew	0° Skew	Caltrans Estimate
Stiffness	434.1 kip/in. (760 kN/cm)	709.9 kip/in. (1243 kN/cm)	585.0 kip/in. (1024 kN/cm)
Passive Resistance	509.8 kip (2268 kN)	383.7 kip (1707 kN)	321.8 kip (1431 kN)

7 CONCLUSIONS AND RECOMMENDATIONS

7.1 Conclusions

1. The backwall skew angle appeared to have no effect on the peak passive resistance. Peak passive resistance was actually higher for the 30° skew test than for the 0° skew test, although this difference may be attributed to differences in compressive strength and differences in concrete placement.
2. Class II cellular concrete strength (with similar placement and curing procedures) is very sensitive to wet density, which is the greatest predictor of backfill strength for low-density cellular concrete. Wet density should be sampled frequently to ensure there are consistent material properties throughout the backfill.
3. In contrast to flowable fill (Wagstaff 2016), the Class II cellular concrete used in these tests did not experience any significant reduction in passive force after reaching the peak value. This is similar to the behavior of granular backfills and is modeled well using the PYCAP program.
4. Initial peak passive resistance was mobilized with displacements approximately equal to 1.7-2.6% of the wall height (5.5 ft (1.68 m) wall). This is between the 3-5% that has been suggested for conventional backfill materials and the 0.75-2% displacement observed for CSLM (flowable fill) backfills.

5. The horizontal peak passive force can be computed within an error of 20% or less using the Rankine equation for cohesive soil using a cohesion equal to half of the UCS and a friction angle of zero.

7.2 Recommendations for Future Research

Further research should be conducted to verify the results of this study. Although no skew effects were observed between the 30° and 0° skew tests, the two tests cannot be directly compared owing to the small differences in concrete placement and testing. Future research could better control these variables to provide a better comparison.

The results of this study are only applicable to cellular concrete cured and produced in a way similar to that used in this research. A denser cellular concrete would likely behave different than the low-density concrete tested in this study. Since the results of this study cannot be extrapolated to denser concretes, further research is necessary to make conclusions about the passive resistance of other classes of cellular concrete. This study was also conducted in a hot, dry climate; cellular concrete placed in a different climate may behave differently.

The cellular concrete tested exhibited behavior similar to that of a geofoam. Since the UCS of geofoam changes based on the rate of applied load, it would useful to determine if cellular concrete performs similarly. If the pile cap were displaced into the cellular concrete at a faster or slower rate, the passive resistance of the cellular concrete could change.

REFERENCES

Cellular Concrete Solutions. *Simplifying Construction on Marginal Lands*, 2009. cellular-concrete.com. Accessed 16 May 2016.

Duncan, J.M. and R.L. Mokwa. "Passive Earth Pressures: Theories and Tests." *Journal of Geotechnical and Geoenvironmental Engineering* (2001): 248-257.

Elastizell Corporation of America. *What is Elastizell?* elastizell.com/what.html. Accessed 7 October 2016.

FHWA. *LRFD Seismic Analysis and Design of Bridges Reference Manual.* Rep. No. FHWA-NHI-15-004. 2014.

FHWA. *Recording and coding guide for the structure inventory and appraisal of the nation's bridges*. Rep. No. FHWA-PD-96-001. Washington, D.C., 1995.

Franke, B.W. "Passive Force on Skewed Abutments with Mechanically Stabilized Earth (MSE) Wingwalls Based on Large-Scale Tests." *All Theses and Dissertations,* 2013. scholarsarchive.byu.edu/etd/3909.

Fredrickson, A. "Large Scale Testing of Passive Force Behavior for Skewed Bridge Abutments with Gravel and Geosynthetic Reinforced Soil (GRS) Backfills." *All Theses and Dissertations*, 2015. scholarsarchive.byu.edu/etd/5513.

Filz, G., A. Reeb, A. Grenoble, and F. Abedzadeh. "Material Properties for Analysis of Deep Mixing Support Systems." *Deep Foundations Institute* (2015): 823-834.

Grutzeck, M.W. "Cellular Concrete." Cellular Ceramics: Structure, Manufacturing, Properties and Applications. Ed. Michael Scheffler and Paolo Colombo. Wiley-VCH, 2005. 193-223.

Jessee, S.J. "Skew Effects on Passive Earth Pressures Based on Large-Scale Tests." *All Theses and Dissertations,* 2012. scholarsarchive.byu.edu/etd/3202

Jones, M.R. and A. McCarthy. "Heat of hydration in foamed concrete: effect of mix constituents and plastic density." *Cement and Concrete Research* (2006): 36:1032-1041.

Jones, M.R. and A. McCarthy. "Preliminary views on the potential of foamed concrete as a structural material." *Magazine of Concrete Research* (2005): 57:21-31.

Kaviani, P., F. Zareian, and E. Taciroglu. *Performance-Based Seismic Assessment of Skewed Bridges*. Pacific Earthquake Engineering Research Center. Rep. No. 2014/01, 2014.

Kearsley, E.P. and P.J. Wainwright. "The effect of high fly ash content on the compressive strength of foamed concrete." *Cement and Concrete Research* (2001): 105-112.

Kearsley, E.P. and P.J. Booysens. "Reinforced foamed concrete, can it be durable." *Concrete/Beton* (1998): 91:5-9.

Lee, M.Y., D.R. Bronowski, and R.D. Hardy. *Laboratory Constitutive Characterization of Cellular Concrete*. Sandia National Laboratories. Rep. No. 2004-1030, 2004.

Legatski, L.M. and A.E. Mansour. *Properties and Proportioning of Elastizell Cellular Concrete*. University of Michigan Research Institute. Project. No. 2326, 1961.

Legatski, L. personal communication. 22 June 2016. Email.

Lemnitzer, A.A., E.R. Nigbor, A. Shamsabadi, A. Wallace, and J.P. Stewart. "Lateral Performance of Full-Scale Bridge Abutment Wall with Granular Backfill." *Journal of Geotechnical and Geoenvironmental Engineering* (2009): 506-514.

Leo, C.J., M. Kumruzzaman, H. Wong, and J.H. Yin. "Behavior of EPS geofoam in true triaxial compression tests." *Geotextiles and Geomembranes* (2008): 175-180.

Marsh, A.K. "Evaluation of Passive Force on Skewed Bridge Abutments with Large-Scale Tests." *All Theses and Dissertations,* 2013. scholarsarchive.byu.edu/etd/3921.

Maw, R. and R. Cole. "Cellular Concrete Laboratory Testing Program Laboratory Testing Observations and Results." Gerhart Cole Inc., 2015.

Meyer, R.D. II. "Passive Earth Pressures: Design Parameters for Common Force-Displacement Approaches." M.S. Project, Brigham Young University, 2012.

Nambiar, E.K.K. and K Ramamurthy. "Models relating mixture composition to the density and strength of foam concrete using response surface methodology." *Cement & Concrete Composites* (2006): 752-760.

Nambiar, E.K.K. and K. Ramamurthy. "Models for strength prediction of foam concrete." *Materials and Structures* (2008): 247-254.

Nambiar, E. K.K. and K. Ramamurthy. "Shrinkage Behavior of Foam Concrete." *Journal of Materials in Civil Engineering* (2009): 631-636.

Nambiar, E.K.K. and K Ramamurthy. "Sorption characteristics of foam concrete." *Cement and Concrete Research* (2007): 37:1341-1347.

Nichols, D. and K.M. Rollins. personal communication, 2012.

NRMCA. "Flowable Fill." *Concrete in Practice*, 2000. Ch 17.

Palmer, W.D. Jr. *Advances in Lightweight*, 2009. www.concreteconstruction.net/how-to/materials/advances-in-lightweight_o. Accessed 9 June 2016.

Panesar, D.K. "Cellular concrete properties and the effect of synthetic and protein foaming agents." *Construction and Building Materials* (2013): 575-584.

Ramamurthy, K. and E.K.K. Nambiar. "A classification of studies on properties of foam concrete." *Cement and Concrete Composites* (2009): 388-396.

Ramamurthy, K. and E.K.K. Nambiar. "Models relating mixture composition to the density and strength of foam concrete using response surface methodology." *Cement & Concrete Composites* (2006): 752-760.

Rollins, K.M. and A. Sparks. "Lateral Resistance of Full-Scale Pile Cap with Gravel Backfill." *Journal of Geotechnical and Geoenvironmental Engineering* (2002): 711-723.

Rollins, K.M., T.M. Gerber, and L. Heiner. *Passive Force-Deflection Behavior for Abutments with MSE Confined Approach Fills*. Utah Department of Transportation. Rep. No. UT-10.15, 2010.

Scott, E.G. “Passive Force on Bridged Abutments and Geofoam Inclusions with Large-Scale Test.” M.S. Project, Brigham Young University 2015.

Tada, S. "Material design of aerated concrete: an optimum performance design." *Materials and Construction* 19 (1986): 21-6.

Tam, C.T., T.Y. Lim, and S.L. Lee. et al. "Relationship between strength and volumetric composition of moist-cured cellular concrete." *Magazine of Concrete Research* (1987): 39.138:12-18.

Tikalsky, P.J., J. Pospisil, and W. MacDonald. "A method for assessment of the freeze-thaw resistance of preformed foam cellular concrete." *Cement and Concrete Research* (2004): 34:889-893.

Wagstaff, K.B. "Evaluation of Passive Force on Skewed Bridge Abutments with Controlled Low-Strength Material Backfill." *All Theses and Dissertations*, 2016. scholarsarchive.byu.edu/etd/5824.

Zemajtis, J.Z. *Role of Concrete Curing*. www.cement.org/for-concrete-books-learning/concrete-technology/concrete-construction/curing-in-construction. Accessed 18 November 2016.

Zollo, R.F. and C.D. Hays. "Engineering Material Properties of a Fiber Reinforced Cellular Concrete." *ACI Materials Journal* (1998): 631-635.